Theses and Dissertations

2003

Evaluation of real-time pseudodynamic testing algorithms for seismic testing of structural assemblages

Oya Mercan
Lehigh University

Follow this and additional works at: http://preserve.lehigh.edu/etd

Recommended Citation

Mercan, Oya

Evaluation of Real-Time Pseudodynamic Testing Algorithms for Seismic Testing…

May 2003

Evaluation of Real-Time Pseudodynamic Testing Algorithms

for Seismic Testing of Structural Assemblages

by

Oya Mercan

A Thesis

Presented to the Graduate and Research Committee

of Lehigh University

in Candidacy for the Degree of

Master of Science

in

Civil Engineering

Lehigh University

May, 2003

This thesis is accepted and approved in partial fulfillment of the requirements for the Master of Science.

April 25, 2003

_____
Date

Dr. James M. Ricles, Thesis Advisor

Dr. Arup K. SenGupta, Chairperson of Department

Acknowledgements

I would like to first thank to my advisor Professor James M. Ricles. I was fortunate to work with him. His academic vision, advice, guidance, motivation and support made this thesis possible.

The financial support provided by the Lehigh University ATLSS Research Center and National Science Foundation is gratefully acknowledged.

Thanks to each of my friends for all their support. There are too many names and for the fear of leaving one out accidentally I will not try. I just want you all know that I cherish our friendships.

Finally, I would especially like to thank to my family; annecim, babacim, Yavuz abi, Fatih and Hatice. Thanks for everything...

TABLE OF CONTENTS

List of Tables

List of Figures

Chapter 2

Chapter 3

Chapter 4

Chapter 6

Chapter 7

Chapter 8

ABSTRACT

The conventional pseudodynamic method is an experimental technique to simulate the seismic response of structural models. It is a displacement-control approach, which utilizes feedback signals from a test structure and a numerical integration algorithm to sequently solve the equations of motion to determine the target displacement to be imposed on the structure for selected time interval. Since the strain rate effect can be neglected for most steel structures, a conventional pseudodynamic test performed quasi-statically at a reasonable rate is able to simulate the earthquake response reasonably well.

With the introduction of the use of velocity-dependent devices (e.g., viscoelastic dampers, friction dampers, rubber bearings) to mitigate earthquake hazards in structures, there currently exists the need to perform large-scale real-time testing to evaluate the performance of these types of structures. Conventional pseudodynamic testing would not properly account for load-rate effects. In this case, the test structure has to be loaded dynamically in real time.

The objective of this study is to evaluate selected conventional and real-time pseudodynamic testing algorithms. The effect of using different algorithms in testing structures with rate dependent components is evaluated through numerical simulations. Error propagation characteristics of three different algorithms are investigated in a consistent manner for both conventional and real-time pseudodynamic testing.

A new algorithm based on Newmark Explicit method that enables real-time testing is also presented. In this method the Newmark Explicit algorithm is modified, whereby two independent integrations are separately performed for even and odd time steps with a

1

filtering technique employed to remove the artificially introduced higher frequencies that create instability in rate dependent test simulations.

Based on the numerical analyses performed, recommendations for attaining reliable conventional and real-time pseudodynamic test results are discussed.

Chapter 1   Introduction

1.1   General

Since its first application in the 1970's, the conventional pseudodynamic method has been effectively used in several seismic simulations. Extensive analytical and experimental studies have been published to establish the baseline of the procedure (Shing and Mahin, 1984; Shing and Mahin, 1985).

Early tests conducted with this method in Japan, the United States and Europe were carried out with an explicit time integration scheme, such as the Newmark Explicit or Central Difference method.

The major source of inaccuracies for the pseudodynamic (PSD) method was found to be the propagation of experimental errors. This issue was extensively investigated for the conventional PSD method of testing, and conclusions were drawn related with the detrimental effects of different types of experimental errors (Shing and Mahin, 1983; Nakashima and Kato, 1987; Shing and Mahin, 1987).

Implicit integration schemes based on the Alpha Method (Hilber et al., 1977) have been developed which have superior energy dissipation and stability properties. The implicit Alpha Method for PSD testing was first proposed by Thewalt and Mahin (1987). Nakashima proposed another unconditionally stable algorithm, the Operator-Splitting Method (Nakashima et al., 1990). This method enables PSD testing with substructuring to be conveniently performed. Several additional studies on the properties of implicit schemes have been published (Shing and Manivannan, 1990; Shing and Vannan, 1991; Bursi and Shing, 1996).

Recently, mainly for earthquake hazard mitigation purposes, various new structural components and devices such as viscous dampers, friction dampers and rubber bearings have been introduced. Because of their velocity dependency characteristics, the conventional pseudodynamic testing based on quasi-static loading is no longer able to capture the seismic response of structures having load rate-dependent devices. The use of a shake table would not be a viable option, since it prohibits large-scale test to be performed due to specimen weight limitations. Through the advances in computer hardware and controllers, there have been some studies involving fast pseudodynamic testing, with numerical integration algorithms for conventional PSD testing modified appropriately (Nakashima and Kato, 1992; Nakashima and Masaoka, 1999; Shing et al., 2002). The purpose of these studies has been to develop a means of performing real-time testing of large-scale structures.

Conventional PSD tests are performed slowly where the dynamic effects (i.e. velocity related and inertia forces) are accounted for in the solution of the equations of motion. As noted previously, in some applications it is necessary to perform the PSD test at, or near real-time.

To ensure continuous loading in real-time, the numerical integration algorithm used in the testing must be able to have the next step target displacement ready, before the current step loading is completed. Using the conventional PSD algorithms and performing the test quickly cannot achieve this. Various attempts have been made in modifying some of the existing explicit and implicit algorithms to satisfy this requirement. A number of problems encountered with these efforts have already been

documented in the literature (Nakashima and Kato, 1992, Nakashima and Masaoka, 1999).

1.2   Objectives and Scope

The purpose of this study is to evaluate selected integration algorithms for both conventional and real-time PSD testing of structural systems subjected to earthquake loading. Through numerical simulations, certain characteristics of the selected integration schemes are evaluated; related observations, conclusions and remarks are provided. Information from previous research results is also given, enabling this study to be used as a general reference.

To evaluate the performance of selected real-time PSD algorithms, numerical simulations of real-time PSD tests of structural systems including a visco-elastic (VE) damped frame were carried out. The VE dampers are load-rate dependent devices.

Many studies have shown that the PSD method is sensitive to experimental error. This source and effect of experimental error has been explored analytically and numerically in great detail for conventional PSD method (Shing and Mahin, 1983; Nakashima and Kato, 1987; Shing and Mahin, 1987; Shing and Manivannan, 1990; Thewalt and Roman, 1994; Bursi and Shing, 1996). However, no such systematic study exists for real-time PSD testing methods. In this report, error propagation characteristics of three different algorithms are numerically investigated in a consistent manner for both conventional and real-time pseudodynamic testing.

A new algorithm based on the Newmark Explicit method that enables real time testing is also developed. In this method, the conventional Newmark Explicit algorithm is

5

modified such that two independent integrations are separately performed for even and odd time steps, and a filter is employed to remove the artificially introduced higher frequencies that create instability in the load rate-dependent test simulations. The use of the filter maintains the "smoothness" between the motions in the even and odd time steps. An error propagation analysis is also performed for this new method.

Based on the numerical analyses conducted, the effect of using different PSD algorithms in testing structures with load-rate dependent components is evaluated, and recommendations for attaining reliable test results are presented in this report.

1.3 Organization of the Thesis

This thesis focuses on the integration algorithms for conventional and real-time PSD tests.

Background information and summaries of previous studies in both conventional and real-time PSD method are presented in Chapter 2. Basic experimental schemes and problems encountered, along with the applied solutions are also explained.

After an overall introduction to direct step-by-step integration algorithms, the theoretical background for three selected algorithms, including the details related to the newly developed staggered Newmark Explicit scheme with Alpha-Beta Tracker filter is given in Chapter 3.

In Chapter 4, a 4-story moment resisting frame (MRF) and a VE-damped MRF, which are used in the numerical simulations of conventional and real-time PSD tests, are introduced. The structural idealizations and the design procedure for sizing the VE dampers are explained.

The results of PSD testing simulations for conventional and real-time PSD method using three different algorithms are presented in Chapter 5. Both linear and nonlinear structural response cases are considered.

In Chapter 6, velocity characteristics of the algorithms are examined and the rate dependent restoring force effect on simulation results is evaluated.

Chapter 7 describes the experimental error sources. The error types that have been introduced in the numerical simulations in this study are discussed in this chapter. A review of the previous studies on this subject is also given.

Systematic error analyses were performed for both conventional and real-time PSD test simulations. The behavior of each algorithm in the case of several possible experimental error scenarios was investigated. The results of error propagation simulations are illustrated in Chapter 8.

Finally, Chapter 9 summarizes the study. A summary and general conclusions are given; observations and areas requiring further research are identified.

Chapter 2 Pseudodynamic Testing Background

2.0   General

This chapter contains background information about conventional and real-time pseudodynamic (PSD) methods of testing. While summarizing previous research done on this subject, the general experimental schemes and problems encountered, along with the applied solutions are also explained.

2.1   Conventional Methods of Seismic Testing

There are three experimental laboratory techniques that are typically used to evaluate the seismic behavior of structures: quasi-static testing, shaking table testing and the conventional PSD method of testing.

In quasi-static testing the structure or its component is subjected to a predetermined cyclic displacement history and the behavior of the elements is observed. The deformation history imposed may be arbitrary or it may be computed using a dynamic analysis before the testing. Quasi-static testing permits a careful measurement and observation of the behavior of the test structure. It is commonly used and economical, however, it is limited because the deformation history does not necessarily correspond to the true earthquake response of the specimen since the dynamic analysis performed beforehand may not accurately predict the true seismic behavior of the structure.

Perhaps the most realistic method for evaluating the dynamic response of a given structure is to place it on a shaking table and subject it to properly scaled ground motion time histories. However, these tests are expensive and must be performed on small-scale test structures. To account for scaling effects, the time scale of the acceleration record

must be compressed; consequently there is very little time to observe the behavior of the specimen during the seismic simulation. As a result, while the response may represent actual seismic behavior, the combined effects of small-scale specimens, short duration testing and cost limit the use of shaking table tests.

The conventional PSD method is an experimental technique to simulate the seismic response of large-scale structural models. It is a displacement-control approach, which utilizes feedback signals from the structure and a numerical integration algorithm to determine the target displacement to be imposed on the structure at each time step.

In a conventional PSD test, the test structure is first idealized as discrete parameter system such that the governing equations of motion can be represented by a system of second order ordinary differential equations in time. This procedure is called a semidiscretization. The inertial and viscous damping characteristics are analytically prescribed and the excitation history is numerically specified. During the test the equations of motion are solved by direct step-by-step numerical integration to obtain target displacements for each time step. The target displacements computed in each time step are quasi-statically imposed on the test structure by hydraulic actuators. The restoring forces developed by the structural deformations are measured by the load transducers at the end of the time step and subsequently used to compute the target displacements to be imposed in the next time step. This process is repeated (as illustrated in Figure 2.1) until the whole response history of the test specimen is obtained.

The use of experimentally measured restoring forces from the deformed specimen eliminates the uncertainties associated with nonlinear stiffness or resisting force characteristics of the structure.

As explained earlier, in order to perform a conventional PSD test, the test structure is first idealized as discrete parameter system having mass concentrated at a limited number of degrees of freedom. In order to represent the vibration characteristics accurately it is wise to select the dynamic degrees of freedom at locations where the structural mass is actually concentrated, such as the story levels of multi-story buildings with heavy floor systems.

The damping characteristics of the test structure are often modeled by a viscous damping mechanism. Appropriate viscous damping coefficients can be determined from a vibration test. During a conventional PSD test, other types of damping mechanisms, such as Coulomb damping due to friction or hysteretic damping due to inelastic deformations, are accounted for through the measured resisting forces. Also, as hysteretic damping is the dominant energy dissipation mechanism in a structure deformed beyond elastic limits, failure to assign the exact viscous damping properties does not have a significant effect on response when considerable inelastic deformations occur (Shing and Mahin, 1984).

Since the strain rate effect can be neglected for most steel structures, the conventional PSD method of testing performed quasi-statically at a slow rate is able to realistically simulate the earthquake response.

Conventional PSD method of testing overcomes the limitations of size and mass of the specimen that are present in shaking table test, while using the same equipment necessary for performing quasi-static testing. However, structures with significant distributed mass or having material properties or components that are load-rate sensitive may not be able to have their response to seismic loading accurately captured by the conventional PSD method of testing.

Since its first application in the 1970's (Takanashi et al., 1975) the conventional PSD method of testing has been effectively used in several seismic simulations. The method however has three major sources of inaccuracies. The first is the idealization of the test structure as discrete parameter system, the second is the computational error inherent in the numerical solution of the equations of motion, and the third is the experimental feedback error introduced during a test. The third source of inaccuracies, namely propagation of experimental errors, appears to be the main source of inaccuracies in conventional PSD testing.

Of the conventional methods of seismic testing, only shake table testing can account for load-rate effects.

2.2   Real-time Methods of Seismic Testing

Recently, mainly for earthquake hazard mitigation purposes, various new structural components and devices such as viscous dampers, friction dampers and rubber bearings have been introduced in structures. Because of the velocity dependent vibration characteristics of these devices, the conventional pseudodynamic testing method based on quasi-static loading is no longer appropriate to determine the seismic response of

11

structures equipped with these devices. In this case, the test structure has to be loaded dynamically in real time.

The steps explained for conventional PSD testing is also valid for real-time PSD testing. The major difference between the two is the use of dynamic actuators in the latter. Furthermore, in order to impose the calculated displacements in a fast and precise manner, and with an accurate velocity control, sophisticated control technologies and an efficient computation scheme are required.

To load the structure dynamically in real time, the displacements have to be computed in such a manner to enable continuous actuator motion. In the numerical integration algorithms used for the conventional method of PSD testing, target displacements for the next time step are computed from the restoring forces developed due to deformations imposed by the current time step displacements. As a result, the next time step target displacements are not available at the instant when the loading for the current step displacements is completed. Although this is not a problem for conventional PSD testing, for real-time PSD testing the numerical algorithm needs to have the target displacements ready prior to the completion of the current time step.

As the purpose of real-time testing is to simulate earthquake response of structures with velocity dependent components and devices, the velocity characteristics of the numerical algorithms becomes more important. A test structure equipped with rate dependent components can only be tested realistically when a displacement history that closely resembles the earthquake response is imposed at the same rate as the structure would experience during the actual earthquake. Otherwise the test structure will not

develop the actual resisting forces, and consequently will not exhibit the actual seismic behavior.

One other point that one has to be careful about with real-time PSD method of testing is the effect of inertial forces. When the actuators impose a high level of acceleration to a test structure having heavy mass, the forces measured by the load cells include a considerable amount of inertial force. This effect cannot be neglected in real-time testing.

Another method of real-time seismic testing, called the Effective Force Testing (EFT) method, employs a force control algorithm that enables real-time earthquake simulation studies of large-scale structures. Unlike the PSD method of testing, there is no computational time required to determine the required force signal in the EFT method. Once the structural mass and ground acceleration record to be simulated are known, the complete force history to be applied to the structure is calculated before the test. Although the testing scheme is conceptually simple, its implementation has been considered to be problematic. An experimental investigation of the EFT method using an SDOF system was conducted at the University of Minnesota, and a direct application of the method was found to be ineffective because the actuator was unable to apply force at the natural frequency of the structure due to actuator control-structure interaction (Dimig et al., 1999).

2.3   Previous Studies in Conventional PSD Method of Testing

The method in its current form was first reported by Takanashi et al. in 1975 (Takanashi et al., 1975). Early tests conducted with this method in Japan, the United

13

States, and Europe were carried out with an explicit time integration scheme, such as the Newmark Explicit or Central Difference method.

Several sources of inaccuracies, such as structural idealization effects, strain-rate effects, uncertainties associated with assigning energy dissipation properties, and propagation of experimental error were closely studied (Shing and Mahin, 1984). Certain systematic experimental errors were found to be detrimental to pseudodynamic testing, particularly in multi-degree-of-freedom tests (Shing and Mahin, 1983; Shing and Mahin, 1985; Nakashima and Kato, 1987).

Various efforts have been made to find ways to modify the algorithms to suppress the error growth. Modifying the measured reactional force by using the initially estimated stiffness of the analyzed system and the displacement error detected in each step of loading, and using this modified reactional force in solving the equations of motion was proposed by Nakashima and Kato in order to reduce the experimental error effects (Nakashima and Kato, 1987). As an extension of this method they also proposed another algorithm, where instead of using the initial stiffness of the structure, the instantaneous stiffness is used to modify the reactional force (Nakashima and Kato, 1987).

Shing and Mahin recommended the use of a modified Newmark explicit algorithm with numerical energy dissipation in order to suppress the spurious growth of the high frequency modes of a multi-degree of freedom (MDOF) system (Shing and Mahin, 1983).

14

Explicit numerical integration schemes are conditionally stable whereas implicit integration schemes are generally unconditionally stable. Conditional stability of explicit methods is not a weakness when dealing with problems where using a small time step is required by accuracy considerations (i.e., structural impact problems). Also explicit schemes are computationally economical compared to implicit algorithms.

The solution of nonlinear differential equations by an implicit method usually requires iterative corrections, which are highly undesirable for testing nonlinear systems because the restoring forces developed depend on the displacement history of the structure. The internal displacement cycles performed during iterative corrections may result in an erroneous convergence. In order to circumvent this problem, explicit integration methods were initially recommended for conventional PSD testing in the early studies (Shing and Mahin, 1984; Mahin and Shing, 1985; Nakashima and Kato, 1987).

To avoid fabrication and testing of the entire specimen, the substructure PSD method of testing (referred to also as hybrid testing) was developed. This method is a practical and an economical alternative, where only a portion of the structure is experimentally tested and its degrees of freedom are coupled to an analytical model of the remaining part of the structure, as shown in Figure 2.2.

Although hybrid PSD testing had been suggested when the PSD test was first devised, its implementation remained limited due to the large number of degrees of freedom involved. In hybrid testing, the number of DOF is the sum of the DOFs of the analytical

and experimental models. There is a tendency to use many DOFs in the analytical models to achieve better accuracy.

When many DOFs have to be considered, such as in the case of hybrid testing or more complex specimens which have many experimental degrees of freedom, because of the conditionally stable nature of explicit algorithms the integration time interval required is unavoidably very small. As the number of time steps in a test is increased, problems with error propagation also increase. It would be advantageous to decide on the time interval to ensure accuracy in the responding modes, rather than as a stability constraint.

To achieve an unconditional numerical stability condition, the integration operator must be implicit. The first successful implicit scheme for PSD testing of inelastic MDOF systems was developed by Thewalt and Mahin (Thewalt and Mahin 1987, Thewalt and Mahin 1995). The main concern with an implicit algorithm, as explained above, is the requirement of an iterative procedure to evaluate the response of a nonlinear system. This is not only computationally inefficient, but it may also induce undesirable loading and unloading hystereses, creating problems for structures whose response is highly sensitive to history of imposed deformations. Although implicit, the scheme developed by Thewalt and Mahin did not involve numerical iteration. This was accomplished by using an analogue electronic device in the displacement control loop to correct the predictor displacements, which were based on the uninterrupted feedback of the instantaneous structural resisting forces developed. They used the Alpha Method developed by Hilber (Hilber et al., 1977) as the integration algorithm; however, other implicit algorithms can also be used. Although it is reported to be more reliable and far superior than the existing

implicit schemes, it is more difficult to implement because of the additional hardware required.

Another scheme that has been developed is the adaptation by Nakashima (Nakashima et al, 1990) of the Operator-Splitting method developed by Hughes and Liu (1978) to hybrid testing involving experimental models (i.e., test subassemblies) which have high frequency components introduced by the interface degrees of freedom. The Operator-Splitting Method is an unconditionally stable algorithm, which is based on a predictor-corrector approach. It requires neither numerical iteration nor an electronic device to obtain an accurate solution.

Shing et al. (1991) developed a third scheme to overcome the difficulties of using the implicit method developed by Thewalt and Mahin. Instead of using an analogue electronic device to correct the predictor displacement, the scheme Shing et al (1991) uses a numerical iteration that is based on the initial stiffness of the structure. To reduce the risk of overshooting the displacements, and to have a more or less uniform convergence rate for all DOFs, a displacement reduction factor was introduced. The displacement reduction factor prevents the undesired loading and unloading hystereses during iterations due to overshooting the target displacement.

2.4 Previous Studies in Real-Time PSD Method of Testing

The first real-time PSD test was performed by Nakashima et al. (1992) using a single-degree of freedom (SDOF) system with a single actuator. A slightly modified central difference algorithm was used, where a staggered integration scheme was used to separately compute target displacements for the even and odd time steps, as illustrated in

17

Figure 2.3. For example, the displacement at time step (2n+1) was computed using the displacements from steps (2n-1) and (2n-3) and the restoring force from time step (2n-1). Likewise, displacement at time step (2n+2) was computed using the displacements from steps (2n) and (2n-2) along with the restoring force from step (2n). As a result, while the actuator is leading the test structure to the target displacement during time step (2n+1), the target displacement for time step (2n+2) can be computed. Repeating this procedure enabled continuous real-time loading.

The Central Difference method is a conditionally stable integration scheme. For a staggered integration the stability criterion is even more severe. The scheme was devised with the electronic technologies of late 1980's. Due to the relatively slow operating speeds of the computers at the time, the integration time interval had to be relatively large. As a result, only an SDOF system with primary frequency of at most 1 Hz could be tested.

In the 1990's Horiuchi et al. (1996) developed a special computing and controlling mechanism to perform real-time PSD testing. To ensure real time loading, parallel computing techniques along with a special computer programming language developed by Horiuchi et al. were used. The requirement of a special device and inflexible nature of the programming language hindered the wide acceptance and use of this system.

In 1999 Nakashima and Masaoka presented a method for conducting real-time PSD tests of multi-degree of freedom structures (Nakashima and Masaoka, 1999). They again used the Central Difference algorithm as the direct integration scheme. In an attempt to overcome the problem of having the target displacement available for the next time step

18

when the target displacement of the current time step is reached, they proposed to extrapolate the target displacement beyond the current time step. As a result the actuators kept moving as the target displacement for the next time step was being calculated. When it then became available, an interpolation scheme was used to ensure that the calculated target displacement at the end of this next time step was reached. The method is shown schematically in Figure 2.4.

The problem with this method was that a significant velocity change occurs in the interval where the algorithm switches from extrapolation to interpolation. Since the main reason for real-time testing is to simulate the response of structures with rate dependent characteristics, accurate velocity control is very important and such a velocity change is undesirable.

2.5 Current Studies in Real-Time PSD

Several studies are currently being carried out on real-time substructure PSD testing in Europe, through the European Union-funded networks such as CASACADE and ECOLEADER, and in USA. The latter is a part of the NSF-funded NEES initiative for tele-networking of earthquake engineering test laboratories across the United States (http://www-civil.eng.ox.ac.uk/people/msw/rts.html).

Under the current NEES program (http://www.nsf.gov), the University of Colorado at Boulder is in the process of developing a Fast Hybrid Test (FHT) system (Shing et al., 2002). The integration scheme that is proposed for the FHT system is an implicit algorithm. This method, referred to as the "Alpha Method with a Fixed Number of Iterations", is one of the algorithms that are going to be evaluated in this report.

19
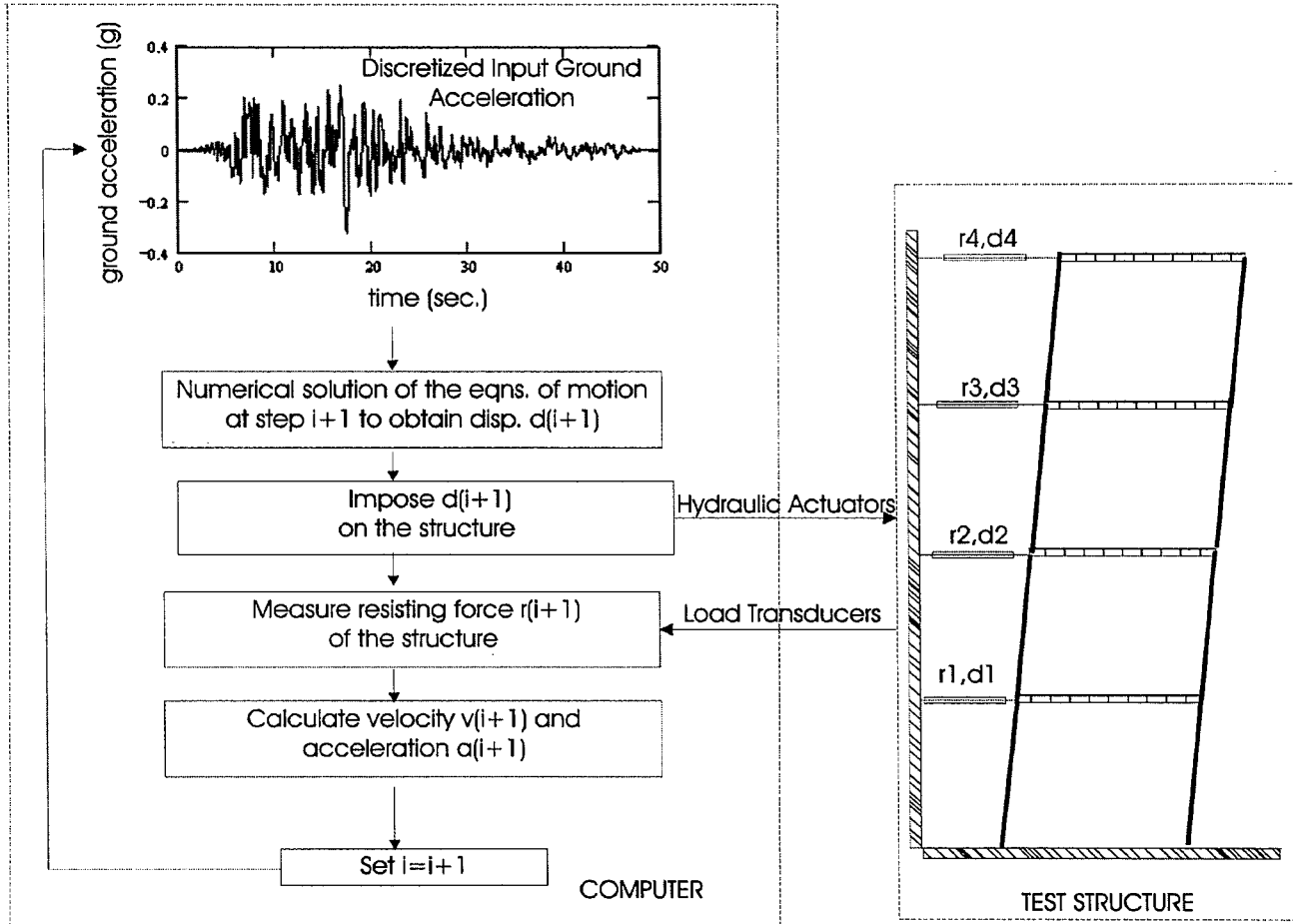
Figure 2.1   Conventional PSD Method Experimental Scheme
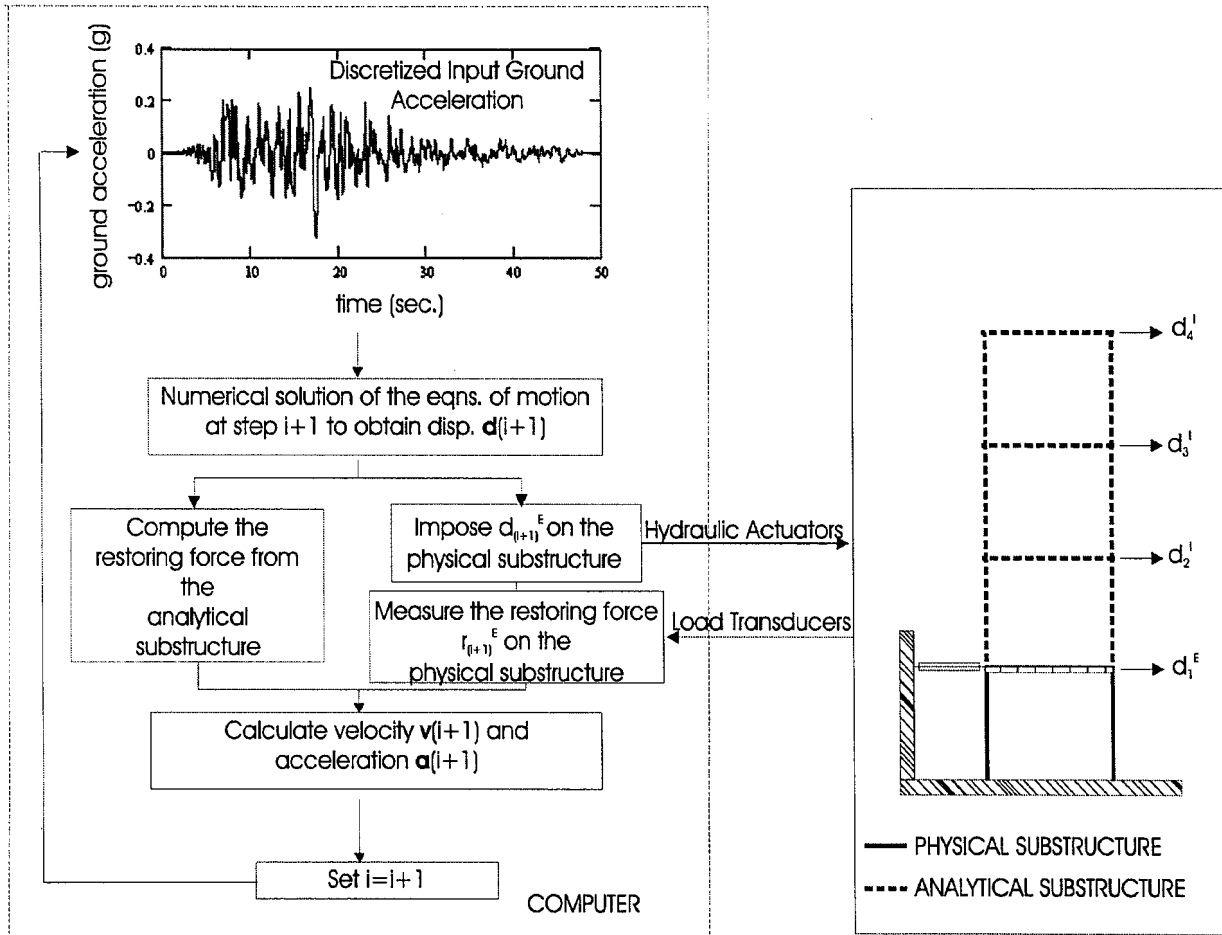
Figure 2.2 Substructure PSD Method Experimental Scheme
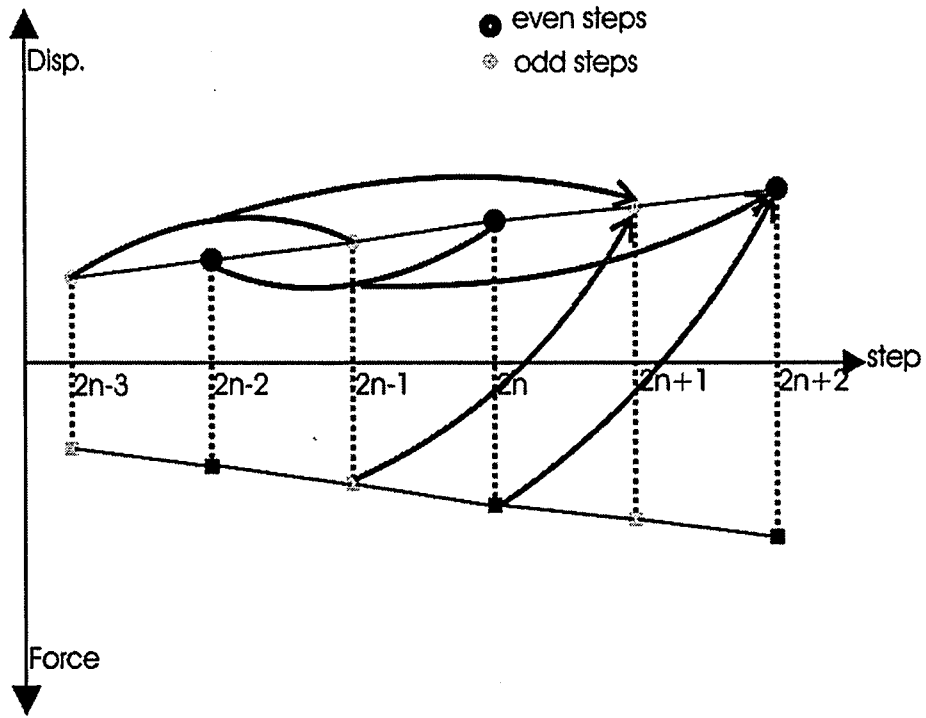
Figure 2.3   Staggered Integration (Nakashima et al., 1992)
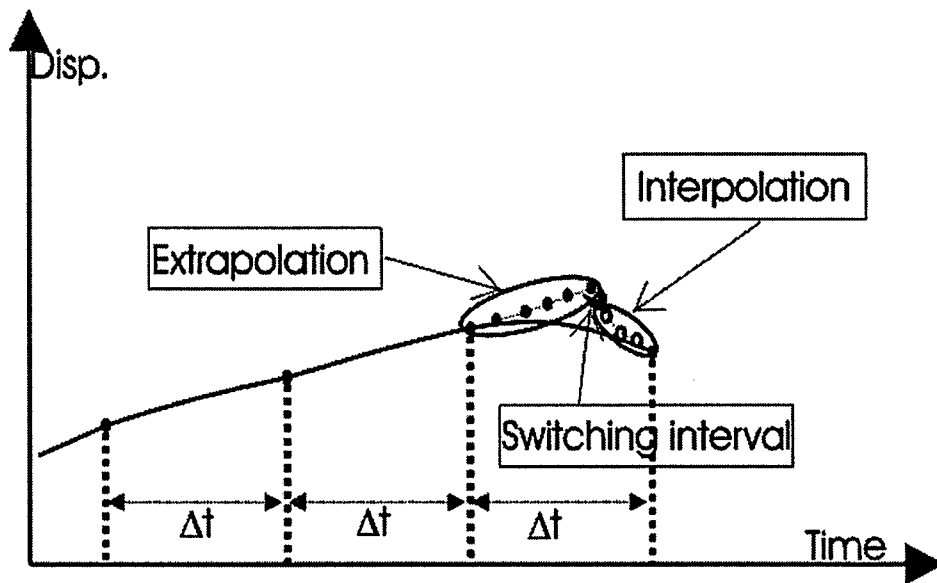
Figure 2.4   Velocity change in interval where extrapolation switches to interpolation
(Nakashima and Masaoka, 1999)

22

Chapter 3 Theoretical Background

3.0   General

This chapter presents background information about numerical integration algorithms for PSD testing. After a brief introduction to the numerical integration algorithms, linear and nonlinear stability aspects are presented. Derivations and detailed explanations are provided for three numerical integration algorithms that are investigated in this study. Information about a filter employed in a newly proposed real-time testing algorithm is also presented.

3.1   Numerical Integration Methods

In most numerical solutions of transient continuum mechanics or structural problems, the governing partial differential equations are first discretized in space. This procedure is called semidiscretization, and it reduces the problem to a system of ordinary differential equations (ODE) in time, which in turn must be integrated to complete the solution process.

The most popular methods for integrating the resulting ODE's are direct integration methods. In a direct integration method the time duration of interest is divided into steps and the solution is sequentially computed at each time step. Direct integration methods are a viable means to solve nonlinear problems where modal analysis procedures are not applicable.

Direct integration methods can be classified into two basic categories, namely: explicit and implicit methods. The explicit methods allow the displacements for the next time step to be determined from the accelerations, velocities and displacements at the current time step. Since only simple vector operations are required, the computational effort needed at each time step is small, and as a result their implementation into a computer program is relatively easy. Explicit algorithms are however only conditionally stable. The time step size is restricted by numerical stability requirements, which may result in a time increment much smaller than that needed for accuracy, thus increasing the cost of the explicit method.

In implicit methods, the displacements at the next time step for multi degree of freedom systems are determined by solving a system of equations. For nonlinear structures these equations are nonlinear and require, in many cases, iterative solutions of linear equation systems (equilibrium iterations) within each time step. As a result, implicit algorithms require a much greater computational effort at each time step and are more difficult to implement and to use than explicit algorithms. However, they can be made unconditionally stable so that in many cases the time step is restricted in size only by accuracy requirements, and therefore relatively large time steps can be used.

In the PSD test method, the equations of motion for an idealized structure can be solved using either explicit or implicit direct step-by-step integration methods. Equation (3.1) expresses the equations of motion:

$$\mathbf{M}\ddot{u}(t) + \mathbf{C}\dot{u}(t) + \mathbf{r}(t) = \mathbf{P}(t) \qquad (3.1)$$

where, $\mathbf{M}$, $\mathbf{C}$ are the mass and damping matrices, $\mathbf{P}(t)$ is the external load vector, $\mathbf{r}(t)$ is the restoring force vector, and $\dot{\mathbf{u}}(t), \ddot{\mathbf{u}}(t)$ are the nodal velocity and acceleration vectors, respectively. The restoring force $\mathbf{r}(t)$ is measured at a specified target displacement corresponding to the applied load $\mathbf{P}(t)$ and state of the structure. In the PSD test method $\mathbf{M}$ and $\mathbf{C}$ are analytically defined, unless the test is performed in real-time when there are inertia and damping forces that become part of the measured restoring force.

3.1.1 Stability Analysis

Stability of an integration method implies that the initial conditions for the equations of motions must not be artificially amplified over a large number of time steps. Stability also implies that any errors in the displacements, velocities, or accelerations at time t due to round off in the computer do not grow in the integration (Bathe and Wilson, 1976).

Bathe and Wilson (1976) state that an integration method is unconditionally stable if the solution for any initial conditions does not grow without any bound for any time step Δt, in particular when $\dfrac{\Delta t}{T_n}$ is large, where T_n is the natural period of the structure. The method is only conditionally stable if the above only holds provided that $\dfrac{\Delta t}{T_n}$ is smaller than a certain value, usually called the stability limit.

The procedure to determine the stability of an integration scheme can be summarized as follows:

(1) Establish a recursive relationship, (since the behavior of the numerical solution for arbitrary initial conditions is examined, no load is specified) where,

$$\hat{X}_{t+n\Delta t} = A^n \hat{X}_t$$ (3.2)

$\hat{X}_{t+n\Delta t}, \hat{X}_t$: vectors of solution quantities (e.g., displacements, velocities)

A^n : integration approximation matrix

(2) Perform spectral decomposition of the integration matrix A^n.

$$A^n = PJ^nP^{-1}$$ (3.3)

P : matrix of eigenvectors of A^n.

J^n : Jordan form of A^n with eigenvalues λ_i of A^n on its diagonal.

(3) Evaluate the spectral radius of A^n as:

$$\rho(A^n) = \max|\lambda_i| \; ; \qquad i = 1,2...$$ (3.4)

The stability criterion is based on the values of $\rho(A^n)$. J^n is bounded for $n \rightarrow \infty$, therefore the integration scheme is stable, if and only if when $\rho(A^n) \leq 1$.

3.1.2 Nonlinear Stability Analysis

Analytical techniques for evaluating the stability and accuracy of numerical integration methods in solving linear differential equations have been well established as explained above.

The stability and accuracy properties of numerical integration methods in solving nonlinear differential equations are not very well understood due to the lack of an

26

analytical evaluation technique (Shing and Mahin, 1984). These properties were usually

evaluated via numerical experiments, which sometimes leads to contradictory results.

As explained by Shing and Mahin (1984), it is possible that unconditionally stable

implicit methods can become unstable when applied to nonlinear problems with large

integration time intervals. The explanation is twofold: first, solving a nonlinear equation

by means of an implicit integration method requires an approximate solution procedure,

such as iterative correction. The additional errors introduced by an approximate solution

procedure will affect the stability and accuracy of the solution. Secondly, a nonlinear

solution can be unstable because of the spurious energy growth, which may occur in

numerical solutions of nonlinear equations.

Since explicit integration methods can provide a direct solution for a nonlinear

equation, with no iterations involved, there are no problems associated with an

approximate solution procedure.

Disregarding the energy effects, the stability and accuracy characteristics of the

explicit methods for linear systems are locally valid for nonlinear systems by the fact that

a nonlinear system can be considered as a piecewise linear system, in which the tangent

stiffness will dictate the numerical characteristics. This implies that the size of the time

step Δt selected for a linear system will remain conservative if the system becomes

nonlinear and the nonlinearity is the softening type. The opposite will be true for a

hardening system.

3.2 PSD Testing Algorithm: Newmark Explicit Method

In 1959, N.M. Newmark developed a family of direct integration methods based on the following equations:

$$\dot{u}_{i+1} = \dot{u}_i + (1-\gamma)\Delta t \ddot{u}_i + \gamma \Delta t \ddot{u}_{i+1} \tag{3.5}$$

$$u_{i+1} = u_i + \Delta t \dot{u}_i + (0.5 - \beta)(\Delta t)^2 \ddot{u}_i + \beta(\Delta t)^2 \ddot{u}_{i+1} \tag{3.6}$$

The parameters β and γ define the variation of acceleration over a time step and determine the stability and accuracy characteristics of the method. Typically a value of $\frac{1}{2}$ is used for γ, with β ranging from $\frac{1}{6}$ to $\frac{1}{4}$. When $\gamma = \frac{1}{2}$ and $\beta = \frac{1}{4}$ the method is an implicit integration method with the acceleration constant over the integration step (this method is often referred to as constant average acceleration). For $\gamma = \frac{1}{2}$ and $\beta = \frac{1}{6}$ the method is again an implicit one but the acceleration varies linearly over the time step, and for $\gamma = \frac{1}{2}$ and $\beta = 0$ the method becomes an explicit method.

Newmark's method is stable when

$$\frac{\Delta t}{T_n} \leq \frac{1}{\pi\sqrt{2}} * \frac{1}{\sqrt{\gamma - 2\beta}} \tag{3.7}$$

For $\gamma = \frac{1}{2}$ and $\beta = \frac{1}{4}$ this condition becomes $\frac{\Delta t}{T_n} \leq \infty$; which indicates that the constant average acceleration method is an unconditionally stable algorithm. For

$\gamma = \frac{1}{2}$ and $\beta = \frac{1}{6}$ this condition becomes $\frac{\Delta t}{T_n} \leq 0.551$; which indicates that the linear

acceleration algorithm stable if $\frac{\Delta t}{T_n} \leq 0.551$. Finally, for $\gamma = \frac{1}{2}$ and $\beta = 0$ this condition

becomes $\frac{\Delta t}{T_n} \leq \frac{1}{\pi}$. Therefore, the Newmark Explicit method is stable only if $\frac{\Delta t}{T_n} \leq \frac{1}{\pi}$ or

$\omega_n * \Delta t \leq 2$, where ω_n is the highest natural frequency.

If γ and β set equal to 0.5 and 0, respectively, Equations (3.5) and (3.6) become for

an MDOF system:

$$\mathbf{v}_{i+1} = \mathbf{v}_i + 0.5\Delta t \mathbf{a}_i + 0.5\Delta t \mathbf{a}_{i+1} \tag{3.8}$$

$$\mathbf{d}_{i+1} = \mathbf{d}_i + \Delta t \mathbf{v}_i + 0.5(\Delta t)^2 \mathbf{a}_i \tag{3.9}$$

From Equation (3.9) the displacements $\mathbf{d}_{i+1}$ at the time t_{i+1} are related to the

displacements $(\mathbf{d}_i)$, velocities $(\mathbf{v}_i)$ and accelerations $(\mathbf{a}_i)$ from the current time step t_i,

while the velocities $\mathbf{v}_{i+1}$ from Equation (3.8) are related to $\mathbf{v}_i$ and $\mathbf{a}_i$ at the time t_i as

well as accelerations $\mathbf{a}_{i+1}$ at the time t_{i+1}.

Considering the equation of motion at time t_{i+1},

$$\mathbf{M}\mathbf{a}_{i+1} + \mathbf{C}\mathbf{v}_{i+1} + \mathbf{r}_{i+1} = \mathbf{P}_{i+1} \tag{3.10}$$

and upon substituting for $\mathbf{v}_{i+1}$ from Equation (3.8) the equations of motion become:

$$(\mathbf{M} + 0.5\Delta t \mathbf{C})\mathbf{a}_{i+1} = (\mathbf{P}_{i+1} - \mathbf{r}_{i+1} - \mathbf{C}\mathbf{v}_i - 0.5\Delta t \mathbf{C}\mathbf{a}_i) \tag{3.11}$$

Solving for the accelerations $\mathbf{a}_{i+1}$:

$$\mathbf{a}_{i+1} = (\mathbf{M} + 0.5\Delta t \mathbf{C})^{-1} (\mathbf{P}_{i+1} - \mathbf{r}_{i+1} - \mathbf{C}\mathbf{v}_i - 0.5\Delta t \mathbf{C}\mathbf{a}_i) \qquad (3.12)$$

Equations (3.8), (3.9) and (3.12) are used to formulate the PSD test method based on the Newmark Explicit Algorithm.

The test method is summarized in Figure 3.1 and described below:

(1) The target displacements $\mathbf{d}_{i+1}$ for the next time step are calculated from Equation (3.9).

(2) These target displacements are imposed to the test structure and the restoring forces $\mathbf{r}_{i+1}$ are measured.

(3) The accelerations $\mathbf{a}_{i+1}$ and velocities $\mathbf{v}_{i+1}$ for this new time step are computed from Equations (3.12) and (3.8), respectively.

(4) The process is repeated (i.e., steps (1) through (3)) for each subsequent time step.

3.3   PSD Testing Algorithm: Alpha Method with Fixed Number of Iterations

This method was developed based on the Hilber α-method (Hilber et al., 1977), where:

$$\mathbf{d}_{i+1} = \mathbf{d}_i + \Delta t \mathbf{v}_i + (\Delta t)^2 [(0.5 - \beta)\mathbf{a}_i + \beta \mathbf{a}_{i+1}] \qquad (3.13)$$

$$\mathbf{v}_{i+1} = \mathbf{v}_i + \Delta t [(1 - \gamma)\mathbf{a}_i + \gamma \mathbf{a}_{i+1}] \qquad (3.14)$$

$$\mathbf{M}\mathbf{a}_{i+1} + (1 + \alpha)\mathbf{C}\mathbf{v}_{i+1} - \alpha\mathbf{C}\mathbf{v}_i + (1 + \alpha)\mathbf{r}_{i+1} - \alpha\mathbf{r}_i = (1 + \alpha)\mathbf{P}_{i+1} - \alpha\mathbf{P}_i \qquad (3.15)$$

30

α, β and γ are integration constants. To attain unconditional stability and a favorable energy-dissipation property, it is recommended (Hilber et al., 1977) to use $\beta = (1-\alpha)^2 / 4$ and $\gamma = 1/2 - \alpha$, with $-1/3 \le \alpha \le 0$.

If $\mathbf{v}_{i+1}$ from Equation (3.14) is substituted into the equilibrium equation (Equation (3.15)) the accelerations $\mathbf{a}_{i+1}$ at time t_{i+1} (i.e., at the end of current time step) are obtained, where:

$$\mathbf{a}_{i+1} = (\mathbf{M} + (1+\alpha)\mathbf{C}\gamma)^{-1}[(1+\alpha)\mathbf{P}_{i+1} - \alpha\mathbf{P}_i - \mathbf{C}\mathbf{v}_i - (1+\alpha)\mathbf{C}\Delta t\mathbf{a}_i$$

$$+ (1+\alpha)\mathbf{C}\Delta t\gamma\mathbf{a}_i - (1+\alpha)\mathbf{r}_{i+1} + \alpha\mathbf{r}_i] \qquad (3.16)$$

Defining $\overline{\mathbf{M}} = (\mathbf{M} + (1+\alpha)\gamma\mathbf{C})$ Equation (3.16) becomes:

$$\mathbf{a}_{i+1} = \overline{\mathbf{M}}^{-1}[(1+\alpha)\mathbf{P}_{i+1} - \alpha\mathbf{P}_i - \mathbf{C}\mathbf{v}_i - (1+\alpha)(1-\gamma)\mathbf{C}\Delta t\mathbf{a}_i - (1+\alpha)\mathbf{r}_{i+1} + \alpha\mathbf{r}_i] \qquad (3.17)$$

The displacements $\mathbf{d}_{i+1}$ from Equation (3.13) are therefore equal to:

$$\mathbf{d}_{i+1} = \mathbf{d}_i + \Delta t\mathbf{v}_i + (\Delta t)^2(0.5 - \beta)\mathbf{a}_i +$$

$$(\Delta t)^2 \beta\overline{\mathbf{M}}^{-1}[(1+\alpha)\mathbf{P}_{i+1} - \alpha\mathbf{P}_i - \mathbf{C}\mathbf{v}_i - (1+\alpha)(1-\gamma)\mathbf{C}\Delta t\mathbf{a}_i - (1+\alpha)\mathbf{r}_{i+1} + \alpha\mathbf{r}_i] \qquad (3.18)$$

To calculate the displacements at the next time step $(i+1)$, the current time step information $(\mathbf{d}_i, \mathbf{v}_i, \mathbf{a}_i, \mathbf{P}_i)$ and next time step information $(\mathbf{r}_{i+1}, \mathbf{P}_{i+1})$ need to be known. Externally applied loads ($\mathbf{P}$) are user-defined and therefore are known at all times. However, $\mathbf{r}_{i+1}$ depends on $\mathbf{d}_{i+1}$. The displacement responses have to be calculated iteratively if the exact stiffness of the analyzed structure is not explicitly known.

31

Predictor displacements $\hat{\mathbf{d}}_{i+1}$ can be defined by only using the explicit terms in Equation (3.18):

$$\hat{\mathbf{d}}_{i+1} = \mathbf{d}_i + \Delta t \mathbf{v}_i + (\Delta t)^2 (0.5 - \beta)\mathbf{a}_i +$$

$$(\Delta t)^2 \beta \overline{\mathbf{M}}^{-1}[(1+\alpha)\mathbf{P}_{i+1} - \alpha \mathbf{P}_i - \mathbf{C}\mathbf{v}_i - (1+\alpha)(1-\gamma)\mathbf{C}\Delta t \mathbf{a}_i + \alpha \mathbf{r}_i] \tag{3.19}$$

The next time step displacements can now be written in terms of the predictor displacements and the remaining implicit terms:

$$\mathbf{d}_{i+1} = \hat{\mathbf{d}}_{i+1} - (\Delta t)^2 \beta \overline{\mathbf{M}}^{-1}(1+\alpha)\mathbf{r}_{i+1} \tag{3.20}$$

When both sides of Equation (3.20) are multiplied by $\overline{\mathbf{M}}$:

$$\overline{\mathbf{M}}\mathbf{d}_{i+1} = \overline{\mathbf{M}}\hat{\mathbf{d}}_{i+1} - (\Delta t)^2 \beta(1+\alpha)\mathbf{r}_{i+1} \tag{3.21}$$

Since Equation (3.20) is implicit, iterations will need to be performed in each time step. In the kth iteration performed during time step (i+1), Equation (3.21) becomes:

$$\overline{\mathbf{M}}\mathbf{d}_{i+1}^{(k)} = \overline{\mathbf{M}}\hat{\mathbf{d}}_{i+1} - (\Delta t)^2 \beta(1+\alpha)\mathbf{r}_{i+1}^{(k)} + \overline{\mathbf{M}}\mathbf{e}_{i+1}^{R(k)} \tag{3.22}$$

where $\mathbf{e}_{i+1}^{R(k)}$ is the vector of convergence error, and is defined later.

Subtracting Equation (3.21) from Equation (3.22) leads to a relationship between the displacement increment $\Delta \mathbf{d}_{i+1}^{(k)}$ and the restoring force increment $\Delta \mathbf{r}_{i+1}^{k}$ and error $\mathbf{e}_{i+1}^{R(k)}$ for iteration k.

$$\overline{\mathbf{M}}\Delta \mathbf{d}_{i+1}^{(k)} = -(\Delta t)^2 \beta(1+\alpha)\Delta \mathbf{r}_{i+1}^{(k)} - \overline{\mathbf{M}}\mathbf{e}_{i+1}^{R(k)} \tag{3.23}$$

If the secant stiffness $\mathbf{K}_{sec}$ for the displacement increment is known, then a relationship between the restoring force and displacement increments can be established:

$$\Delta \mathbf{r}_{i+1}^{(k)} = \mathbf{K}_{sec} \Delta \mathbf{d}_{i+1}^{(k)} \tag{3.24}$$

Since the secant stiffness is not known in a PSD test, the initial stiffness $\mathbf{K}$ is used as $\mathbf{K}_{sec}$, and Equation (3.24) becomes:

$$\Delta \mathbf{r}_{i+1}^{(k)} = \mathbf{K} \Delta \mathbf{d}_{i+1}^{(k)} \tag{3.25}$$

Substituting this relationship into Equation (3.23):

$$[\overline{\mathbf{M}} + (\Delta t)^2 \beta(1+\alpha)\mathbf{K}]\Delta \mathbf{d}_{i+1}^{(k)} = -\overline{\mathbf{M}} \mathbf{e}_{i+1}^{R(k)} \tag{3.26}$$

Defining $\mathbf{K}^* = \overline{\mathbf{M}} + (\Delta t)^2 \beta(1+\alpha)\mathbf{K}$ Equation (3.26) becomes:

$$\mathbf{K}^* \Delta \mathbf{d}_{i+1}^{(k)} = -\overline{\mathbf{M}} \mathbf{e}_{i+1}^{R(k)} \tag{3.27}$$

Using the equations derived above, Shing et al. (2002) developed an integration scheme for real-time PSD testing by introducing an iterative solution method that does not require slowing down or stopping the actuators at the end of a time step. The method is illustrated in Figure 3.2, where first the predictor displacement $\hat{\mathbf{d}}_{i+1}$ for the next target displacement is computed from Equation (3.19). The algorithm proceeds with iteration steps. Using Equation (3.20) (Eq.1 in Figure 3.2) the next step displacement $\mathbf{d}_{i+1}$ is computed. For the first iteration, in Eq. 1 the corrected restoring force (See Eq. 4 in Figure 3.2) during the last iteration of the current time step is used as $\mathbf{r}_{i+1}$. $\mathbf{r}_{i+1}^m$ in Figure 3.2 is the measured restoring force.

A conventional Newton iteration method to eliminate the convergence error would lead to decreasing incremental corrections as the solution converges to the exact values. This is not desirable for real-time testing, because either the actuators have to slow down or signals have to be sent to the actuators controllers at an increasing speed. To have a more or less uniform incremental correction in each iteration step, Shing at al. (2002) developed a scheme involving a fixed number of iterations, where computed target displacement $\mathbf{d}_{i+1}^{c(k+1)}$ for iteration k is:

$$\mathbf{d}_{i+1}^{c(k+1)} = \mathbf{d}_{i+1}^{c(k)} + \frac{(\mathbf{d}_{i+1} - \mathbf{d}_{i+1}^{m(k)})}{n-k} \tag{3.28}$$

In Equation (3.28) (Eq.2 in Figure 3.2) n is the total number of iterations, k is the iteration index, m designates a measured quantity and c is for calculated target command quantities.

In the second term of Equation (3.28), $(n-k)$ is in the denominator, where n is fixed and k increases as the iteration proceeds. That leads to a more or less uniform incremental correction for the command displacements $\mathbf{d}_{i+1}^{c(k+1)}$. The second term of Equation (3.28) has the measured displacements $\mathbf{d}_{i+1}^{m(k)}$ in the numerator; thereby this equation is capable of correcting for any time lag in the actuator response by overshooting the command displacement for the next correction.

By rearranging Equation (3.22), the convergence errors after the $(n-1)^{th}$ iteration can be calculated as follows:

$$\mathbf{e}_{i+1}^{R(n-2)} = \mathbf{d}_{i+1}^{m(n-2)} - \hat{\mathbf{d}}_{i+1} + (\Delta t)^2 \beta(1+\alpha)\overline{\mathbf{M}}^{-1}\mathbf{r}_{i+1}^{m(n-2)} \tag{3.29}$$

Using the displacement increments corresponding to these convergence errors (Equation (3.27)), the displacements are updated:

$$\mathbf{d}_{i+1} = \mathbf{d}_{i+1}^{m(n-2)} - \mathbf{K}^{*-1}\overline{\mathbf{M}}\mathbf{e}_{i+1}^{R(n-2)} \qquad (3.30)$$

Equation (3.30) appears as Eq. 3 in Figure 3.2. Establishing the relationship between the displacement and restoring force increments using the initial stiffness as explained above (Equation (3.25)), the restoring forces are updated; where:

$$\mathbf{r}_{i+1} = \mathbf{r}_{i+1}^{m(n-2)} + \underline{\mathbf{K}\mathbf{K}}^{*-1}\overline{\mathbf{M}}\mathbf{e}_{i+1}^{R(n-2)} \qquad (3.31)$$

By means of these equilibrium corrections performed to eliminate the convergence errors the displacement and restoring force values are made available for the calculation of the predictor displacement for the next time step while the actuators are imposing the displacement during the last iteration substep n. As a result, the structure continues to be loaded in real time without any pause. In the Alpha Method with a Fixed Number of Iterations, the computational effort for each iteration is rather small. As a result, the actuators can receive uninterrupted commands at fixed time intervals and a continuous actuator motion with a more or less constant speed is provided.

The Alpha Method is an unconditionally stable implicit scheme, which is an advantage when a large number of DOFs exist in the test. The correction scheme provided at the end of the time step is proven to be effective in eliminating spurious higher-mode response that could otherwise be introduced by experimental errors (Shing et al., 1991).

3.4 PSD Testing Algorithm: Newmark Explicit Real-Time

As explained in Chapter 2, the first real-time PSD test was performed by Nakashima et al. (1992) using a modified central difference algorithm with staggered integration involving the even and odd time steps. Since the test system used by Nakashima et al. was devised with the electronic technologies of late 1980's, the integration time interval had to be relatively large. As a result, only an SDOF system with the fundamental frequency at most about 1 Hz could be tested.

In this study, the staggered integration idea was applied to the Newmark Explicit integration scheme for real-time PSD testing. No stability problem was observed in numerical simulations of the method applied towards PSD-testing of frames without VE dampers. However the method was not stable for rate-dependent real-time PSD test simulations. This stability problem was solved by employing Alpha-Beta Tracker filter (Grewal and Andrews, 1993; Cunningham, 1992). In Chapter 3 the steps of the algorithm and the filter will be presented. The reason for the instability and the contribution of the filter to the solution will be explained in detail in Chapter 6, where rate-dependent restoring force effects will be presented.

In the staggered integration scheme the displacements, velocities and accelerations of the first three time steps (i=0,1,2) are numerically calculated using the standard Newmark Explicit algorithm. These results then become the initial conditions for the staggered integration.

Equations (3.8), (3.9) and (3.12) of the standard Newmark Explicit algorithm are modified resulting in the following staggered integration algorithm procedure:

For $i = 3...N$

(1) Determine target displacements for the next time step i :

$$\mathbf{d}_i = \mathbf{d}_{i-2} + \Delta T \mathbf{v}_{i-2} + 0.5(\Delta T)^2 \mathbf{a}_{i-2} \qquad (3.32)$$

(2) Impose next step displacements and measure the resisting forces $\mathbf{r}_i$

(3) Determine the accelerations for the next time step i :

$$\mathbf{a}_i = [\mathbf{M} + 0.5\Delta T \mathbf{C}]^{-1}(\mathbf{P}_i - \mathbf{r}_i - \mathbf{C}\mathbf{v}_{i-2} - 0.5\Delta T \mathbf{C}\mathbf{a}_{i-2}) \qquad (3.33)$$

(4) Determine velocities for the next time step i :

$$\mathbf{v}_i = \mathbf{v}_{i-2} + 0.5\Delta T \mathbf{a}_{i-2} + 0.5\Delta T \mathbf{a}_i \qquad (3.34)$$

(5) Set $i = i + 1$ (Go to Step (1))

Here i is the time step counter, N is the total number of time steps and $\Delta T = 2\Delta t$, where Δt is the time step size.

As stated above, the solutions associated with time steps i=0, 1 and 2 are used as initial conditions. From Equation (3.32) the displacements at time steps i=3 and 4 can be calculated right away. Once the actuators impose the displacement at time step 3 and measure the restoring force, the acceleration and velocity at time step 3 are computed and, with this information the displacement at time step 5 can be determined. Note that while these operations are taking place, the actuators are not waiting but leading the structure to the already known displacement for time step 4. By repeating this procedure the structure is loaded without any pause between time steps.

No systematic stability analysis was performed for the proposed scheme, however since the time step is twice as large for integration process, $\omega_n \Delta t \leq 1$ is expected to be valid for cases involving rate-independent materials.

For the rate-dependent simulations, where the apparent velocity, (obtained as the ratio of displacement increment over time step size) is used to calculate the restoring force developed in the VE dampers, the above staggered integration scheme was observed to be numerically unstable.

This problem has been overcome by employing an "Alpha –Beta Tracker Filter" to filter out artificially-induced high frequencies. The method is described next, with simulation results given in Chapter 5.

3.4.1 The Alpha-Beta Tracker (Position and Rate Estimation)

The Alpha-Beta tracker is an observer, which estimates the range x and the range rates of a target on the basis of a sequence y_i, $i = 1,2...$, of measurements. It has been used in the radar industry. The observer has a filter structure similar to that of a Kalman filter. Below is a description of the Alpha-Beta Tracker formulation:

$$x = \frac{c}{2} \Delta t_c \qquad (3.35)$$

where c is the velocity of light, and Δt_c is the actual time for the signal to reach the target and return back to the radar. Suppose Δt is the measured value of Δt_c. Denoting the measured value of range by y.

$$y = \frac{c}{2}\Delta t = \frac{c}{2}(\Delta t_c + \xi) = x + v \qquad (3.36)$$

In Equation (3.36) y is the measured signal, x is the original signal and v is the noise in the signal.

Suppose that x_k is the current range (at time k), and s_k is the current range rate (at time k). Using the following definitions:

$\hat{x}_{k(+)}$ - estimate of x_k based on all measurements up to and including y_k

$\hat{s}_{k(+)}$ - estimate of s_k based on all measurements up to and including y_k

$\hat{x}_{k(-)}$ - estimate of x_k based on all measurements up to and including y_{k-1}

And designating $\hat{x}_{k(-)}$ as a predicted or *a priori* estimate of $\hat{x}_k$, and $\hat{x}_{k(+)}$ as an updated or *a posteriori* estimate of $\hat{x}_k$, with a priori and a posteriori estimate related by:

$$\hat{x}_{k(-)} = \hat{x}_{k-1(+)} + T\hat{s}_{k-1(+)} \qquad (3.37)$$

In Equation (3.37) T is the interval between the pulses.

The residual between the measured signal and priori estimate at time k, $(y_k - \hat{x}_{k(-)})$ is the basis for which a correction is to be made:

$$\hat{x}_{k(+)} = \hat{x}_{k(-)} + \alpha(y_k - \hat{x}_{k(-)}) \qquad (3.38)$$

where α is the gain for the correction. The residual for the range rate s is given by Equation (3.39)

$$\Delta \hat{s}_k = \frac{1}{T}(y_k - \hat{x}_{k(-)}) \qquad (3.39)$$

Further the estimate for s_k (i.e., a posteriori estimate of s_k) is obtained from:

$$\hat{s}_{k(+)} = \hat{s}_{k-1(+)} + \frac{\beta}{T} * (y_k - \hat{x}_{k(-)}) \qquad (3.40)$$

where β is the gain for velocity correction. Typically β is chosen in the interval of 0.2 to 0.4 and $\alpha = 2\sqrt{\beta} - \beta$. Further information can be found in references (Grewal and Andrews, 1993; Cunningham, 1992).

3.4.2 Implementation of the Alpha-Beta Tracker Filter

The filter is used to remove the noise from the calculated displacement signals of the Newmark Explicit Real-Time PSD test method with staggered integration. The calculated displacements of the first three steps are considered to be corrected values since they are used as initial conditions.

The algorithm is shown schematically in Figure 3.3. The details are given below.

For $i = 3...N$

- Assign initial slope estimates s_{i-1}

(1) Calculate the next time step displacements using the corrected displacements from previous time steps:

$$\mathbf{d}_{noise\_i} = \mathbf{d}_{corrected\_i-2} + \Delta T \mathbf{v}_{i-2} + 0.5(\Delta T)^2 \mathbf{a}_{i-2} \qquad (3.41)$$

40

(2) Calculate the predicted displacements:

$$\mathbf{d}_{predicted\_i} = \mathbf{d}_{corrected\_i-1} + \Delta t \mathbf{s}_{i-1} \tag{3.42}$$

(3) Calculate the corrected next time step displacements:

$$\mathbf{d}_{corrected\_i} = \mathbf{d}_{predicted\_i} + \alpha(\mathbf{d}_{noise\_i} - \mathbf{d}_{predicted\_i}) \tag{3.43}$$

(4) Update the slope estimates:

$$\mathbf{s}_i = \mathbf{s}_{i-1} + (\frac{\beta}{\Delta t})(\mathbf{d}_{noise\_i} - \mathbf{d}_{predicted\_i}) \tag{3.44}$$

(5) Impose the corrected next time step displacements

and measure the resisting forces $\mathbf{r}_i$.

(6) Calculate next time step accelerations:

$$\mathbf{a}_i = [\mathbf{M} + 0.5\Delta T\mathbf{C}]^{-1}(\mathbf{P}_i - \mathbf{r}_i - \mathbf{C}\mathbf{v}_{i-2} - 0.5\Delta T\mathbf{C}\mathbf{a}_{i-2}) \tag{3.45}$$

(7) Calculate next step velocities:

$$\mathbf{v}_i = \mathbf{v}_{i-2} + [0.5\Delta T]\mathbf{a}_{i-2} + [0.5\Delta T]\mathbf{a}_i \tag{3.46}$$

(8) Set $i = i+1$ (Go to Step (1))

$\mathbf{s}_{i-1}$ in the above algorithm when $i = 3$, (i.e., $\mathbf{s}_2$) is a vector of zeros.

- specify external loads $\mathbf{P}_{i+1}$
- compute next step displacements
  $$\mathbf{d}_{i+1}=\mathbf{d}_i+\Delta t\mathbf{v}_i+[0.5(\Delta t)^2]\mathbf{a}_i$$

$i=i+1$

- impose $\mathbf{d}_{i+1}$ to the structure
- measure restoring forces $\mathbf{r}_{i+1}$

calculate the accelerations and velocities:
- $\mathbf{a}_{i+1}=(\mathbf{M}+0.5\Delta t\mathbf{C})^{-1}[\mathbf{P}_{i+1}\text{-}\mathbf{r}_{i+1}\text{-}\mathbf{C}\mathbf{v}_i\text{-}0.5\Delta t\mathbf{C}\mathbf{a}_i]$
- $\mathbf{v}_{i+1}=\mathbf{v}_i+0.5\Delta t(\mathbf{a}_i+\mathbf{a}_{i+1})$
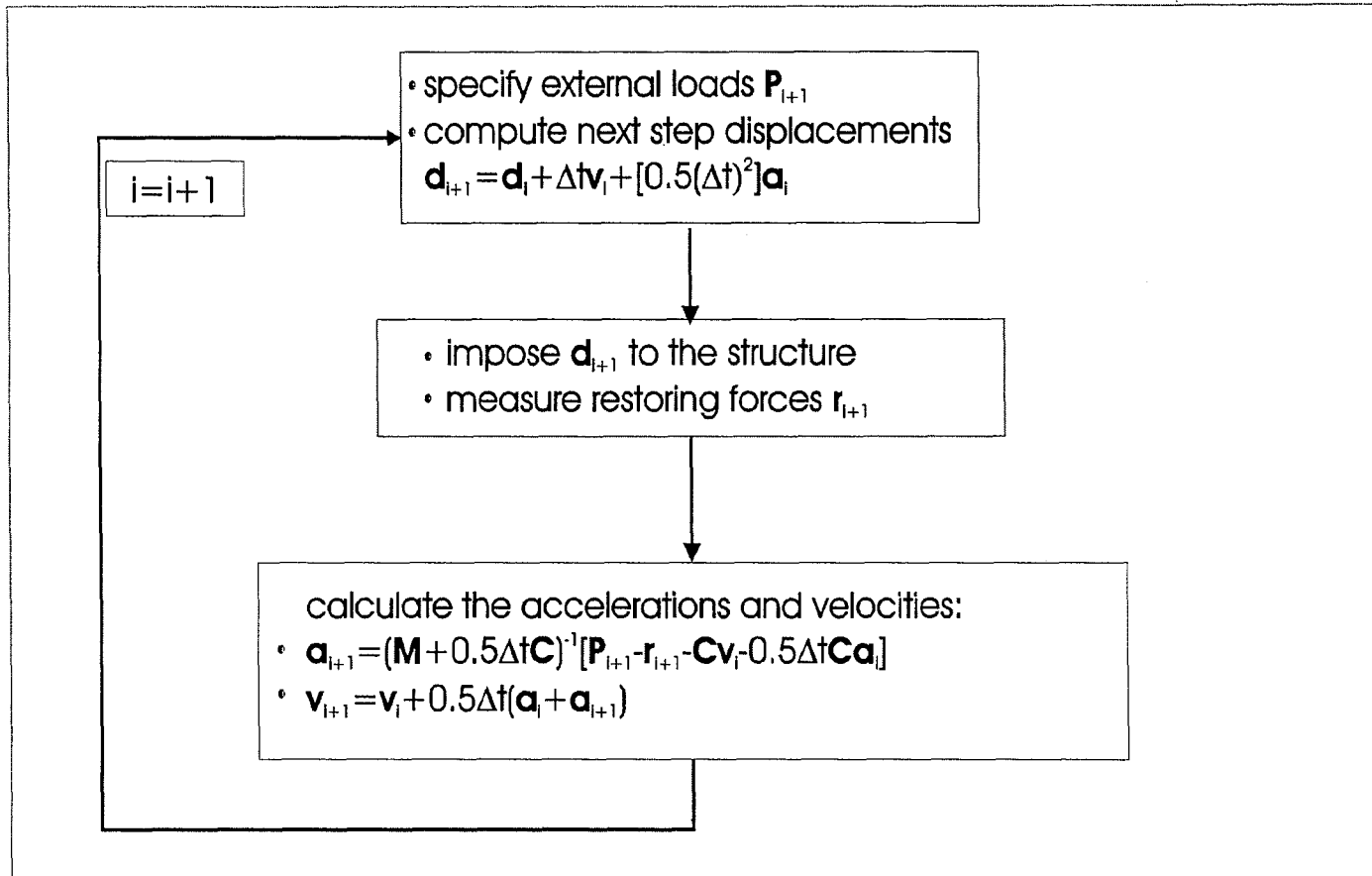
Figure 3.1   PSD Algorithm Based on Newmark Explicit Method

$k=0$ to $n-1$

$r^{m(0)}_{i+1}=r_i$

$d^{m(0)}_{i+1}=d_i$

$K^*=\overline{M}+\Delta t2\beta(1+\alpha)K$

$\overline{M}=M+(1+\alpha)\gamma\Delta tC$

$i=i+1$

-specify external load P_{i+1}

-compute predictor displacement

$\hat{d}_{i+1}=f(d_i,v_i,a_i,P_i,P_{i+1})$

$k=0$

$d_{i+1}=d^{m(n-2)}_{i+1}-K^{*-1}\overline{M}e^{R(n-2)}_{i+1}$ [Eq.3]

$r_{i+1}=r^{m(n-2)}_{i+1}-KK^{*-1}\overline{M}e^{R(n-2)}_{i+1}$ [Eq.4]

$d_{i+1}=\hat{d}_{i+1}-\Delta t^2\beta(1+\alpha)\overline{M}^{-1}r^{m(k)}_{i+1}$ [Eq.1]

$d^{c(k+1)}_{i+1}=d^{c(k)}_{i+1}+\dfrac{(d_{i+1}-d^{m(k)}_{i+1})}{n-k}$ [Eq.2]

-impose $d^{c(k+1)}_{i+1}$ to the structure

$k=k+1$

$e^{R(n-2)}_{i+1}=d^{m(n-2)}_{i+1}-\hat{d}_{i+1}+\Delta t^2\beta(1+\alpha)\overline{M}^{-1}r^{m(n-2)}_{i+1}$

-measure the displacement $d^{m(k+1)}_{i+1}$

-measure the restoring force $r^{m(k+1)}_{i+1}$
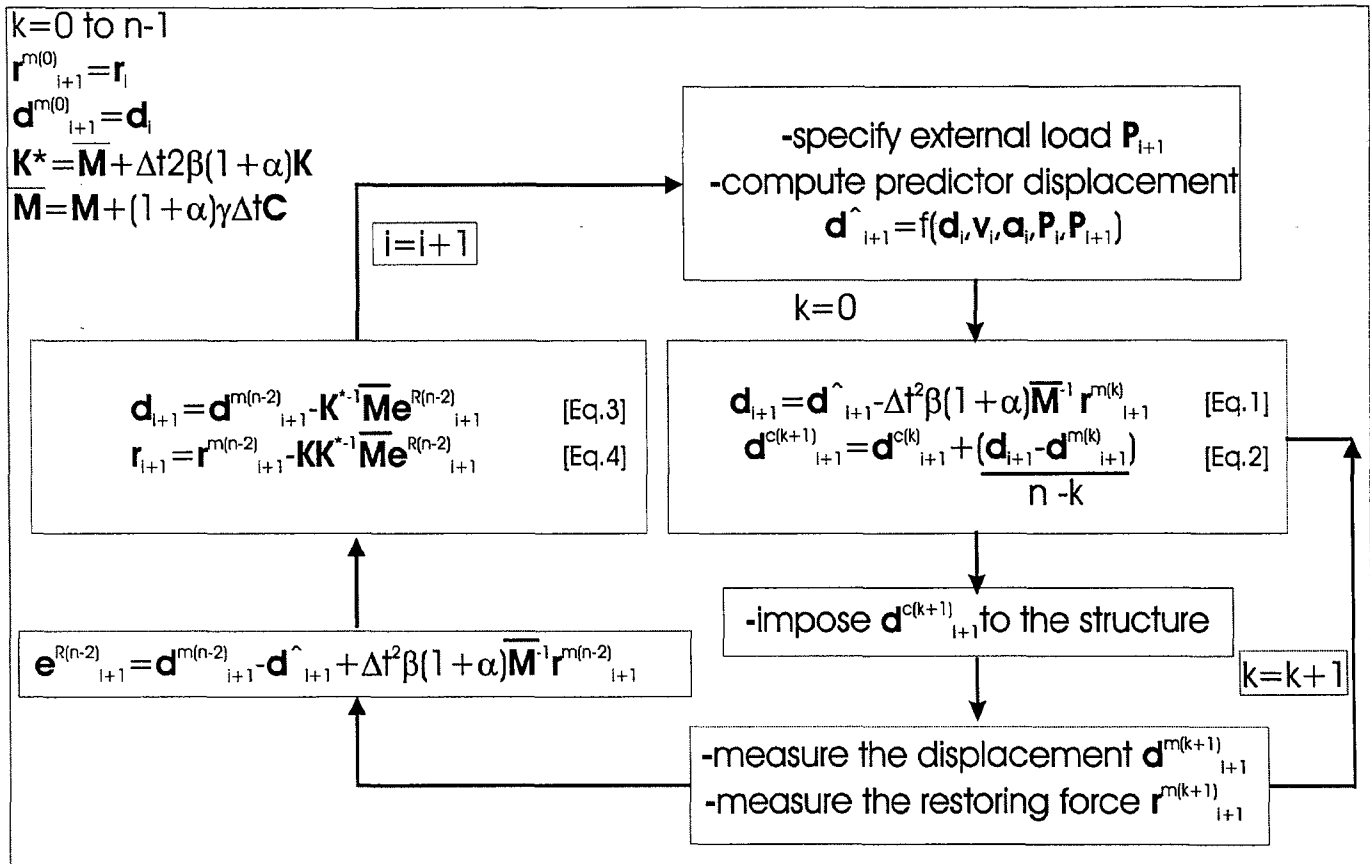
Figure 3.2   Real-Time PSD Algorithm Based on Alpha Method with a Fixed Number of Iterations

$\mathbf{d}_{noise\_I+2}=f(\mathbf{d}_{corrected\_I},\mathbf{v}_I,\mathbf{a}_I)$

$\mathbf{d}_{noise\_I+4}=f(\mathbf{d}_{corrected\_I+2},\mathbf{v}_{I+2},\mathbf{a}_{I+2})$

$\mathbf{d}_{noise\_I+3}=f(\mathbf{d}_{corrected\_I+1},\mathbf{v}_{i+1},\mathbf{a}_{i+1})$

$\mathbf{d}_{noise\_I+5}=f(\mathbf{d}_{corrected\_I+3},\mathbf{v}_{I+3},\mathbf{a}_{I+3})$

alpha-beta tracker filter (using $\mathbf{d}_{corrected\_I+1}$)

alpha-beta tracker filter (using $\mathbf{d}_{corrected\_I+3}$)

alpha-beta tracker filter (using $\mathbf{d}_{corrected\_I+2}$)

alpha-beta tracker filter (using $\mathbf{d}_{corrected\_I+4}$)

$\mathbf{d}_{corrected\_I+2}$

$\mathbf{d}_{corrected\_I+4}$

$\mathbf{d}_{corrected\_I+3}$

$\mathbf{d}_{corrected\_I+5}$

impose $\mathbf{d}_{corrected\_I+2}$ and measure $\mathbf{r}_{I+2}$

impose $\mathbf{d}_{corrected\_I+4}$ and measure $\mathbf{r}_{I+4}$

impose $\mathbf{d}_{corrected\_I+3}$ and measure $\mathbf{r}_{I+3}$

impose $\mathbf{d}_{corrected\_I+5}$ and measure $\mathbf{r}_{I+5}$

$\mathbf{a}_{I+2}=f(\mathbf{r}_{i+2},\mathbf{P}_{i+2},\mathbf{v}_I,\mathbf{a}_I)$
$\mathbf{V}_{I+2}=f(\mathbf{v}_I,\mathbf{a}_I,\mathbf{a}_{I+2})$

$\mathbf{a}_{i+3}=f(\mathbf{r}_{i+3},\mathbf{P}_{i+3},\mathbf{v}_{i+1},\mathbf{a}_{i+1})$
$\mathbf{V}_{I+3}=f(\mathbf{v}_{i+1},\mathbf{a}_{i+1},\mathbf{a}_{I+3})$

$\mathbf{a}_{I+4}=f(\mathbf{r}_{I+4},\mathbf{P}_{I+4},\mathbf{v}_{I+2},\mathbf{a}_{I+2})$
$\mathbf{V}_{I+4}=f(\mathbf{v}_{I+2},\mathbf{a}_{I+2},\mathbf{a}_{I+4})$

$\mathbf{a}_{I+5}=f(\mathbf{r}_{I+5},\mathbf{P}_{I+5},\mathbf{v}_{I+3},\mathbf{a}_{I+3})$
$\mathbf{V}_{I+5}=f(\mathbf{v}_{I+3},\mathbf{a}_{I+3},\mathbf{a}_{I+5})$

Figure 3.3   Real-Time PSD Algorithm based on Newmark Explicit Real Time Method

Chapter 4   Idealized MDOF Structure for PSD Test Simulations

4.0   General

This chapter presents the details of the moment resisting frames (MRFs), both with and without VE dampers, which have been used in the numerical simulations of real-time and conventional PSD tests, respectively. Information about the design of the frame and VE dampers is presented. The numerical integration scheme used to calculate the VE damper restoring forces in the simulations is explained.

4.1   Prototype and Scaled MRFs

PSD test simulations were performed on a scaled model of a prototype 4-story MRF. The prototype MRF consisted of wide flange beams with concrete filled steel tubular (CFT) columns (Herrera et al., 2003).

The prototype building was designed according to the International Building Code (IBC) 2000 provisions. It is intended for office use, and assumed to be located in Los Angeles, in soil type D. The equivalent static lateral load procedure outlined in IBC 2000 was used to design the building, where drift was found to control the design. The frame had 4 bays and 4 stories. The design and modeling details, with pushover and time-history analyses results can be found in Herrera et al. (2003).

The results of these analyses showed that MRF's with CFT columns designed in accordance with current U.S. seismic provisions are likely to perform adequately during an earthquake. To refine the design criteria and to calibrate the analytical models that

were developed, experiments were found to be necessary. For this purpose, an experimental study for construction and testing of a three-fifths scale model of the prototype frame was planned. Figure 4.1 shows the 2-bay, 4-story scaled test structure. Analyses were performed by Herrera (Herrera et al., 2003) to ensure that this test frame simulates the response of the prototype frame during the test. The MRF model used in the PSD test simulations was based on the scaled model shown in Figure 4.1.

4.2   Idealized Moment Resisting Frame

As explained in Chapter 2, in a PSD test the structure is first idealized as a discrete parameter system such that the governing equations of motion can be represented by a family of ordinary second order differential equations in time. The idealized structure can be seen in Figure 4.2.

For the PSD test simulations performed during this study, the dynamic degrees of freedom were selected at the story levels where the structural masses were actually concentrated in order to represent the vibration characteristics accurately.

Thus, the inertial force characteristics were represented by lumped mass at each floor level. Rayleigh proportional damping was assumed, with 2% viscous damping assigned in the first and fourth modes.

During the simulations the restoring shear in the frame forces at each floor level were based on the story shear forces developed in the bilinear springs used to model the story shear-drift behaviour. The spring parameters such as the stiffnesses, yield strengths and hardening ratios were obtained from the static pushover analysis performed on the scaled

test frame. This was done by plotting the response for each story (see Figure 4.3). The above-mentioned spring parameters were then approximated through a linear regression analysis (see Figure 4.4).

The numerical values of all these parameters are given in Table 4.1. The modal properties for natural frequency, natural period and viscous damping are given in Table 4.2.

4.3   Idealized MRF with Viscoelastic Dampers

VE dampers have been used in multistory frame structures for the past over 25 years to control wind-induced vibrations. Recently, they have been applied in earthquake resistant design of new buildings, and seismic retrofit of existing buildings, to mitigate seismic hazards.

The force-displacement behavior of VE dampers depends on the frequency of excitation and temperature. Therefore, to evaluate the earthquake response of a structure equipped with VE dampers, or any other rate-dependent components, the experimental simulations should be performed in, or near real time.

The numerical simulations of rate-dependent real-time PSD tests included structural "test specimens" with rate dependent materials, namely VE dampers. The idealized MRF structure with VE dampers shown in Figure 4.5 was used as the "test specimen". The dampers were designed to provide a linear elastic response under the DBE (Design Basis Earthquake), and the resisting forces developed by the dampers were calculated using the

Generalized Maxwell Model. The restoring force calculations for the Generalized Maxwell Model and the design procedure for sizing the dampers are explained below.

4.3.1 Generalized Maxwell Model

The behavior of a viscoelastic material lies between the behavior of elastic materials and viscous materials. Therefore, a viscoelastic material can be represented by a combination of elastic elements (springs) and viscous elements (dash pots). The simplest models are the Kelvin-Voigt element (Figure 4.6(b)), which consists of a spring and a dash pot connected in parallel and a Maxwell element, which consists of a spring and a dash pot connected in series (Figure 4.6(a)). The Generalized Maxwell Model Figure 4.6(c)) is composed of one Kelvin-Voigt element and n Maxwell elements connected in parallel (Fan, 1998).

Fan (1998) solved the equation of motion for the Generalized Maxwell model by using the Newmark numerical integration algorithm. Using static condensation, Fan developed a two-node VE damper finite element; compared its response (where the Generalized Maxwell model had $n = 4$) with that of the 4-parameter fractional derivative model (Kasai et al., 1993) and found good agreement between the two.

4.3.2 State Determination for the Generalized Maxwell Model

The equation of motion for the Generalized Maxwell model can be expressed as:

$$\mathbf{Ku + C\dot{u} = P} \tag{4.1}$$

The DOFs for the model are identified in Figure 4.7, where u_0 is the displacement at the external degree of freedom, and u_1 through u_4 are the displacements at the internal DOFs. Only stiffness and damping terms appear in Equation (4.1), since no mass is associated with the DOFs.

Hence, for a Generalized Maxwell Model with n Maxwell elements:

$$\mathbf{K} = \begin{bmatrix} K_1 & 0 & \cdots & 0 & -K_1 \\ 0 & K_2 & \cdots & 0 & -K_2 \\ \vdots & \vdots & \ddots & 0 & \vdots \\ 0 & 0 & \cdots 0 & K_n & -K_n \\ -K_1 & -K_2 & \cdots & -K_n & K_0 + \sum_{m=1}^{n} K_m \end{bmatrix} \tag{4.2}$$

and

$$\mathbf{C} = \begin{bmatrix} C_1 & 0 & \cdots & 0 & 0 \\ 0 & C_2 & \cdots & 0 & 0 \\ \vdots & \vdots & \ddots & 0 & \vdots \\ 0 & 0 & \cdots 0 & C_n & 0 \\ 0 & 0 & \cdots & 0 & C_0 \end{bmatrix} \tag{4.3}$$

No external load is applied to the internal DOFs, hence the load vector $\mathbf{P}$ is:

$$\mathbf{P} = \begin{bmatrix} P_1 \\ P_2 \\ \vdots \\ P_n \\ P_0 \end{bmatrix} = \begin{bmatrix} 0 \\ 0 \\ \vdots \\ 0 \\ P_0 \end{bmatrix} \tag{4.4}$$

and displacements $\mathbf{u}$ and velocities $\dot{\mathbf{u}}$ are:

$$\mathbf{u} = \begin{bmatrix} u_1 \\ u_2 \\ \vdots \\ u_n \\ u_0 \end{bmatrix} \qquad \dot{\mathbf{u}} = \begin{bmatrix} \dot{u}_1 \\ \dot{u}_2 \\ \vdots \\ \dot{u}_n \\ \dot{u}_0 \end{bmatrix} \tag{4.5}$$

The parameters for the springs K_m and dash pots C_m where $m = 0...n$, are calculated

as:

$$K_m = \frac{A_{ve}}{t_{ve}} E_m \quad , \qquad \text{for } m = 0...n \tag{4.6}$$

$$C_0 = \frac{A_{ve}}{t_{ve}} \beta_{0,ref} E_0 \alpha_T \tag{4.7}$$

$$C_m = \frac{A}{t_{ve}} \tau_{m,ref} E_m \alpha_T \quad \text{for } m = 1...n \tag{4.8}$$

where A_{ve} is the shear area, and t_{ve} is the thickness of the layer. Both are determined as

part of the design procedure. E_0 through E_n, $\beta_{0,ref}$, and $\tau_{1,ref}$ through $\tau_{n,ref}$ are material

properties whose values are established from test data of the damper material, and will be

discussed later. α_T is a shifting function that is used to account for temperature

effects. $\beta_{0,ef}$ and $\tau_{m,ref}$ are the reference values with respect to temperature.

The velocities that generate the VE damper forces are based on the velocities of the

DOFs (i.e., actuators). Because the integration time step used in the simulations is small

(0.005 sec.), the velocity with which the actuators are moving can be estimated by dividing the displacement increment by the time-step size.

This velocity is herein referred to as the "apparent velocity" ($\dot{u}_{app}$).,where:

$$\dot{u}_{app} = \frac{\Delta u}{\Delta t} \qquad (4.9)$$

In Equation (4.9) Δu and Δt are the displacement increment and time step size.

The restoring forces in the VE dampers, were obtained by integrating the equation of motion of the Generalized Maxwell Model using the relationship given by Equation (4.9) for the velocity $\dot{u}$.

The equation of motion for the Generalized Maxwell Model Equation (4.1) for the ith time step is

$$\mathbf{K}\mathbf{u}_i + \mathbf{C}\dot{\mathbf{u}}_i = \mathbf{P}_i \qquad (4.10)$$

From Equation (4.9) $\dot{\mathbf{u}}_i$ can be written as:

$$\dot{\mathbf{u}}_i = \frac{\Delta \mathbf{u}_i}{\Delta t} \qquad (4.11)$$

The displacement at the ith time step can be expressed in terms of the displacement at the previous time step and the displacement increment, where

$$\mathbf{u}_i = \mathbf{u}_{i-1} + \Delta \mathbf{u}_i \qquad (4.12)$$

Upon substituting $\mathbf{u}_i$ and $\dot{\mathbf{u}}_i$ into Equation (4.10), and rearranging:

$$\left[\mathbf{K}+\frac{\mathbf{C}}{\Delta t}\right]\Delta\mathbf{u}_i = \mathbf{P}_i - \mathbf{K}\mathbf{u}_{i-1}$$ (4.13)

For the Generalized Maxwell model with one Kelvin-Voigt element and four Maxwell elements (i.e., $n = 4$), Equation (4.13) becomes:

$$\underbrace{\begin{bmatrix} K_1 + \dfrac{C_1}{\Delta t} & 0 & 0 & 0 & -K_1 \\ 0 & K_2 + \dfrac{C_2}{\Delta t} & 0 & 0 & -K_2 \\ 0 & 0 & K_3 + \dfrac{C_3}{\Delta t} & 0 & -K_3 \\ 0 & 0 & 0 & K_4 + \dfrac{C_4}{\Delta t} & -K_4 \\ -K_1 & -K_2 & -K_3 & -K_4 & K_0 + \sum_1^4 K_m + \dfrac{C_0}{\Delta t} \end{bmatrix}}_{\hat{\mathbf{K}}} \underbrace{\begin{bmatrix} \Delta u_{1i} \\ \Delta u_{2i} \\ \Delta u_{3i} \\ \Delta u_{4i} \\ \Delta u_{0i} \end{bmatrix}}_{\Delta \hat{\mathbf{u}}_i} = \underbrace{\begin{bmatrix} P_{1i} \\ P_{2i} \\ P_{3i} \\ P_{4i} \\ P_{0i} \end{bmatrix} - \begin{bmatrix} A \\ B \\ C^* \\ D \\ E \end{bmatrix}}_{\hat{\mathbf{P}}_i}$$ (4.14)

where $A = K_1\left[u_{1i-1} - u_{0i-1}\right]$ $\qquad$ $B = K_2\left[u_{2i-1} - u_{0i-1}\right]$

$C^* = K_3\left[u_{3i-1} - u_{0i-1}\right]$ $\qquad$ $D = K_4\left[u_{4i-1} - u_{0i-1}\right]$

$E = K_0 u_{0i-1} - A - B - C^* - D$

and $P_{1i} = P_{2i} = P_{3i} = P_{4i} = 0$ since no load is applied to internal DOFs.

Partitioning the matrices of Equation (4.14) in order statically condense out the internal DOFs

$$
\begin{bmatrix}
K_1 + \dfrac{C_1}{\Delta t} & 0 & 0 & 0 & -K_1 \\
0 & K_2 + \dfrac{C_2}{\Delta t} & 0 & 0 & -K_2 \\
0 & 0 & K_3 + \dfrac{C_3}{\Delta t} & 0 & -K_3 \\
0 & 0 & 0 & K_4 + \dfrac{C_3}{\Delta t} & -K_4 \\
-K_1 & -K_2 & -K_3 & -K_4 & K_0 + \displaystyle\sum_1^4 K_m + \dfrac{C_0}{\Delta t}
\end{bmatrix}
\begin{Bmatrix}
\Delta u_{1i} \\ \Delta u_{2i} \\ \Delta u_{3i} \\ \Delta u_{4i} \\ \Delta u_{0i} \\ \Delta u_{exti}
\end{Bmatrix}
=
\begin{Bmatrix}
-A \\ -B \\ -C \\ -D \\ P_{0i} - E \\ P_{loweri}
\end{Bmatrix}
\tag{4.15}
$$

with $\mathbf{K}\hat{a}a$, $\mathbf{K}\hat{a}b$, $\mathbf{K}\hat{b}a$, $\mathbf{K}\hat{b}b$, $\Delta\mathbf{u}_{\text{int}\,i}$, $\mathbf{P}_{upperi}$

results in:

$$
\mathbf{K}\hat{a}a\,\Delta\mathbf{u}_{\text{int}\,i} + \mathbf{K}\hat{a}b\,\Delta u_{ext\,i} = \mathbf{P}_{upperi}
\tag{4.16}
$$

$$
\mathbf{K}\hat{b}a\,\Delta\mathbf{u}_{\text{int}\,i} + K\hat{b}b\,\Delta u_{ext\,i} = P_{loweri}
\tag{4.17}
$$

From Equation (4.16)

$$
\Delta\mathbf{u}_{\text{int}\,i} = \mathbf{K}\hat{a}a^{-1}\left(\mathbf{P}_{upperi} - \mathbf{K}\hat{a}b\,\Delta u_{ext\,i}\right)
\tag{4.18}
$$

Substituting $\Delta\mathbf{u}_{\text{int}\,i}$ into Equation (4.17) results in the equilibrium equations being expressed in terms of the external DOF, where

$$
\underbrace{\left(K\hat{b}b - \mathbf{K}\hat{b}a\,\mathbf{K}\hat{a}a^{-1}\mathbf{K}\hat{a}b\right)}_{K_{ve}^{*}}\Delta u_{exti} = \underbrace{P_{loweri} - \mathbf{K}\hat{b}a\,\mathbf{K}\hat{a}a\,\mathbf{P}_{upperi}}_{P_{vei}^{*}}
\tag{4.19}
$$

In Equation (4.19) K_{ve}^{*} and P_{vei}^{*} are the damper effective stiffness and load respectively.

53

Only the damper element is considered in Equation (4.19) (see Figure 4.7). VE dampers are usually incorporated into a frame through braces. However, the damper and brace are connected in series, enabling their combined behavior to be modeled as such (see Figure 4.8).

The force developed in the damper, P_{0i} is found from Equation (4.19), where

$$P_{0i} = K_{ve}^* \Delta u_{ext\,i} + E + \mathbf{K}\hat{b}a\mathbf{K}\hat{a}a\mathbf{P}_{upperi} \tag{4.20}$$

The force developed in the brace is equal to

$$P_{br\,i} = K_{br}[\Delta u_{ext\_total\,i} - \Delta u_{ext\,i}] \tag{4.21}$$

Where K_{br} is the axial stiffness of the brace and $\Delta u_{ext\_total\,i}$ is the displacement increment at the end of the brace (right hand side in Figure 4.9) and the quantity $[\Delta u_{ext\_total\,i} - \Delta u_{ext\,i}]$ is the deformation increment across the brace.

Equating P_{0i} to $P_{br\,i}$ (since the damper and brace are connected in series) the external displacement acting on the damper is found:

$$\Delta u_{ext\,i} = \frac{(K_{br}\Delta u_{ext\_total\,i} - E - \mathbf{K}\hat{b}a\mathbf{K}\hat{a}a\mathbf{P}_{upperi})}{(K_{ve}^* + K_{br})} \tag{4.22}$$

With the external damper displacement determined from Equation (4.22) the restoring force developed P_{0i} in the damper brace system can be calculated from either the damper or the brace:

$$P_{0i} = K_{ve}^* \Delta u_{ext\,i} + E + \mathbf{K}\hat{b}a\mathbf{K}\hat{a}a\mathbf{P}_{upperi} = P_{br\,i} = K_{br}[\Delta u_{ext\_total\,i} - \Delta u_{ext\,i}] \tag{4.23}$$

The state determination procedure, given the external displacement increment $\Delta u_{ext\_total_i}$ applied to the damper brace system, for the current time step i is summarized below.

(1) Calculate $A, B, C^*, D, E, \hat{\mathbf{K}}, \mathbf{K}\hat{b}a, \mathbf{K}\hat{a}a, \hat{Kb}b, \mathbf{P}_{upper_i}$

(2) Calculate Δu_{ext_i} from Equation (4.22)

(3) Calculate P_{0_i} from Equation (4.23)

(4) Calculate the displacement increment at all DOFs from: $\Delta \hat{\mathbf{u}}_i = \hat{\mathbf{K}}^{-1}\hat{\mathbf{P}}$

(5) Update the displacements:

- $(u_1)_i = (u_1)_{i-1} + (\Delta u_1)_i$
- $(u_2)_i = (u_2)_{i-1} + (\Delta u_2)_i$
- $(u_3)_i = (u_3)_{i-1} + (\Delta u_3)_i$
- $(u_4)_i = (u_4)_{i-1} + (\Delta u_4)_i$
- $(u_0)_i = (u_0)_{i-1} + (\Delta u_{ext})_i$

Note that $\hat{\mathbf{K}}$ and K_{ve}^* would normally have to be calculated at each state determination, since the dashpot coefficients C_0 through C_4 are temperature sensitive (i.e., one may want to consider the temperature rise in the damper that occurs over the course of the simulation). K_{br}, on the other hand is constant and its value can be predefined and stored.

4.3.3 Design of MRF with VE Dampers

The design of the diagonal-braced VE-damped frame used the approach proposed by Fan (1998), where ISD-110 material was assumed for the dampers. There are two stages

55

in the design of frames with dampers. First, the frame is designed without dampers. The second stage involves the design of the dampers and braces. In this study the 4-story structure described previously is used as the frame without dampers.

A VE damper system consists of two parts: a VE damper and the attached braces, which are connected in series. For a diagonal-braced VE-damped frame, with braces inclined at an angle ψ, the brace $(\widetilde{K}_{br})$ and damper $(\widetilde{K}_{ve})$ stiffness in global coordinates are equal to:

$$\widetilde{K}_{br} = K_{br}(\cos^2 \psi) \tag{4.24}$$

$$\widetilde{K}_{ve} = K_{ve}(\cos^2 \psi) \tag{4.25}$$

K_0 denotes the interstory stiffness of the frame without VE dampers (see Figure 4.9).In the design of the VE dampers and braces, two parameters are important: (1) the value α_k, which is the ratio of the stiffness of the brace to the stiffness of the undamped frame at floor level k, (i.e., $\alpha_k = \widetilde{K}_{br\_k} \big/ K_{0\_k}$) and (2) the value β_k, which is the ratio of the global stiffness of the VE damper to the story stiffness of the undamped frame at floor level k, (i.e., $\beta_k = \widetilde{K}_{ve\_k} \big/ K_{0\_k}$).

The preliminary design involves the determination of α_k and β_k for each story ($k = 1 ... number\ of\ floors$). The displacements and the internal forces in the members are then checked to ensure that the frame performs adequately under seismic loading. To

simplify the design, α_k and β_k are constant over the building height, with $\alpha_k = \alpha$ and $\beta_k = \beta$ at all floors.

The design approach proposed by Fan (1998) can be summarized as follows:

(1) Select an appropriate α and a range of β values.

Selecting an appropriate value of α simplifies the analysis. Since the brace and the VE damper are connected in series, when a stiff brace is used, more deformation is directed to the VE damper and the damper becomes more efficient. A range of α from 25 to 40 is appropriate. Steps (2) through (7) below are repeated for each combination of α and β. In the design a value of $\alpha = 30$ and values of $\beta = 0.1$, 0.2, 0.3...2,2.2,2.4...3, 4, 5, 6, 10, 15, 20 were used.

(2) Estimate the first mode deflected shape using static analysis.

A triangular pattern of static lateral forces is applied over the height of the VE-damped structure. The first mode shape is approximated by the lateral displacements at the floor levels, which are obtained from linear elastic analysis under the given loading.

(3) Estimate the fundamental natural period T_1 of the first mode using Rayleigh's Method.

$$T_1 = 2\pi \sqrt{\frac{(\varphi_1^T \mathbf{M} \varphi_1)}{(\varphi_1^T \mathbf{K} \varphi_1)}} \tag{4.26}$$

where in Equation (4.26)

φ_1 is the displacement vector corresponding to the first mode.

K   is the stiffness matrix of the VE-damped frame.

M   is the mass matrix of the VE-damped frame.

(4) Estimate the equivalent viscous damping ratio ξ_s by the Lateral Force Energy (LFE) Method using Equation (4.27).

$$\xi_s = \frac{\eta_{ve}}{2} \frac{\mathbf{F}_{ve}^T \mathbf{u}_{ve}}{\mathbf{F}^T \mathbf{u}} \tag{4.27}$$

Equation (4.27) is based on the proportion of the strain energy in the dampers relative to the total system for a MDOF structure.

In Equation (4.27), $\mathbf{F}_{ve}$ is the vector of forces in the dampers; $\mathbf{u}_{ve}$ is the vector of corresponding VE damper deformations; $\mathbf{F}$ is the vector of applied static lateral forces at the floor levels; and $\mathbf{u}$ is the vector of corresponding floor lateral displacement. η_{ve} is the loss factor, which is dependent on response frequency ω, shear strain γ amplitude, and the ambient temperature T. The loss factor is defined as the loss modulus $E''(\omega,T)$ (complex part of the material stiffness) to the storage modulus $E'(\omega,T)$ (real part of the material stiffness):

$$\eta_{ve} = \frac{E''(\omega,T)}{E'(\omega,T)} \tag{4.28}$$

The storage and loss moduli are determined from Equations (4.29) and (4.30):

$$E'(\omega,T) = E_0 + \sum_{m=1}^{n} \left\{ \left[\frac{(\alpha_T \omega \tau_{m,ref})^2}{1 + (\alpha_T \omega \tau_{m,ref})^2} \right] E_m \right\} \tag{4.29}$$

$$E''(\omega, T) = (\alpha_T \omega \beta_{0,ref})E_0 + \sum_{m=1}^{n} \{[\frac{(\alpha_T \omega \tau_{m,ref})}{1 + (\alpha_T \omega \tau_{m,ref})^2}]E_m\} \tag{4.30}$$

In Equations (4.29) and (4.30), $\beta_{0,ref}$ and $\tau_{m,ref}$ are the values of the parameters β_0

and τ_m at the reference temperature T_{ref}. These reference material parameters are used in

Equations (4.7) and (4.8) to establish the dash pot coefficients for the Generalized

Maxwell Model.

To accounts for temperature changes, by a shifting function α_T is used, where:

$$\alpha_T = \left(\frac{T}{T_{ref}}\right)^p \tag{4.31}$$

In Equation (4.31), T is temperature, and T_{ref} and p are the parameters of the shifting

function. The values for the ISD-110 VE material proposed by Fan (1998) were used for

the material parameters ($E_0 ... E_4, \beta_{0,ref}, \tau_{1,ref} ... \tau_{4,ref}, p$). and are found in Table 4.3. An

ambient temperature of T_{ref} of 24 °C was assumed.

(5) Estimate the earthquake response from a smooth spectrum.

The spectral acceleration is determined from a design spectrum, which is modified to

account for the level of equivalent viscous damping present in the structure. For this, an

equivalent viscous damping-based procedure similar to that in FEMA 273 is used to

adjust the ordinates of the response spectrum that is based on 5% viscous damping.

(6) Compute the equivalent lateral forces.

The design base shear (V) is calculated using the design seismic response coefficient (C_s) and weight of the structure (W), where $V = C_s W$.

Since the structure likely remains elastic during the Design Basis Earthquake (DBE), equivalent lateral forces are based on a triangular distribution of the total base shear.

(7) Perform static analysis under the equivalent lateral forces.

To estimate the displacements, internal forces, and deformations of the structure a static analysis is performed using the equivalent lateral forces obtained in Step (6). The stiffness contribution from only the springs in the Generalized Maxwell Model (i.e., K_0 through K_4) are used in the static analysis in combination with the brace stiffness K_{br} and frame stiffness K_0.

The design performance objectives require the frame to be in operation (damage free) during and after the DBE, and between the Immediate Occupancy and Life Safety levels for the Maximum Considered Earthquake (MCE). To satisfy these requirements, the design criteria considers:

- all the members remain elastic under the DBE.

- the allowable story drift is limited to 1% under DBE.

By repeating the design steps (2) to (7) for the α and β combinations given in step (1) and considering the above-mentioned criteria, the largest value of β was determined to be 1.3 (see Figure4.10). The relationship between β and fundamental period, and

β and the equivalent damping ratio are plotted in Figure 4.11 and Figure 4.12, respectively.

Figure 4.11 and 4.12 indicate that for $\beta = 1.3$, the fundamental period and equivalent viscous damping ratio are equal to 0.763 sec and 35.3, respectively. The value of 0.763 sec is based on Equation (4.26).

Once the value for β is determined, the shear area A_{ve} of each damper can be calculated:

$$A_{vek} = \frac{\beta_k K_{0k} t_{vek}}{\cos^2 \psi_k E'}$$
(4.32)

In Equation (4.32) K_{0k} is the interstory lateral stiffness of the kth story of the frame without the dampers, t_{vek} is the thickness of the layer, (a 1-inch thickness was used for all the dampers), ψ_k is the angle of inclination between the brace at story k and the global horizontal direction (see Figure 4.9), and E' is the storage modulus given by Equation (4.29).

A summary of the damper design is given in Table 4.4, where values for the brace axial stiffness (K_{br}), VE-damper stiffness (K_{ve}), equivalent stiffness of the combined brace and VE-damper (K_{eq}), and the damper shear area (A_{ve}) at each floor level k appear. The modal properties of the idealized MRF with VE-dampers are given in Table 4.5. Comparing the results in Table 4.5 with those of the MRF without VE-dampers (Table 4.2), it is apparent that the addition of the VE-dampers not only increased the

61

damping in the structure, but also shortens the natural frequencies, because the VE-dampers and braces add stiffness to the structure.

The elastic stiffness matrix $\mathbf{K}$ of the MRF with VE-dampers is given in Figure 4.13. It is based on the static stiffness of the dampers (i.e., C_0 through C_4 are taken as zero).

Table 4.1 Structural Properties of Idealized MRF

Floor-k	Mass-m_k [Kips-sec^2/in]	Stiffness-k_k [Kips/in]	Yield Strength $F_{sy,k}$ [Kips]	Strain Hardening Ratio [Kpi/Kpi]
1	0.831	177.9	370.1	0.0185
2	0.831	212.9	327.8	0.0197
3	0.831	172.2	250.6	0.0165
4	0.604	108.9	127.3	0.0165

Table 4.2 Modal Properties of the Idealized MRF

Mode-i	Natural Frequency ω_{ni} [rad/sec]	Natural Period T_{ni} [sec]	Viscous Damping Ratio ξ_{ni}
1	5.48	1.15	0.02
2	14.02	0.45	0.015
3	21.09	0.29	0.017
4	27.95	0.23	0.02

Table 4.3 Properties for ISD-110 VE Material

Material Parameter	Value
E_0	27.7 psi
E_1	393.6 psi
E_2	196.7 psi
E_3	1598.1 psi
E_4	59.4 psi
$\beta_{0,ref}$	0.1226 sec
$\tau_{1,ref}$	0.0401 sec
$\tau_{2,ref}$	0.1356 sec
$\tau_{3,ref}$	0.0062 sec
$\tau_{4,ref}$	1.2395 sec
T_{ref}	24°C
p	-4.449

63

Table 4.4 Damper Design Characteristics

Floor-k	$K_{br\,k}$ [Kips/in]	$K_{ve\,k}$ [Kips/in]	$K_{eq\,k}$ [Kips/in]	$A_{ve\,k}$ [in^2]
1	6670	289	222	2441
2	7498	325	265	2744
3	6061	263	215	2218
4	3835	166	36	1403

Table 4.5 Modal Properties of Idealized MRF with VE Dampers

Mode-i	Natural Frequency $\omega_{n\,i}$ [rad/sec]	Natural Period $T_{n\,i}$ [sec]
1	8.21	0.77
2	21.01	0.29
3	31.59	0.19
4	41.89	0.15
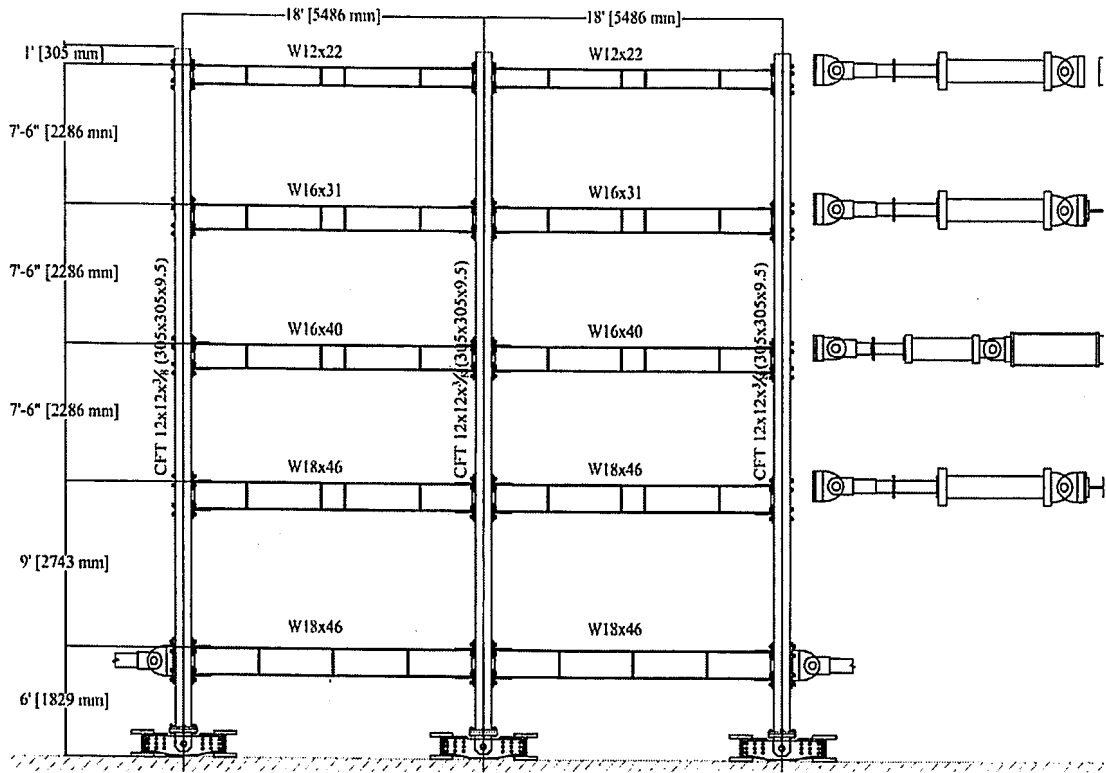
Figure 4.1 Scaled MRF Test Structure (Herrera, 2004)

Rayleigh Proportional
Damping, 2% viscous
damping in 1st and 4th modes
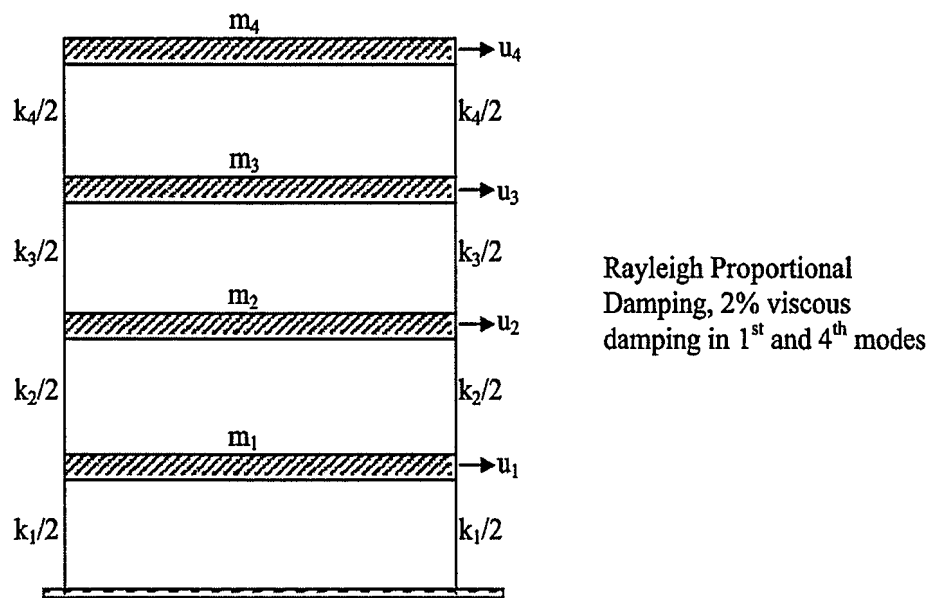
Figure 4.2   Idealized MRF
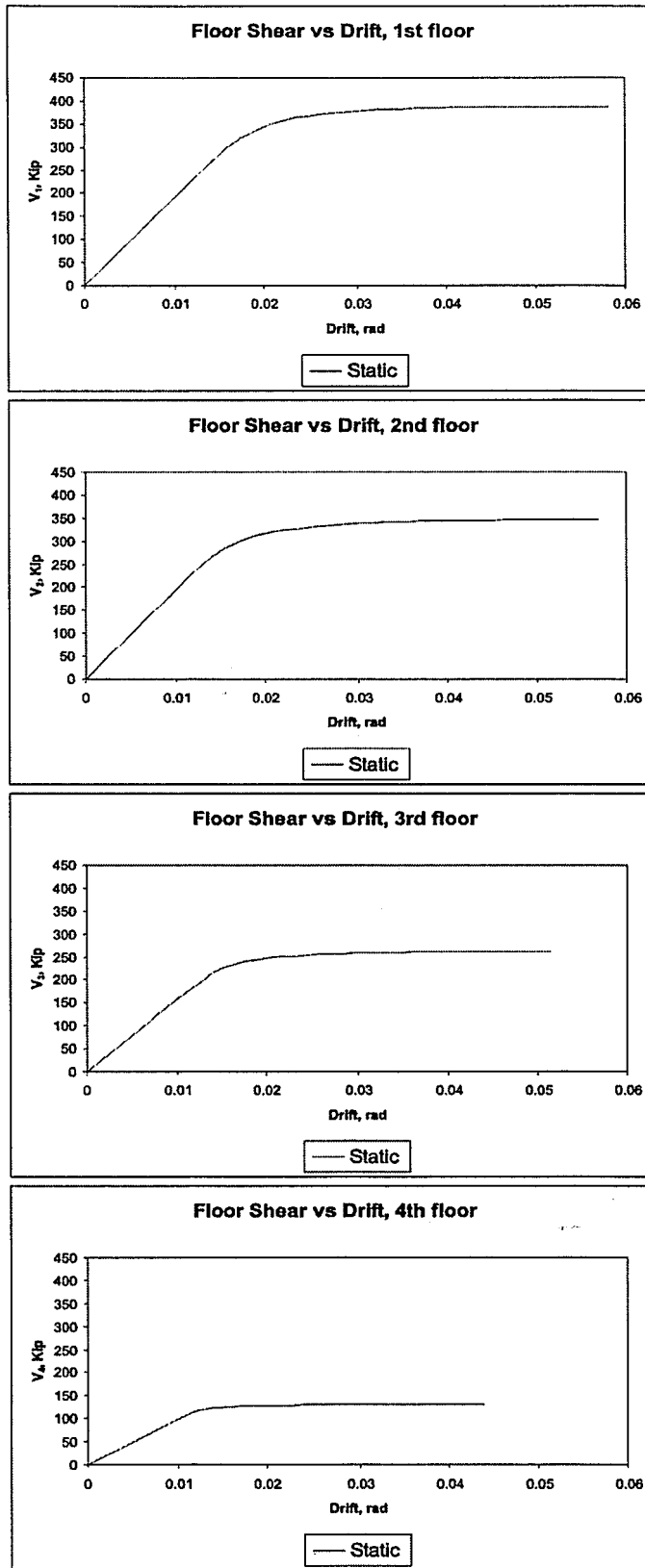
Figure 4.3 Story Shear versus Story Drift Response of Scale Model MRF

66
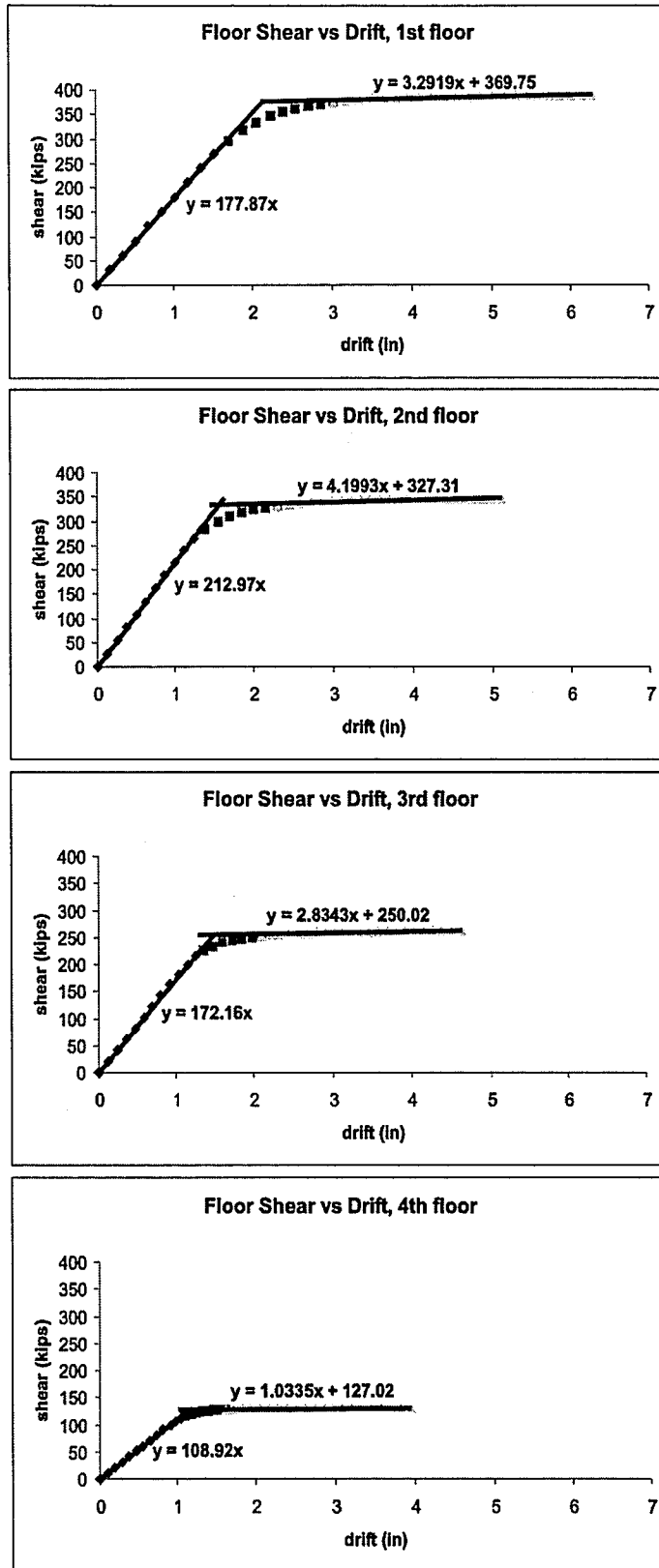
Figure 4.4 Linear Regression Analysis of Story Shear versus Story Drift for Scale Model MRF

Figure 4.5   Idealized MRF with VE-Dampers
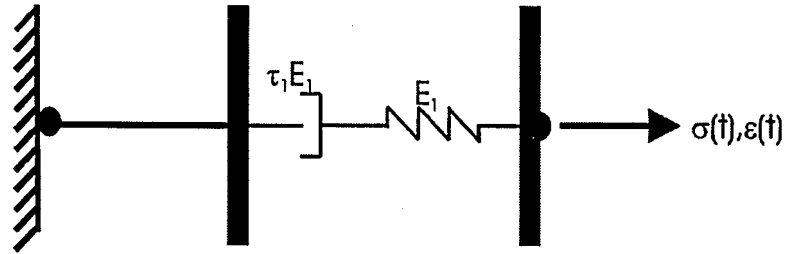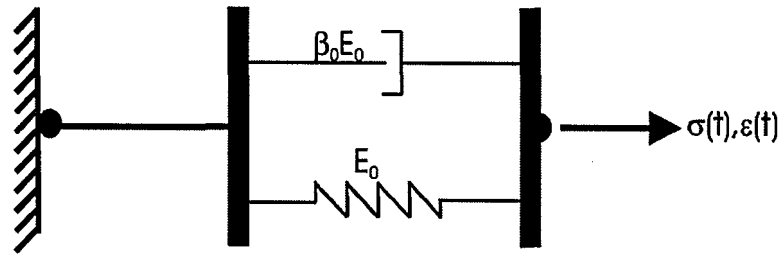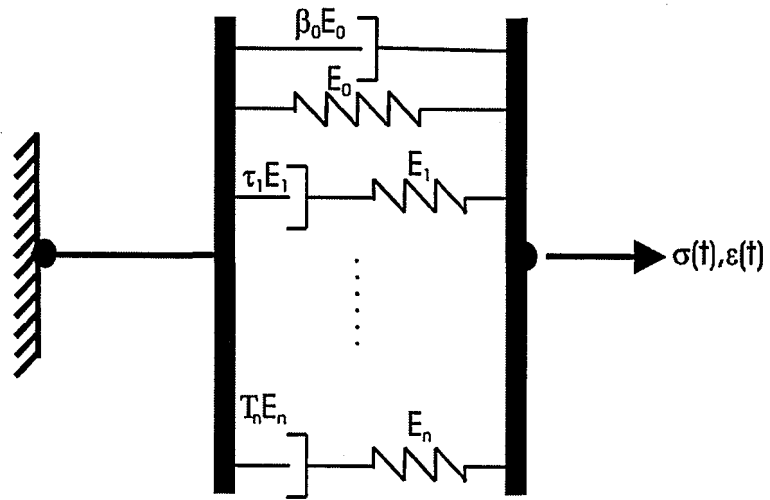
Figure 4.6 Constitive Models for VE Materials
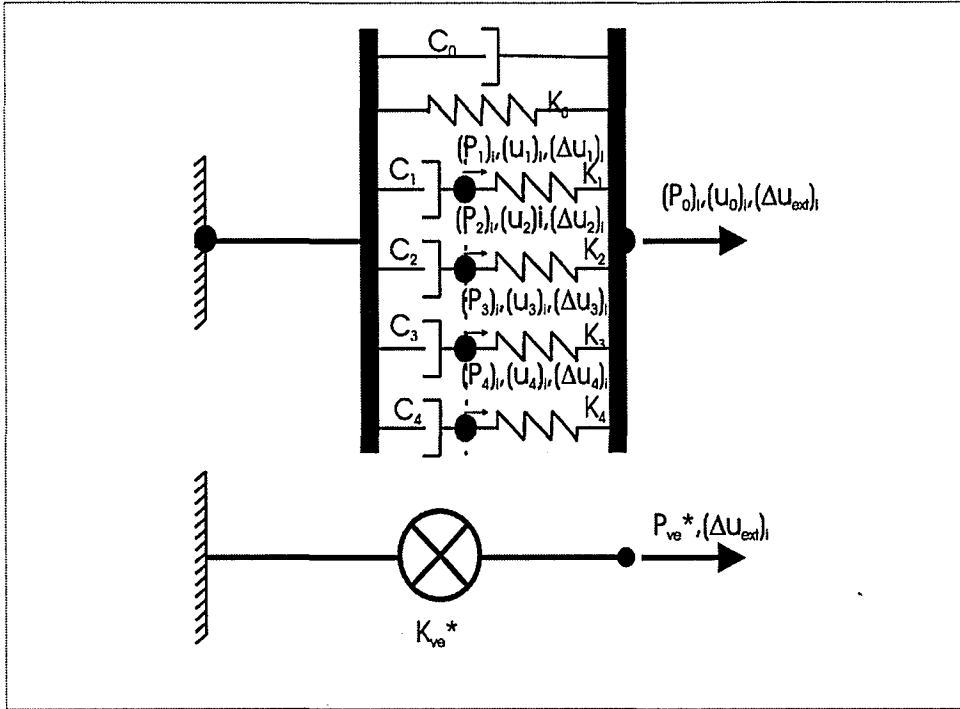
Figure 4.7   Model for VE Damper
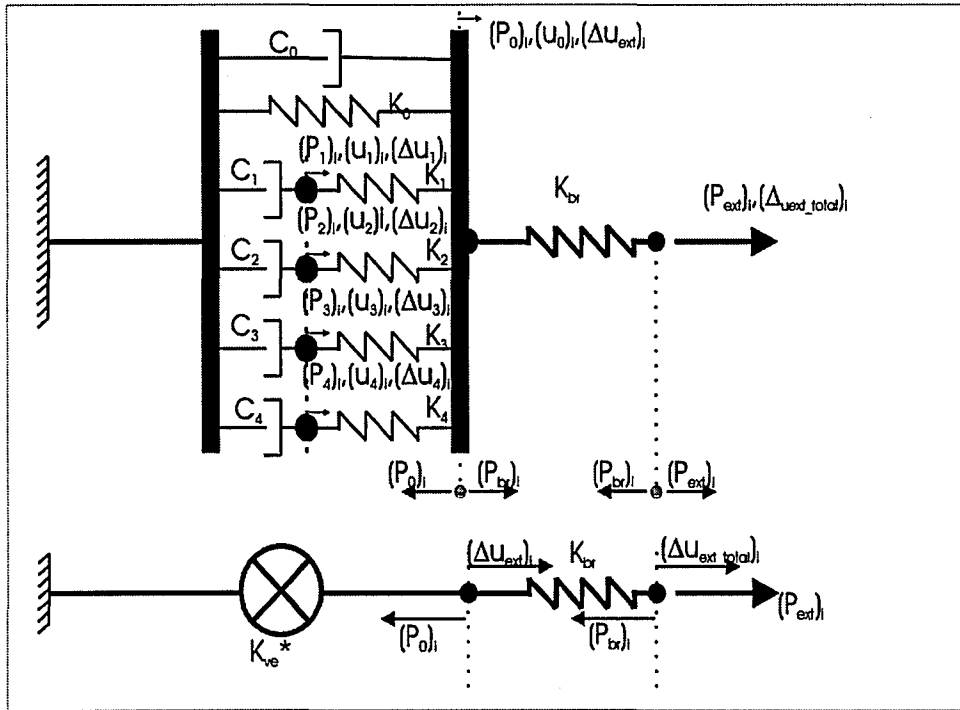
Figure 4.8   Model for VE Damper – Brace System

70
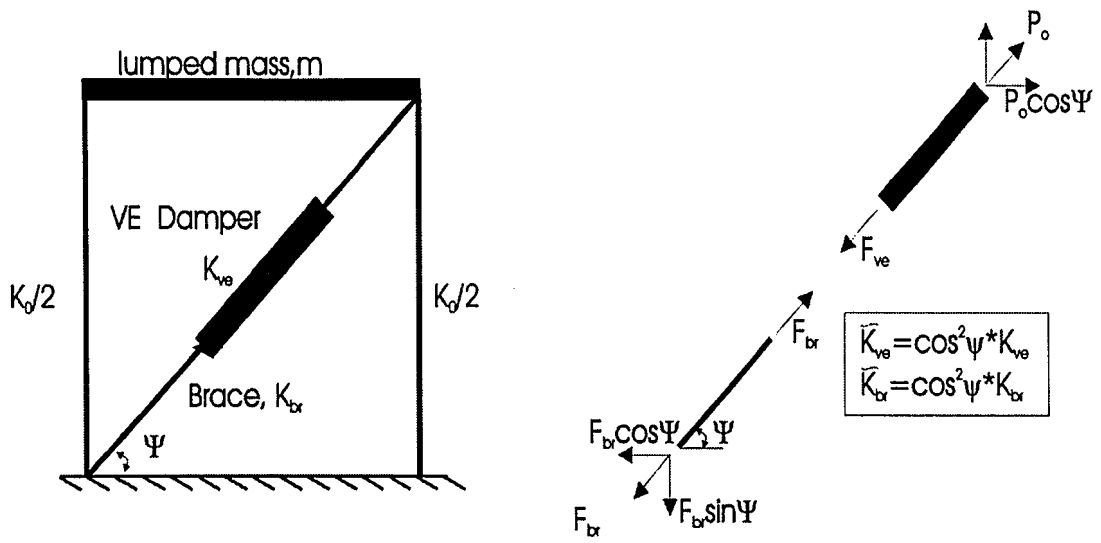
Figure 4.9 Diagonal-Braced VE-Damped Frame
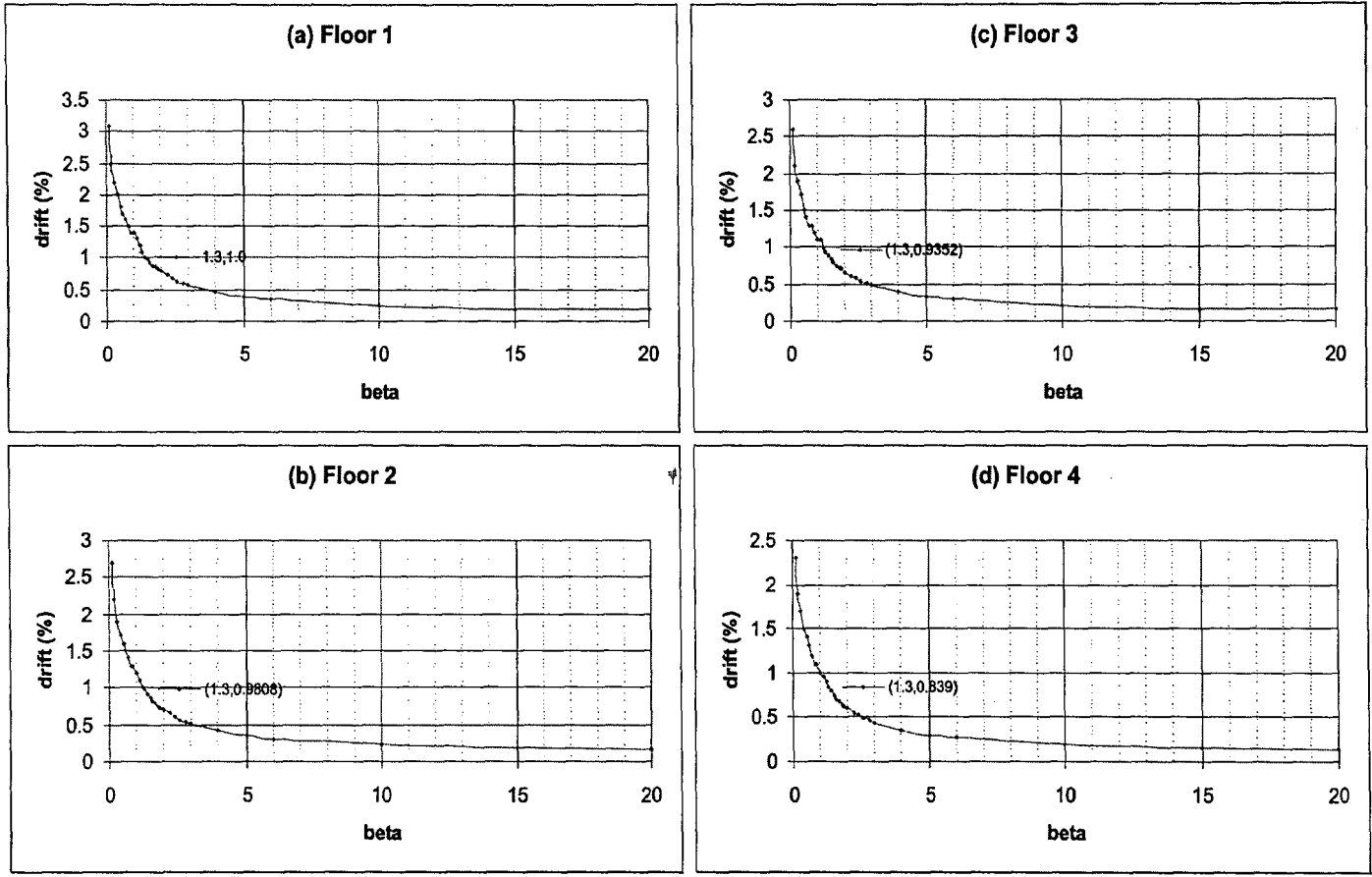
Figure 4.10 β versus Story Drift Relationships
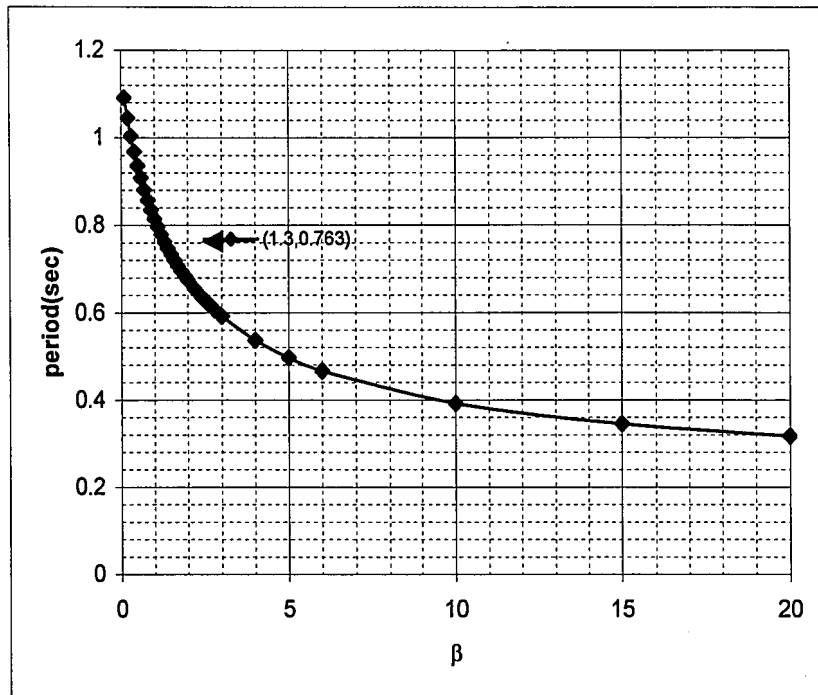
Figure 4.11 Relationship between β and Fundamental Period
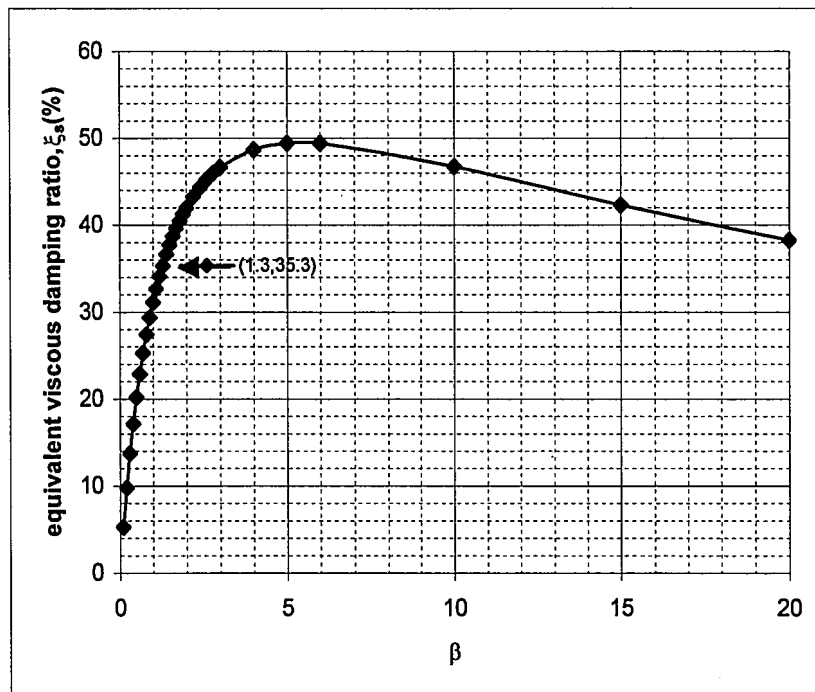
Figure 4.12 Relationship between β and Equivalent Viscous Damping Ratio

$$
\mathbf{K} = \begin{pmatrix} 877.829 & -478.332 & 0 & 0 \\ -478.332 & 865.004 & -386.672 & 0 \\ 0 & -386.672 & 631.307 & -244.635 \\ 0 & 0 & -244.635 & 244.635 \end{pmatrix}
$$

Figure 4.13 Elastic Stiffness Matrix K of the VE-Damped MRF

74

Chapter 5 Pseudodynamic Test Simulations

5.0   General

This chapter presents the results of the numerical PSD test simulations using different step-by-step integration algorithms. Both linear and nonlinear cases are considered for the frames with and without VE dampers.

5.1   Numerical Simulations

The three numerical integration algorithms presented in Chapter 3 were used to perform numerical simulations of the PSD test method. The three algorithms included: (1) Newmark Explicit Method, (2)Alpha Method with a Fixed Number of Iterations, and (3) Newmark Explicit Real-Time Method. The test structure consisted of the MRF, with and without VE dampers, presented in Chapter 4.

The algorithms were programmed in Mathcad (Mathcad 2000 Professional, Mathsoft Inc.), and the analyses were carried out using the 1994 Northridge Earthquake (Canoga Park Station) scaled to the DBE level. The DBE (Design Basis Earthquake) level is the earthquake level that the design lateral forces, used by codes such as the International Building Code (IBC) 2000 [ICC 2000], are based upon. It has an intensity of two thirds of the MCE (Maximum Considered Earthquake). The DBE has a return period of approximately 500 years while the MCE 2500 years.

Four cases were considered in the simulations, and they are identified in Table 5.1.

Case 1 consisted of a linear elastic MRF without VE dampers. The restoring forces were calculated using linear elastic springs with stiffnesses equal to the story stiffnesses (initial stiffnesses of each story obtained from static pushover, see Chapter 4).

Case 2 consisted of an inelastic MRF without VE dampers. The restoring forces were calculated using the story shear-drift relationships for the idealized MRF model presented in Chapter 4.

Case 3 consisted of a linear elastic MRF with VE dampers. The forces developed in the dampers were calculated from the Generalized Maxwell Model. The integration scheme used to integrate the governing equations of motion of the Generalized Maxwell model is explained in Chapter 4. The resisting forces due to the lateral stiffness of the structural members were calculated using the initial linear elastic properties of the MRF. To find the total element forces, at each story level the horizontal component of the damper force was added to the resisting force due to the lateral stiffness of each story.

Case 4 consisted of an inelastic MRF with VE dampers. The forces developed in the dampers were again calculated using the Generalized Maxwell Model. The resisting forces from the MRF were obtained from the story shear-drift relationships of the idealized MRF.

The ground acceleration data for the Canoga Park record was originally provided with a time interval of 0.02 sec. A convergence study was performed to determine the time step size for the Newmark Explicit Method to give an accurate response. Since it assumes a linear variation of acceleration, the response found by using Newmark's method with linear acceleration was accepted as "true response". Convergence of the solution was

achieved using a time step of 0.005 sec. At this time step it was also found that the Newmark Explicit and Newmark's method with linear acceleration gave the same solutions (see Figure 5.1, where the linear acceleration method is identified as "N-beta") Therefore, throughout this study the time step size was selected as 0.005 sec. for simulations using either the Newmark Explicit or Newmark Explicit Real-Time methods.

5.2   Case 1 Results: Linear MRF without VE Dampers

As explained above, numerical simulations of PSD tests for a linear structure, using three different integration algorithms were carried out. Figures 5.2, 5.3, 5.4 and 5.5 show the displacement response history for the first, second, third and fourth story, respectively.

The first plot in each figure (e.g., Figure 5.2(a)) is the response obtained using the Newmark Explicit method. Since a time step of 0.005 sec was used, it is considered as the "true solution". The Alpha Method with a Fixed Number of Iterations was used as the integration scheme for the response in the second plot of each figure (e.g., Figure 5.2 (b)). Ten iterations within a time step of 0.02 sec. were found to be adequate to have an accurate response. The third plot in each figure (e.g., Figure 5.2(c)) is the response obtained using Newmark Explicit Real-Time algorithm with a time step of 0.005.

The last plot of these figures (e.g., Figure 5.2(d)) compares the response from all the three methods together. As can be seen, there is almost no difference between the results and a good agreement exists with the true solution. Therefore, it can be concluded that for PSD test of a rate independent linear structure that all three of the three algorithms give accurate solutions.

77

5.3 Case 2 Results: Inelastic MRF without VE Dampers

Figures 5.6, 5.7, 5.8 and 5.9 show the numerical simulation results of the PSD test simulation for the inelastic MRF.

The first three plots of each figure show the results using each algorithm, with the last plot showing a comparison of the results. These figures illustrate that the three methods give the same results, and that they are in good agreement with the true solution.

5.4 Case 3 Results: Linear MRF with VE Dampers

Figures 5.10, 5.11, 5.12 and 5.13 show the numerical simulation results of the PSD test for the linear MRF with VE dampers. Again, the first three plots of each figure show the results for each method, with the last plot showing a comparison.

In this case the response from Newmark Explicit and Newmark Explicit Real-Time methods are almost the same, however the structure develops more lateral displacement in the response determined using the Alpha Method with a Fixed Number of Iterations.

The discrepancy in the response can be explained by the difference in the apparent velocity (defined in Chapter 4) characteristics of the algorithms. In the Alpha Method, the uniform incremental corrections provided for the displacements cause more or less constant velocities within each time sub step. The dampers therefore cannot develop as much resisting force as they would under the real earthquake and, as a result the structure drifts more. Chapter 6 will present a comprehensive explanation together, with apparent velocity demonstrations of each algorithm.

5.5 Case 4 Results: Inelastic MRF with VE Dampers

Figures 5.14, 5.15, 5.16 and 5.17 show the numerical simulation results of the PSD test for the inelastic MRF with VE dampers. The first three plots of each figure show the results using each algorithm, with the last plot showing a comparison of the results.

The response from the Newmark Explicit and Newmark Explicit Real-Time methods are in close agreement with eachother, with some permanent drift. On the other hand, there are considerably large permanent drifts in the response based on the Alpha Method with a Fixed Number of Iterations, as well as a significant difference with the Newmark Explicit (i.e., 'true solution') and the Newmark Explicit Real-Time methods. This is due to the fact that the apparent velocity is constant within each substep in the Alpha-Method, resulting in smaller damper forces and therefore larger structural displacements. The apparent velocity phenomenon will be discussed in detail in Chapter 6.

The design procedure followed while designing the VE dampers (Section 4.3.3) requires that the VE-damped structure remain elastic under the DBE. However, in the simulations demonstrated, even for Newmark Explicit method (which is considered as the 'true solution', see Chapter 6), there is a slight permanent drift due to some mild inelastic response under the Canoga Park earthquake scaled to the DBE level. For the 'true solution' the maximum drift occurs at the first story with a ductility demand (the ratio of the maximum drift to the yield drift) of 1.06.

Figure 5.18 shows that Canoga Park earthquake has a noticeably large pulse around time $t = 17.5$ sec. During the time history analysis performed under Canoga Park earthquake, the structure yielded and drifted from its initial position due to this pulse and

79

then oscillated about the new deformed position. Figure 5.19 shows the frame shear-drift response, where it can be observed that only a single episode of yielding took place in the frame. The corresponding results for the total shear force-drift responses at each floor are shown in Figure 5.20. The dampers are shown to dissipate energy. The results in Figure 5.19 and 5.20 were obtained from the numerical simulations using the Newmark Explicit method.

5.6 Summary

For the PSD test simulations involving rate-independent materials (i.e., no VE dampers) all the three integration methods gave accurate response for both the linear elastic and inelastic cases (Cases 1 and 2), provided that a small enough time step is chosen for the explicit schemes and a sufficient number of iterations is performed for the implicit scheme (i.e., Alpha Method).

For the PSD test simulations with a rate-dependent (i.e., an MRF with VE dampers), for both linear elastic and inelastic cases (Cases 3 and 4) the Newmark Explicit and Newmark Explicit Real-Time methods gave accurate responses, whereas the Alpha Method with a Fixed Number of Iterations resulted in larger displacements and permanent drift. Although conditionally stable, the Newmark Explicit Real Time algorithm enables real-time testing and agrees well with the 'true solution' for the one earthquake record considered.

Table 5.1 Pseudodynamic Test Simulation Analysis Matrix

Case	Description
1	Linear Elastic MRF
2	Inelastic MRF
3	Linear Elastic MRF with VE Dampers
4	Inelastic MRF with VE Dampers
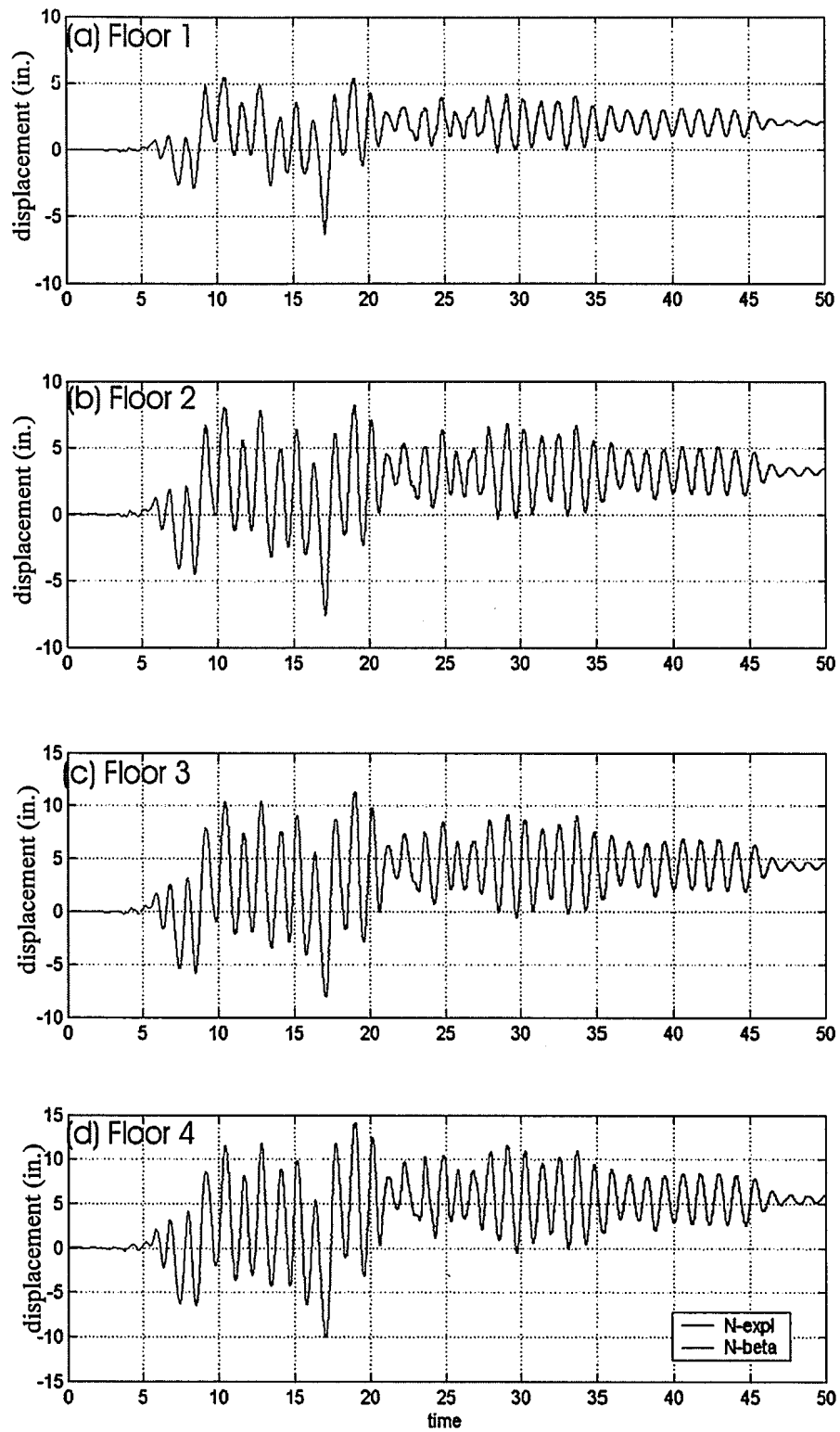
Figure 5.1 Convergence Study, time step size of 0.005 sec.
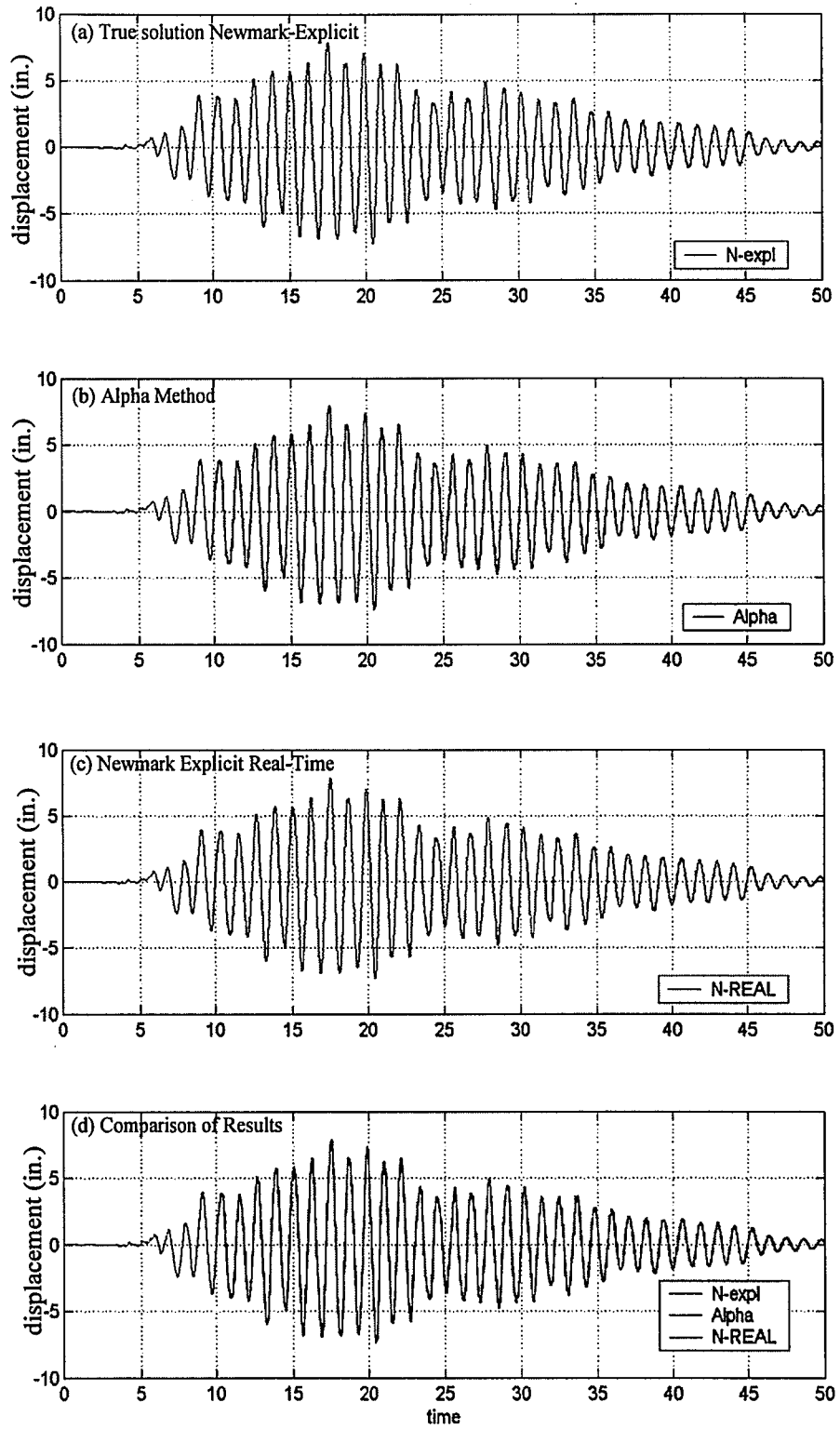
Figure 5.2 Linear MRF without VE Dampers - Story 1

83
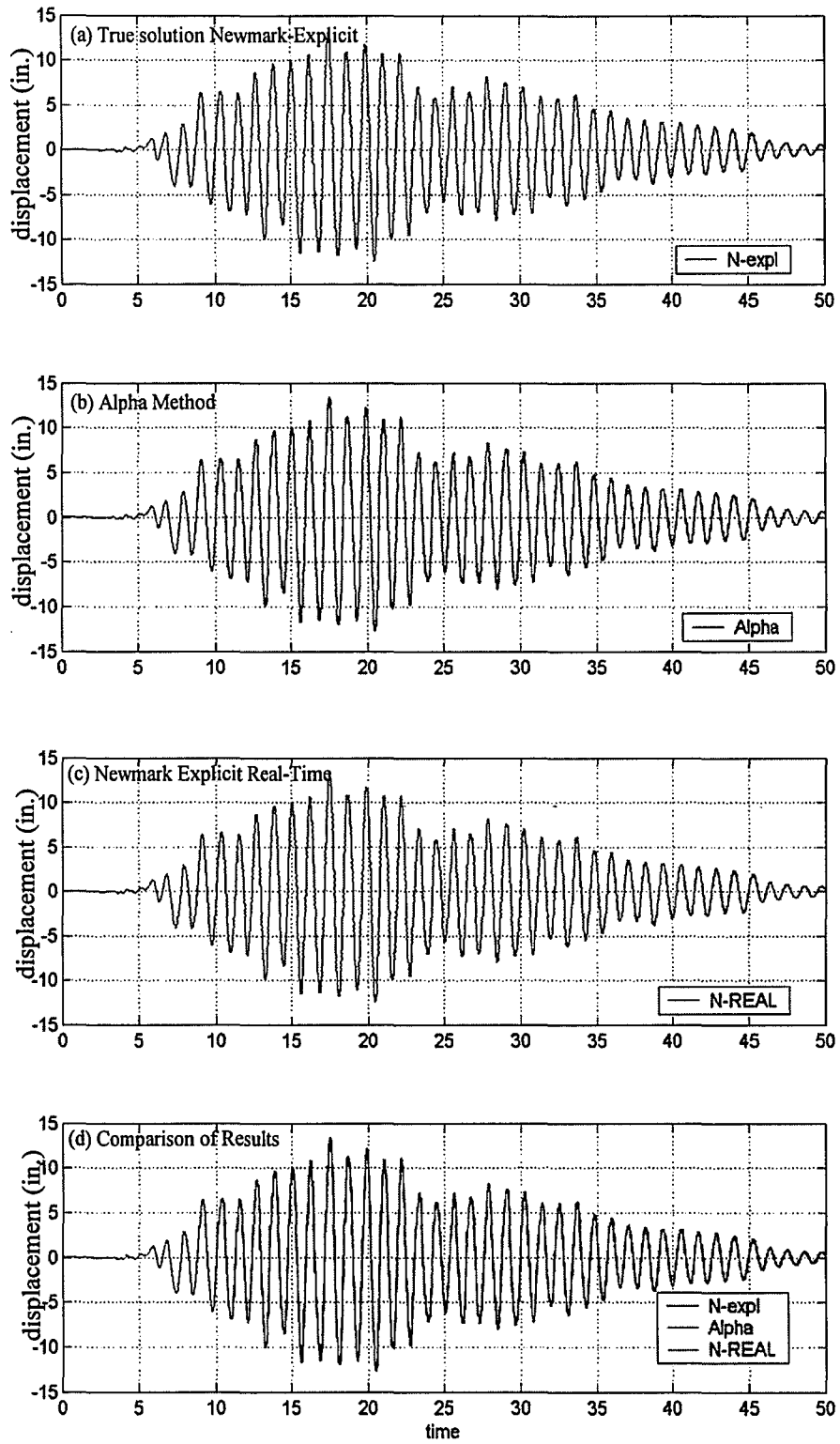
Figure 5.3 Linear MRF without VE Dampers – Story 2
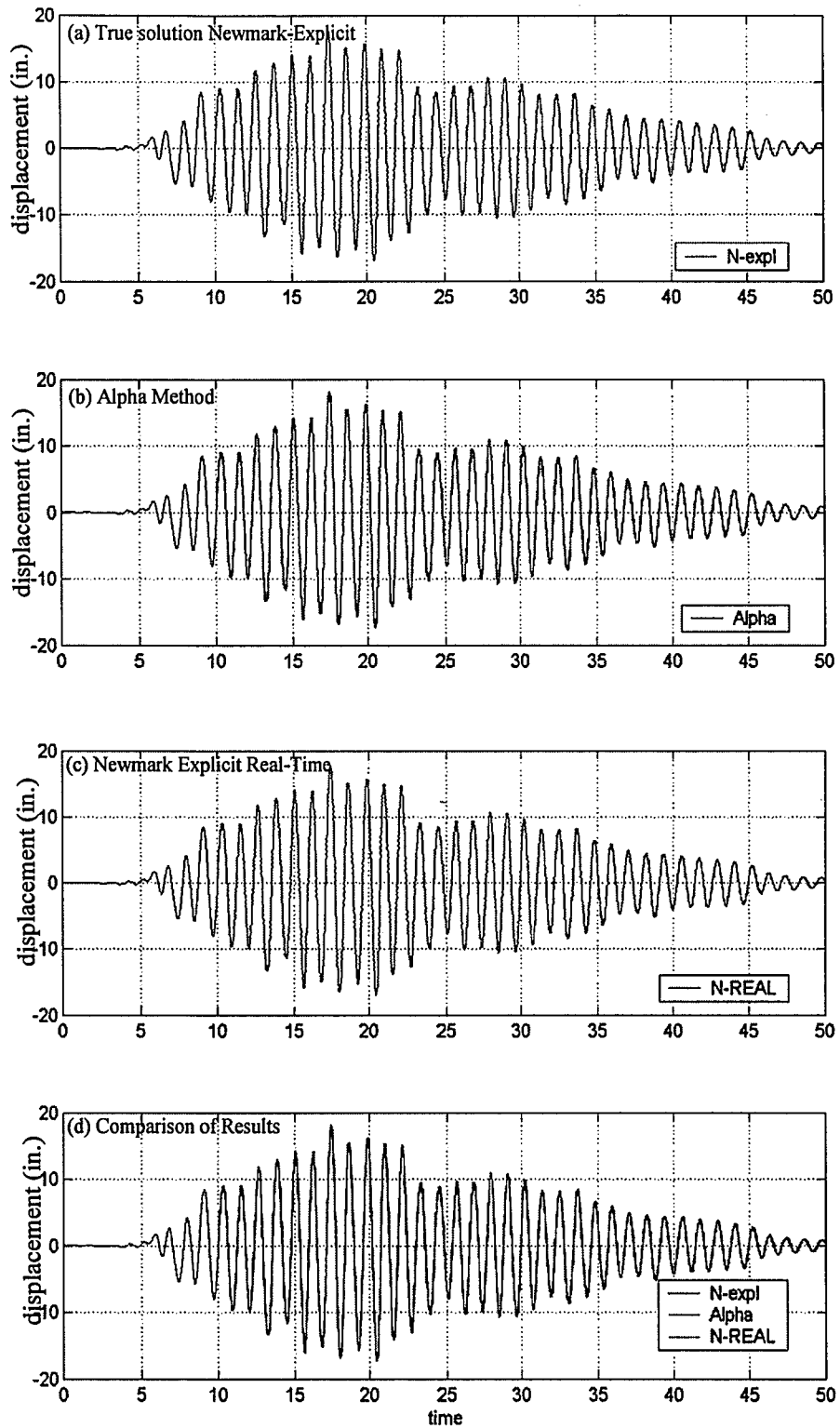
Figure 5.4   Linear MRF without VE Dampers – Story 3
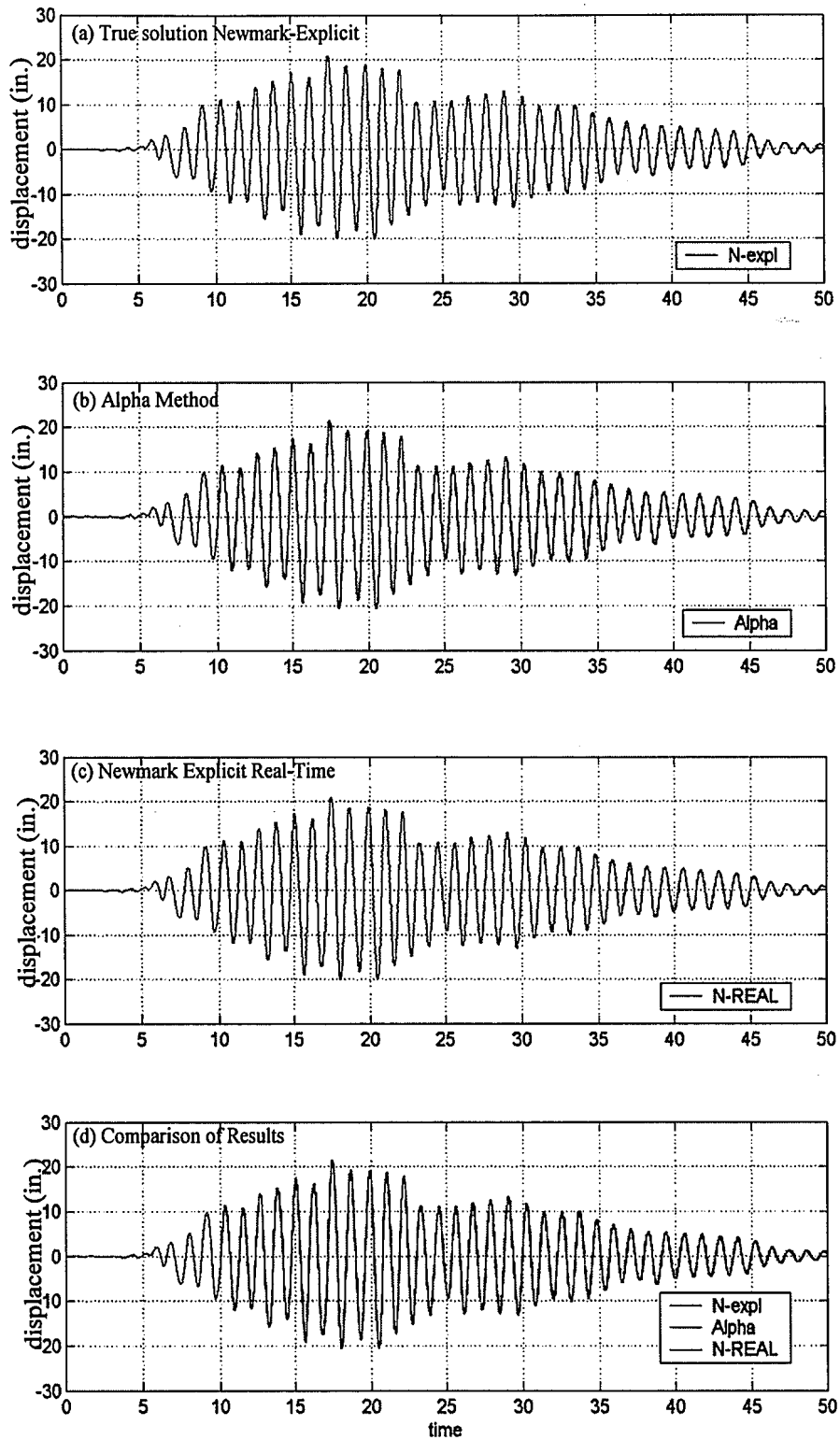
Figure 5.5   Linear MRF without VE Dampers – Story 4
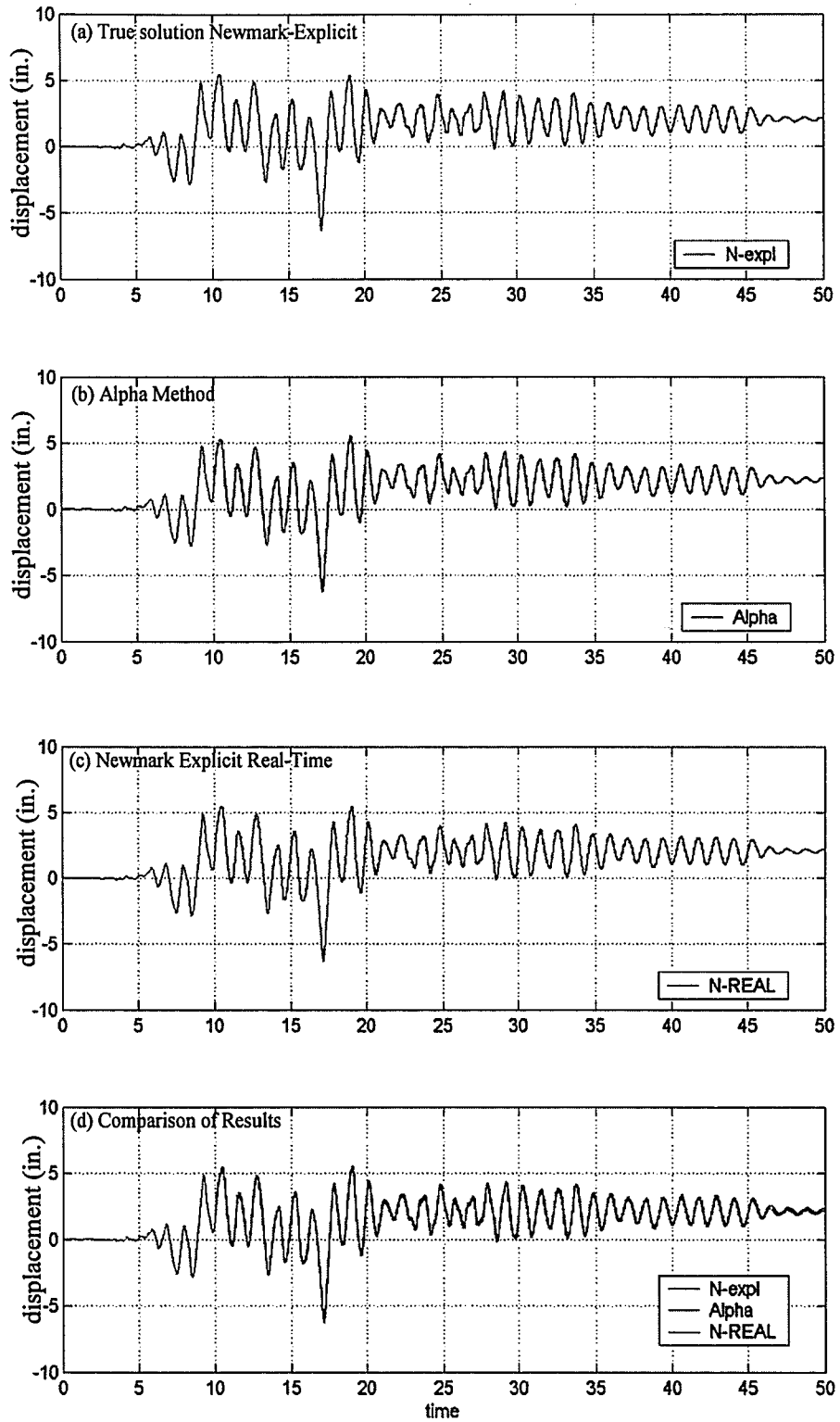
Figure 5.6   Inelastic MRF without VE Dampers– Story 1

87
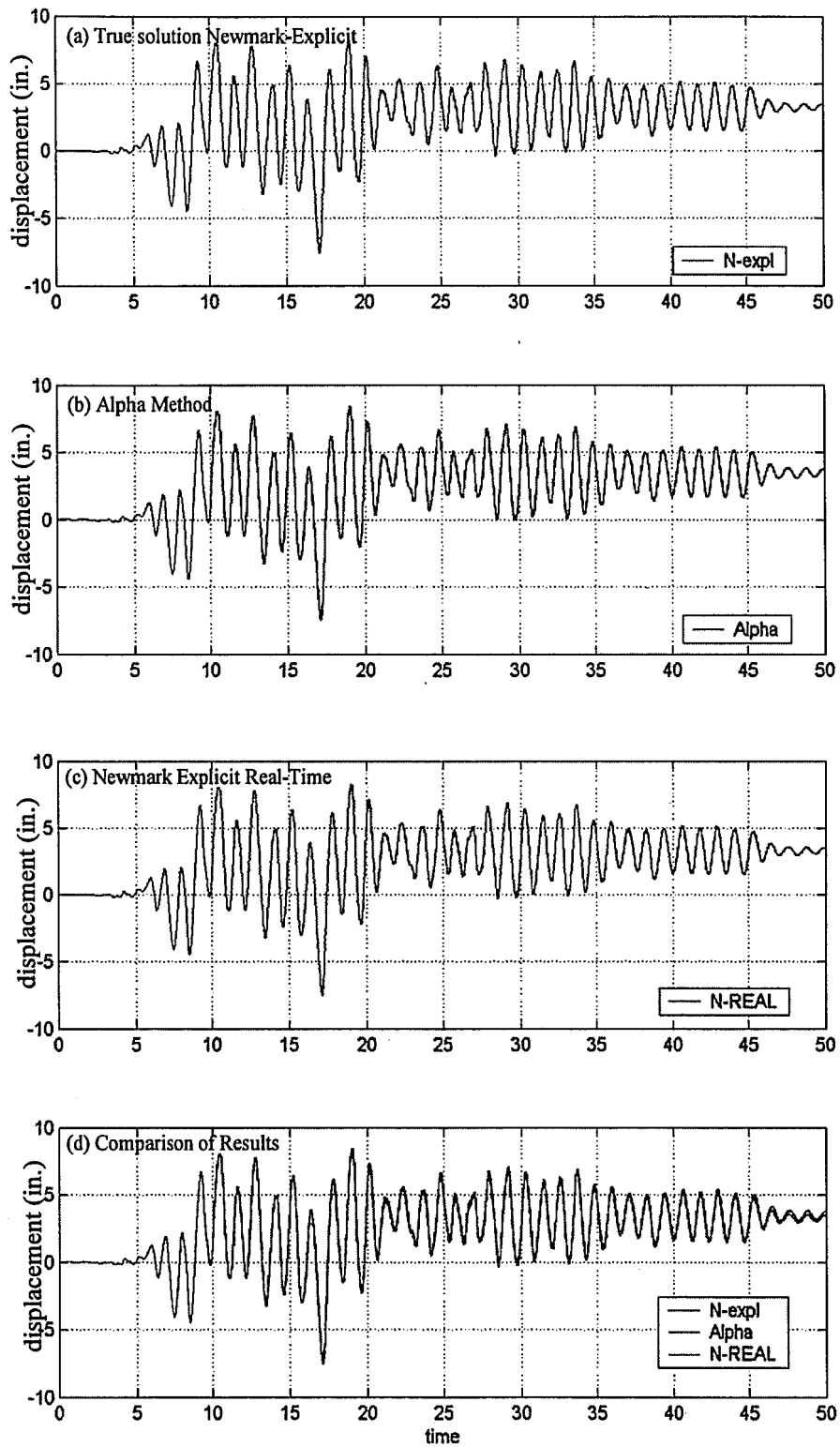
Figure 5.7   Inelastic MRF without VE Dampers – Story 2
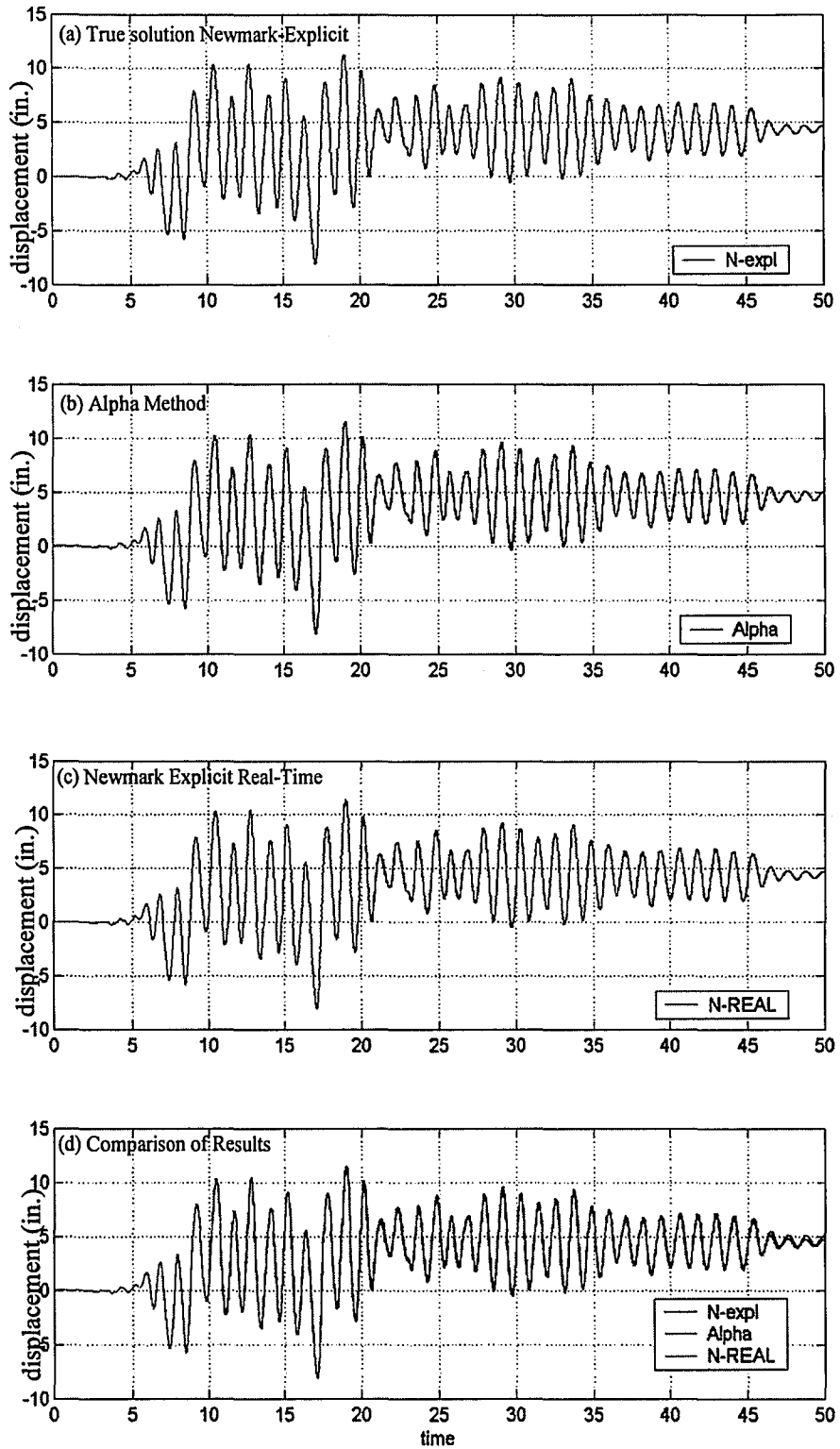
Figure 5.8 Inelastic MRF without VE Dampers – Story 3
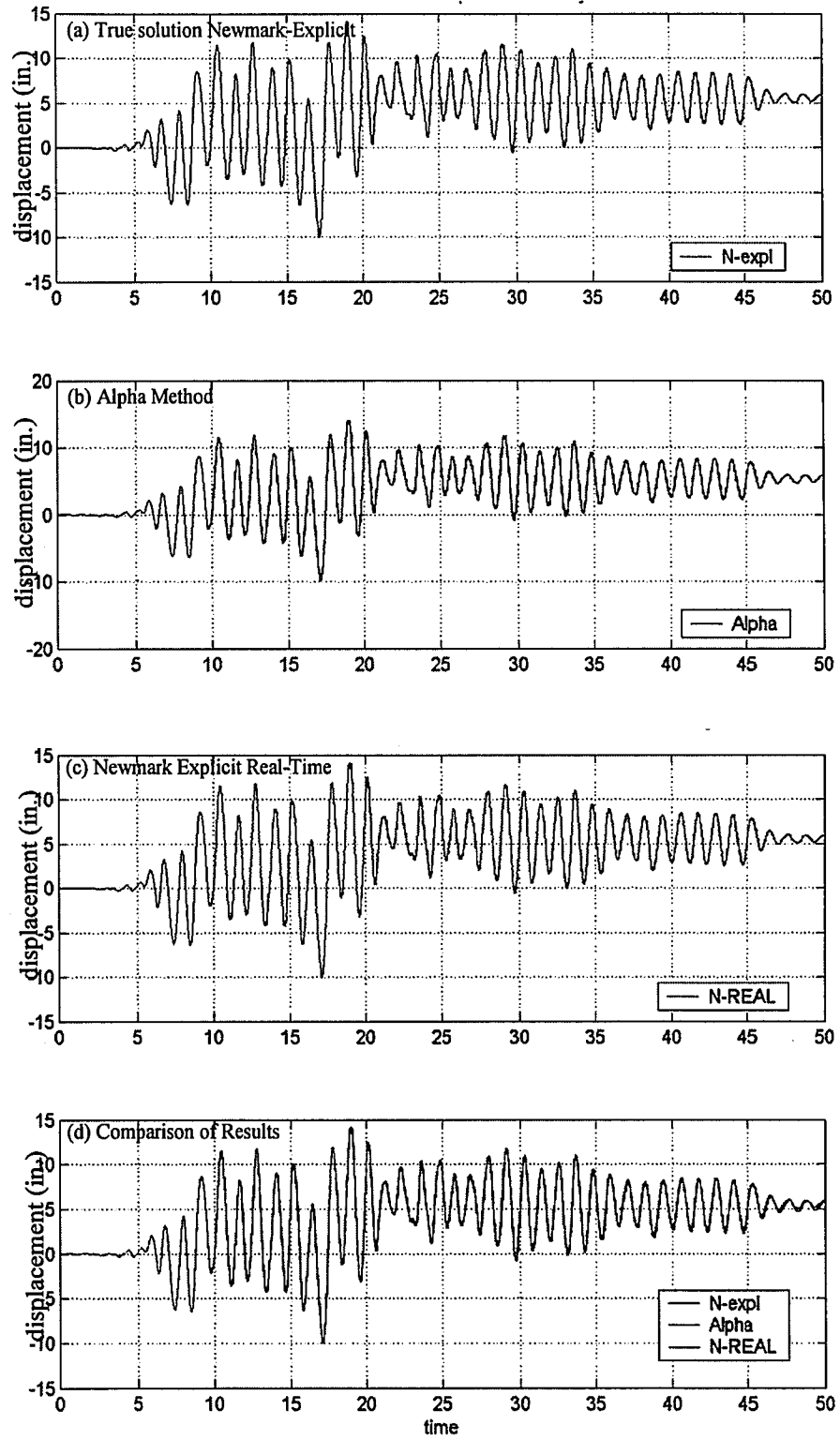
Figure 5.9   Inelastic MRF without VE Dampers – Story 4
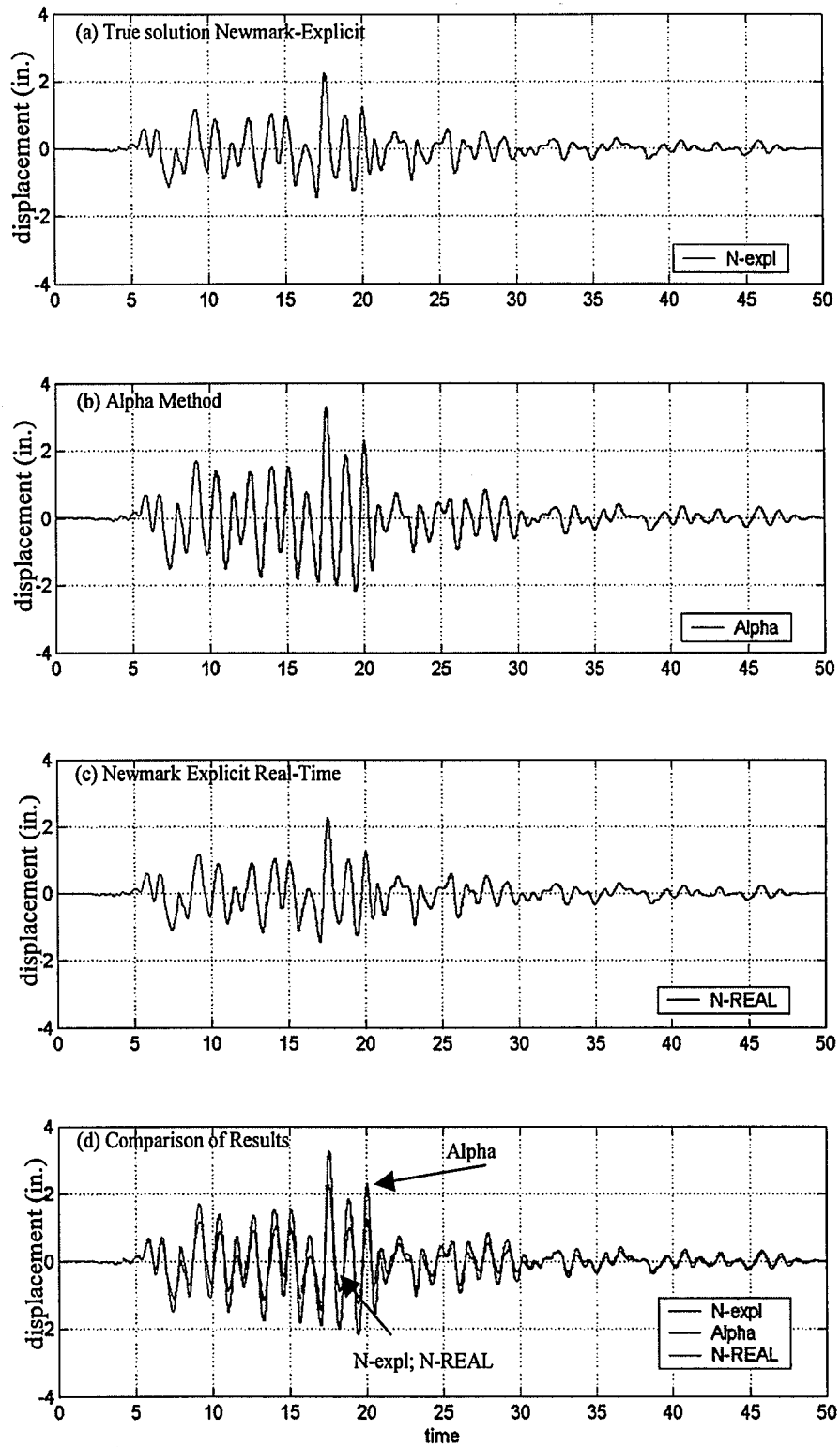
Figure 5.10   Linear MRF with VE Dampers - Story 1

91
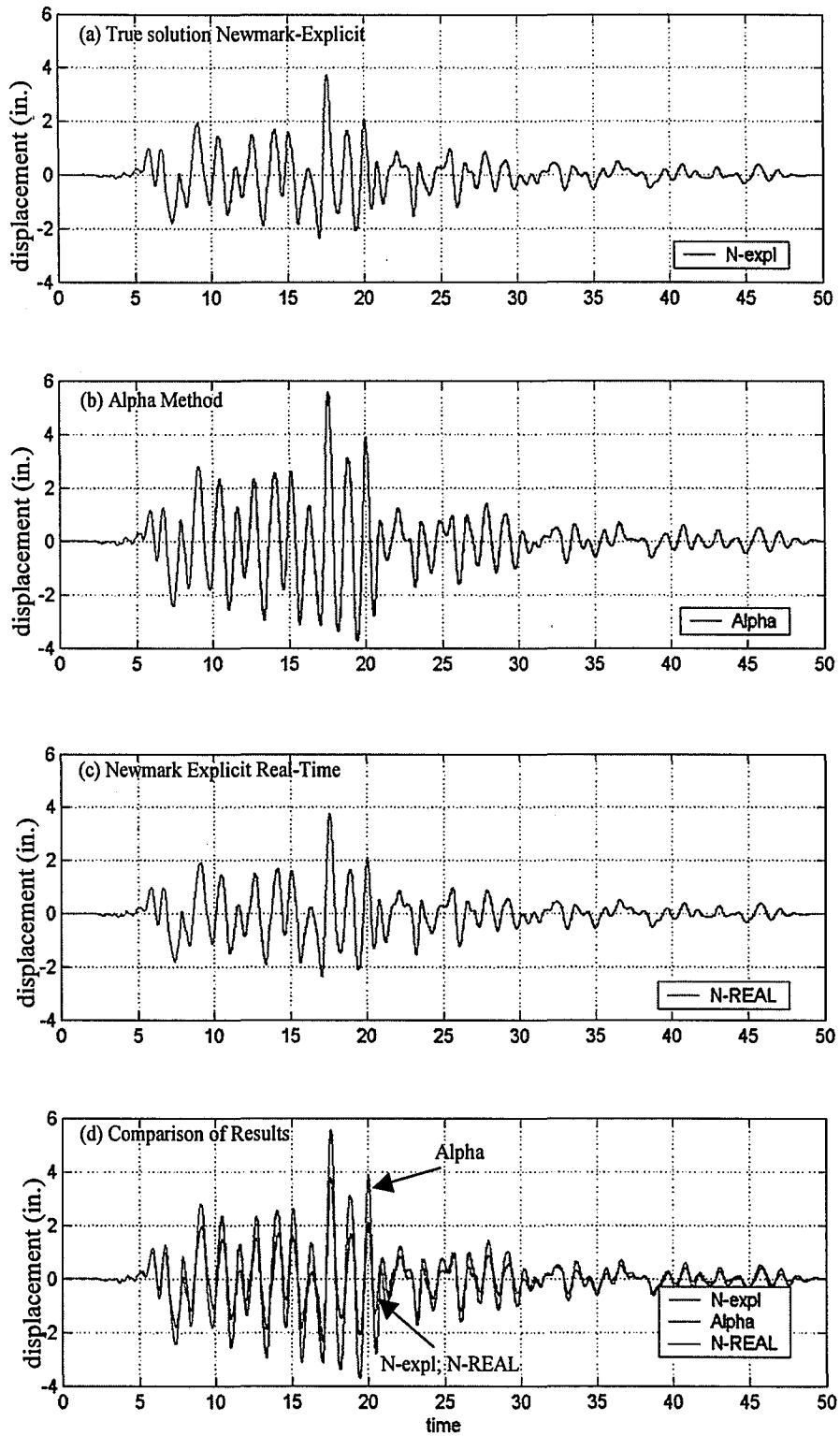
Figure 5.11   Linear MRF with VE Dampers – Story 2
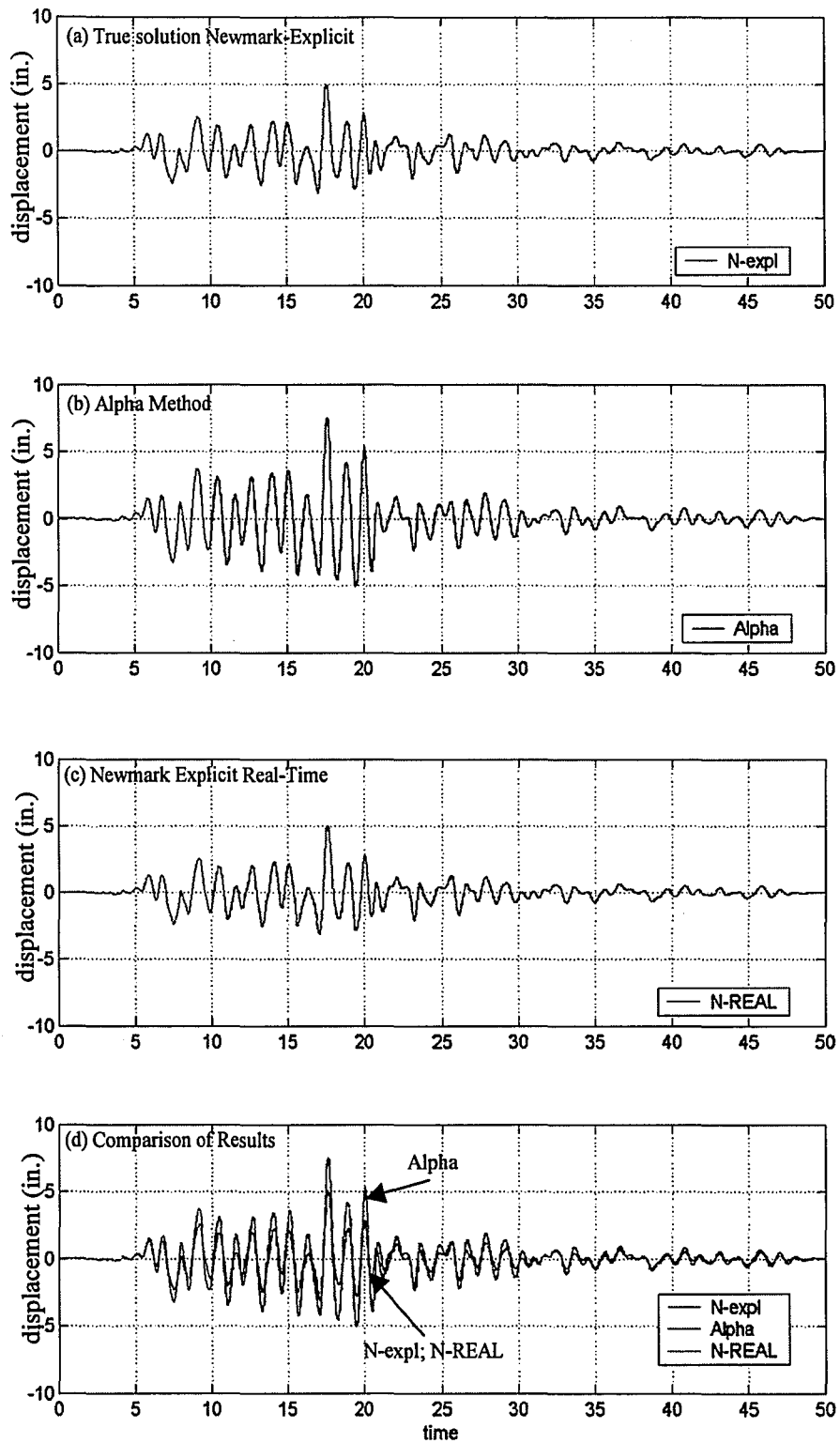
Figure 5.12   Linear MRF with VE Dampers –Story 3

93
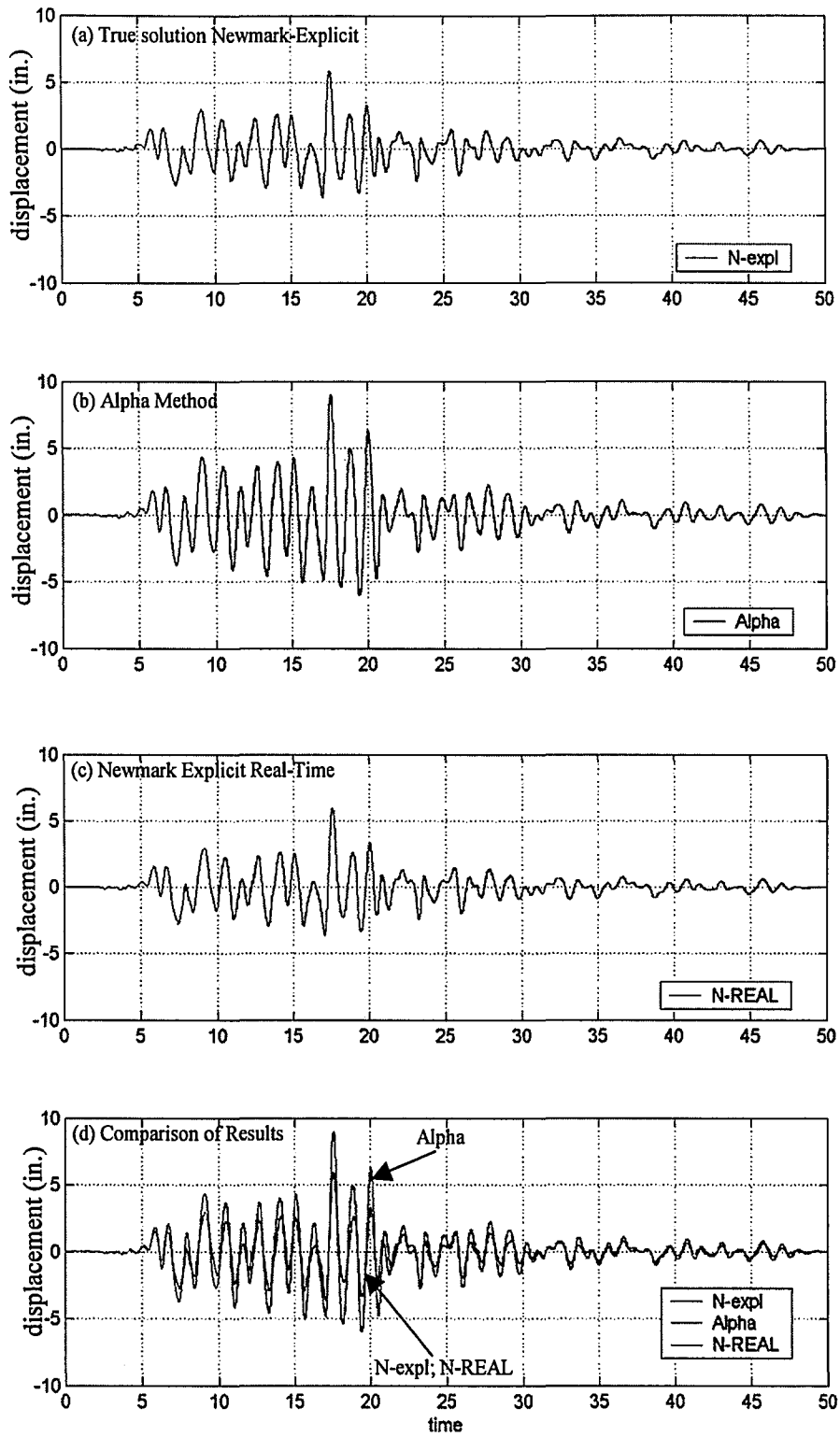
Figure 5.13   Linear MRF with VE Dampers – Story 4
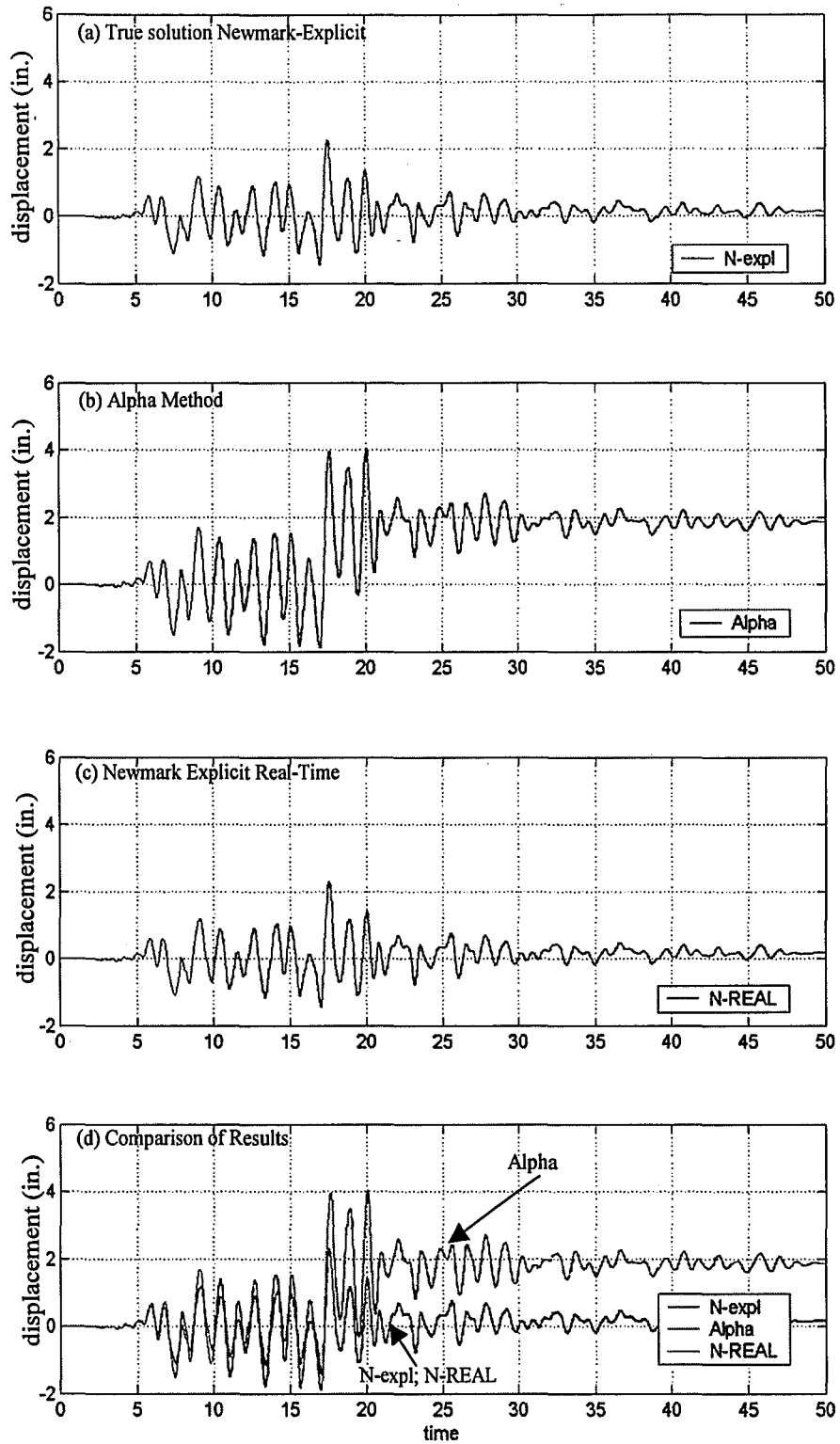
Figure 5.14   Inelastic MRF with VE Dampers– Story 1

95
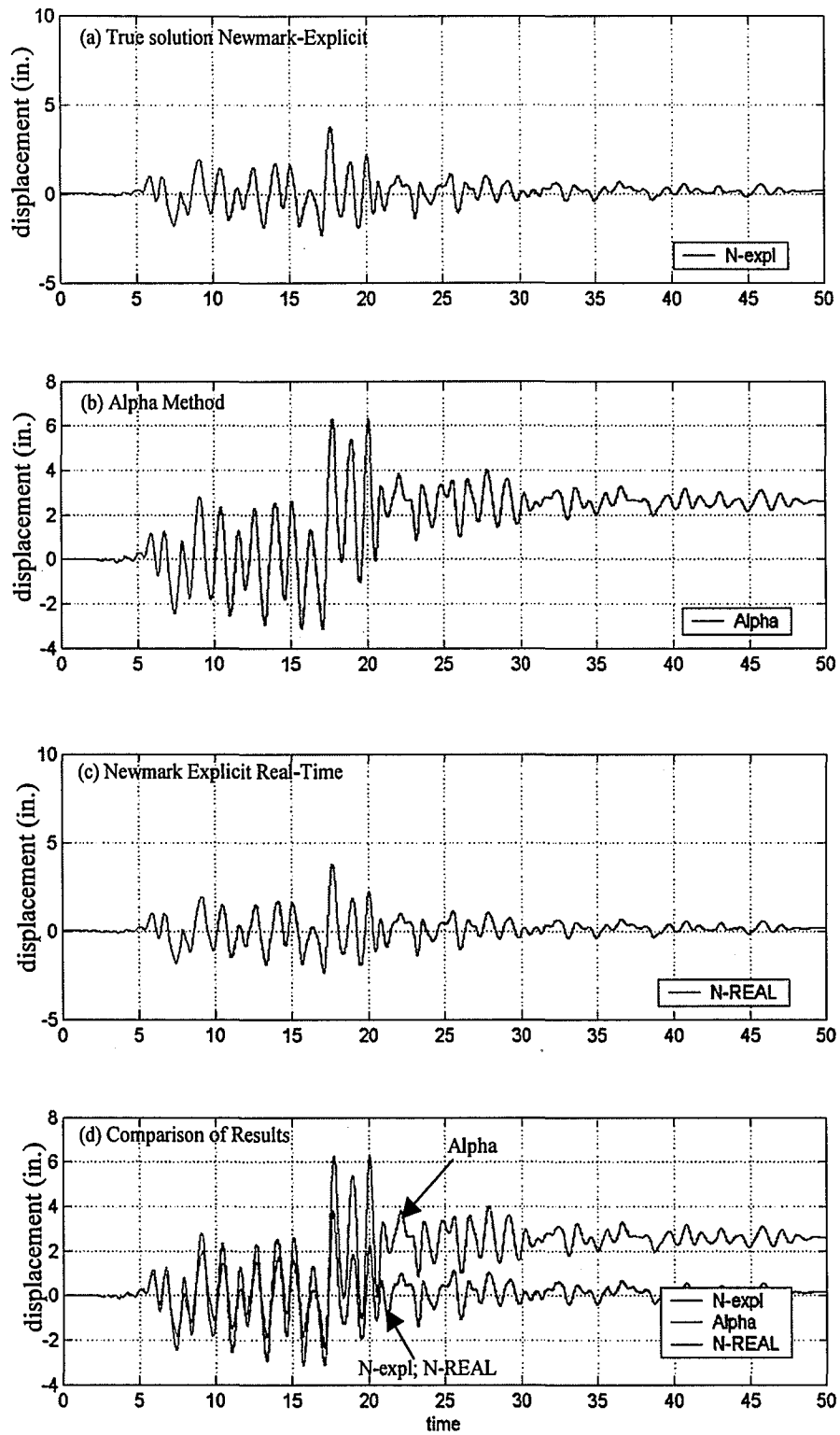
Figure 5.15 Inelastic MRF with VE Dampers – Story 2
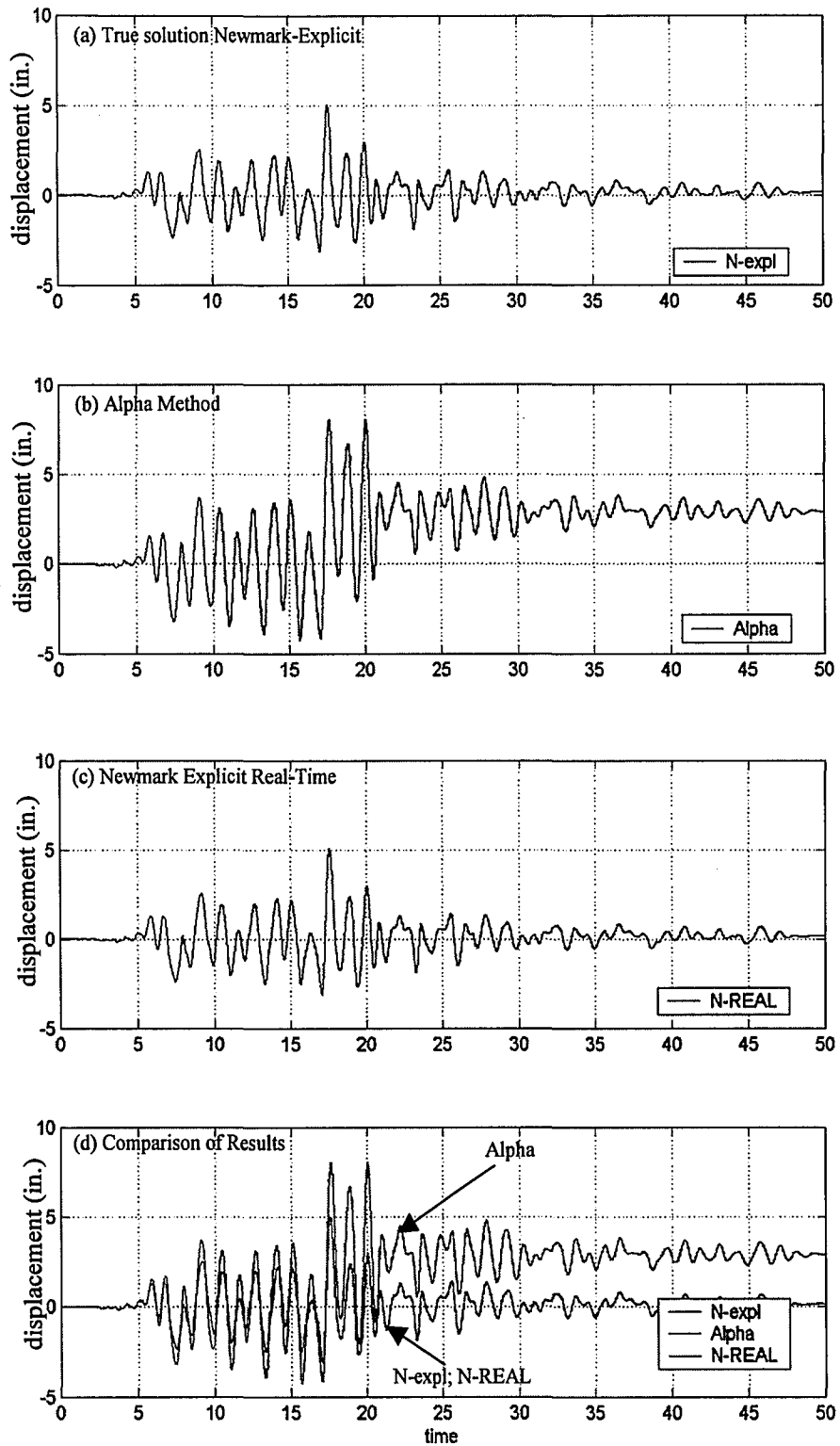
Figure 5.16   Inelastic MRF with VE Dampers – Story 3

97
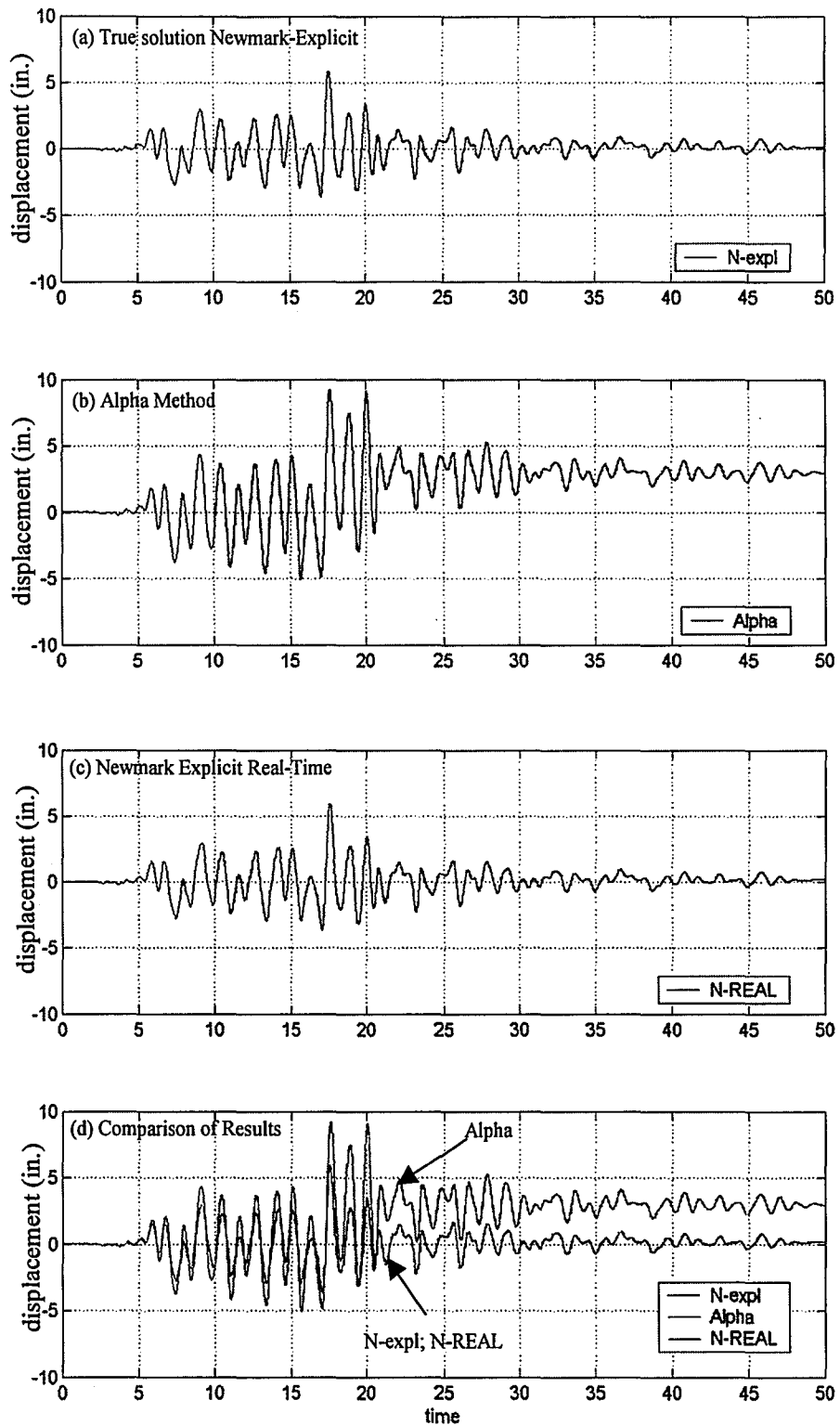
Figure 5.17 Inelastic MRF with VE Dampers – Story 4
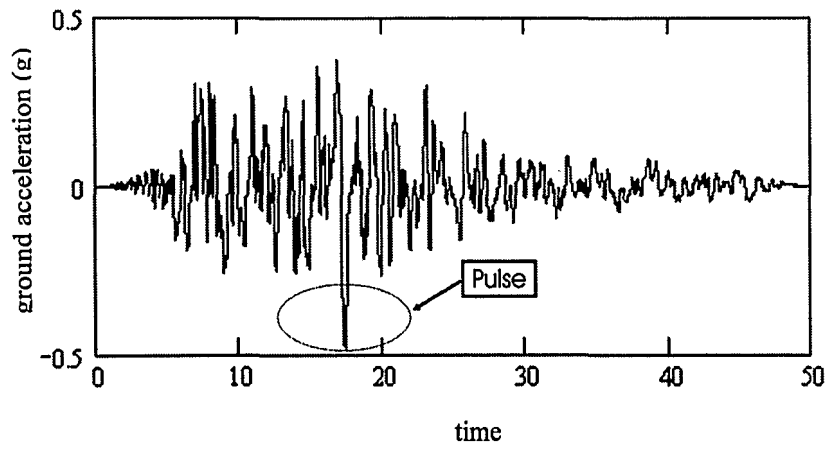
Figure 5.18   Northridge EQ (Canoga Park Station) Scaled to DBE Level
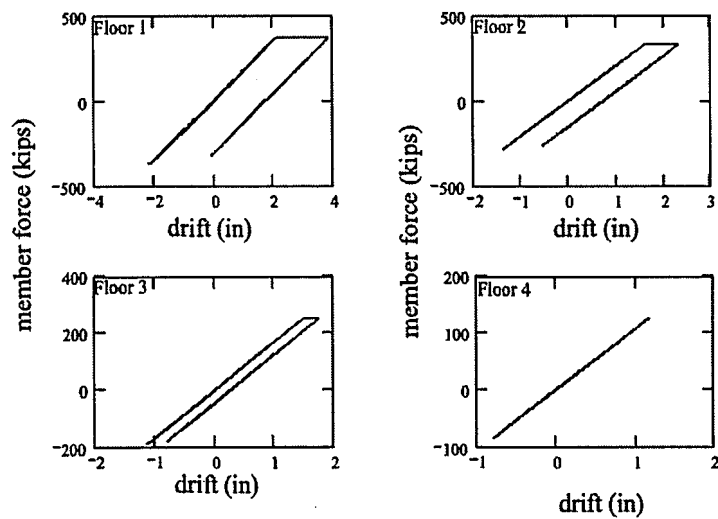
Figure 5.19   Frame Shear – Drift Response

99
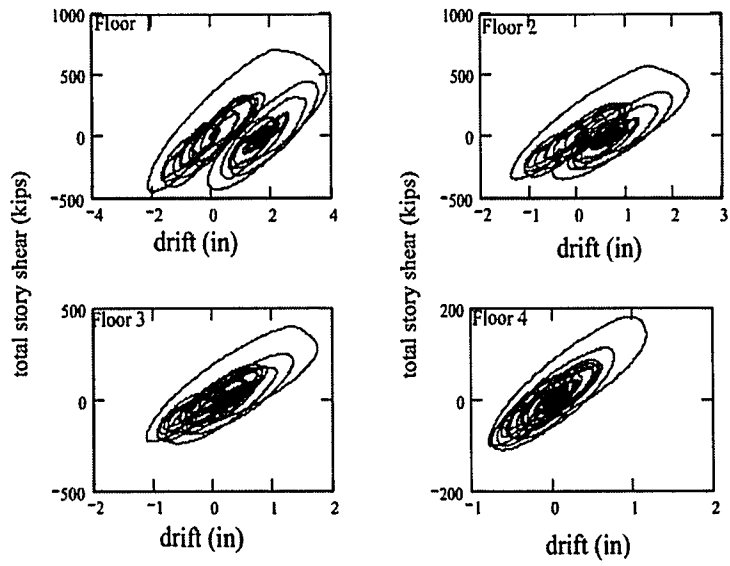
Figure 5.20   Total Story Shear – Drift Response

100

Chapter 6 Rate-Dependent Force Effect

6.0 General

This chapter presents the apparent velocity characteristics of the selected three integration algorithms in order to clarify their rate-dependent restoring force features, and explain the reason for the differences in the response observed in the numerical simulations of the rate-dependent PSD tests.

6.1 Apparent Velocity Characteristics of the Algorithms

As noted previously, when a structure is equipped with rate-dependent devices such as VE dampers or rubber bearings, conventional PSD testing based on quasi-static loading is no longer capable of simulating the true earthquake response. For such a case the test should be conducted in, or near real-time. This cannot be achieved by using conventional PSD testing algorithms and performing the test quickly.

To ensure continuous loading in real time, the numerical integration algorithm used should be able to have the next time step target displacement ready, prior to when the current time step loading is completed. Various attempts have been made in modifying some of the existing explicit and implicit algorithms to satisfy this requirement (see Chapter 2).

During a real-time PSD test, the actuators' task in each step is to apply the target displacement over the time step duration. If the integration time step used is small, the velocities with which the actuators are moving can be calculated by dividing the

displacement increment by the time step size. This "apparent velocity" is the velocity that the structure actually experiences during the test.

As mentioned in Chapter 5, the integration algorithm used is very important for a real-time PSD test to simulate the true seismic response of a structure with rate-dependent components. If the algorithm can provide displacement increments in such a way that the apparent velocities (the velocities experienced by the test structure) match the velocities that would occur during the real earthquake (calculated velocities), the test specimen will develop as much resisting force as it would under the real seismic event and therefore the simulation is realistic. Otherwise, when the apparent velocities deviate from the calculated ones, the displacements and restoring forces developed in the dampers and the overall response obtained from the test are not correct.

In 1992 Nakashima et al. tested (1992) an SDOF system with velocity dependent characteristics using a staggered central difference algorithm, as explained in Section 2.4. To check the accuracy of the velocity control, they compared the computed velocity with the velocity achieved during the test and found a good agreement. The achieved velocity was estimated by differentiating the displacement measured by the LVDT which monitored the structural displacement, which is the same way that the 'apparent velocity' is defined in Section 4.3.2 provided that a small enough time step is used.

In this chapter, the apparent velocity characteristics of the selected three integration algorithms used in the PSD test simulations are examined in order to evaluate their rate dependent force features. The results from the numerical simulations of PSD tests of the inelastic MRF without the VE dampers are presented. This case (identified as Case 2 in

102

Chapter 5) has the largest velocity developed at the DOFs, and for that reason was selected to study the apparent velocity characteristics of the different algorithms. Only time history plots related to the first story response are given. The 'calculated velocity' quantities are those computed by the integration algorithm. The 'apparent velocity' quantities are calculated by dividing the displacement increment by time step size, or in the case of the Alpha Method, the time substep size (i.e., the time between iterations).

6.1.1 Newmark Explicit Method

Figure 6.1(a) shows the comparison of the apparent and calculated velocities for the complete time history, where it can be seen they are almost identical. The time step size used in the simulations was 0.005 sec. This good agreement can also be observed in Figure 6.1(b) where the response over a 0.5 sec duration is shown.

6.1.2 Alpha Method with Fixed Number of Iterations

The velocity calculated by the algorithm and the apparent velocity do not show a very good agreement when the Alpha Method is used.

As explained in Chapter 3, the Alpha Method is an implicit algorithm, which requires iterative corrections for nonlinear systems. Conventional Newton iteration leads to decreasing incremental corrections in successive iterations as the solution converges towards the exact solution. This is undesirable for a real-time PSD test, because either the actuators have to slow down or the signals have to be sent to the actuator controllers at an increasing speed during the iterations. To avoid this problem, an alternative approach was

adopted where a more or less uniform incremental correction is provided in each time step (Shing et al., 2002).

During the simulations with the Alpha Method, ten iterations were performed in every time step. Since the time step size was $\Delta t = 0.02$ sec., the sub step size for each iteration become $\delta t = 0.002$ sec. The effect of this uniform incremental correction approach on the apparent velocity characteristics can be observed from the magnified plots shown in Figure 6.2 (b and c). The apparent velocity, the velocity with which the actuators are actually leading the structure during the test, remains almost constant within the time step. At the end of each time step a sudden change in velocity occurs, generating additional accelerations hence inertial forces.

These phenomena would lead to unrealistic results if a PSD real-time test were performed in a structure with rate-dependent elements.

6.1.3 Newmark Explicit Real-Time Method without Alpha-Beta Tracker Filter

In the Newmark Explicit Real-Time Method, the basic idea is to perform independent integrations for the even and odd time steps (staggered integration) in order that the scheme provides the next time step target displacement prior to the completion of the current time step loading.

Figure 6.3 compares the calculated and apparent velocity from the PSD test simulations for a rate-independent structure performed using the Newmark Explicit Real-Time method with staggered integration. In the simulations, a time step size of $\Delta T = 0.01$

seconds between odd and even time steps respectively with 0.005 sec. $\Delta t = 0.005$ sec. between an odd and even successive time step.

It is evident in Figure 6.3 that there is an oscillation of high frequency that exist in the apparent velocity. This apparent velocity oscillation is due to the fact that the even and odd time step displacements are calculated only from the previous even time step and odd time step information, respectively, leading to local maxima and minima in the displacement response history when the actuators apply the even and odd time step displacements one after the other (see Figure 6.4).

6.1.4   Newmark Explicit Real-Time Method with Alpha-Beta Tracker Filter

The above mentioned apparent velocity problem can only be solved if the information is shared between the even and odd time steps. The Alpha-Beta Tracker filter removes the high frequency in the apparent velocity, by correcting the calculated displacement in each time step using the corrected displacement and slope estimate quantities from the previous time step (see Section 3.4.2).

With the sudden changes in the slope of the displacement history removed, there are no high frequencies artificially introduced into the apparent velocity. Figure 6.5 shows that the apparent and calculated velocities have good agreement when the Alpha-Beta Tracker filter is incorporated into the staggered Newmark Explicit Real-Time Method. This simulation had a similar time step size as that in the simulations using the Newmark Explicit Real-Time Method without the Alpha-Beta Tracker filter.

6.1.5   Rate Dependent Real Time PSD Simulations

The comparison of the restoring forces in the dampers from the numerical simulations of PSD test of the elastic MRF with VE dampers are shown in Figure 6.6. As noted previously, the VE damper forces were calculated based on the apparent velocities, where only the forces from the first story are shown. The simulations involved using the two real-time PSD algorithms: (1) Alpha Method with a Fixed Number of Iterations and, (2) Newmark Explicit Real-Time Method. The results from these simulations are compared to the 'true solution' obtained from Newmark Explicit algorithm which also uses the apparent velocity in damping force calculations and has a time step size of $\Delta t = 0.005$ sec.

For the linear MRF with the VE dampers, as can be seen from Figure 6.6, the restoring force from Newmark Explicit Real-Time algorithm agrees well with the 'true solution'. The Alpha Method with a Fixed Number of Iterations, on the other hand, cannot develop as much resisting force in the dampers and does not agree well with the 'true solution'.

6.2   Summary

The numerical simulations of the rate dependent PSD tests were performed for an MRF with VE dampers. The restoring forces from the dampers were calculated using the Generalized Maxwell Model. Since the 'apparent velocity' is the velocity that the test specimen will experience during real-time PSD test, the governing equations of motion of the Generalized Maxwell Model were integrated using this 'apparent velocity' relationship between displacement increment and velocity (see Chapter 4). This ensured

106

that the restoring forces that would develop in the dampers during the real-time PSD test would be calculated accurately in the numerical simulations.

Although it is not capable of performing real-time PSD testing, the response using the Newmark Explicit algorithm is accepted as the 'true solution' for both rate-dependent and rate-independent PSD test simulations. This is based on selecting a small enough time step, from a convergence study (see Chapter 5) to ensure the accuracy of the solution. Because the apparent and calculated velocities are almost the same for the Newmark Explicit algorithm, the dampers subjected to these apparent velocities in real-time testing will develop realistic resisting forces, simulating what would occur under the real earthquake.

In the rate-dependent PSD test simulations it was observed that the Alpha Method with a Fixed Number of Iterations gave larger displacements and permanent drifts than the 'true solution'. This is due to the fact that the apparent velocity is more or less constant in each time step, resulting in the dampers not developing as large a restoring force. Therefore, it can be concluded that, the use of the Alpha Method with a Fixed Number of Iterations could lead to incorrect results in a PSD real-time test of a structure with rate-dependent elements.

Prior to the introduction of the Alpha-Beta Tracker filter to the Newmark Explicit Real-Time Method having staggered integration, there existed a stability problem for the rate-dependent simulations. This was due to the calculated restoring forces becoming very large (more than 10^{307} kips) due to the apparent velocity characteristics explained in Section 6.1.3. The filter improved the apparent velocity features (Section 6.1.4), and the

Newmark Explicit Real-Time Method became stable and displayed good agreement with the 'true response'.

(a) Complete Time History

(b) Selected Time Window
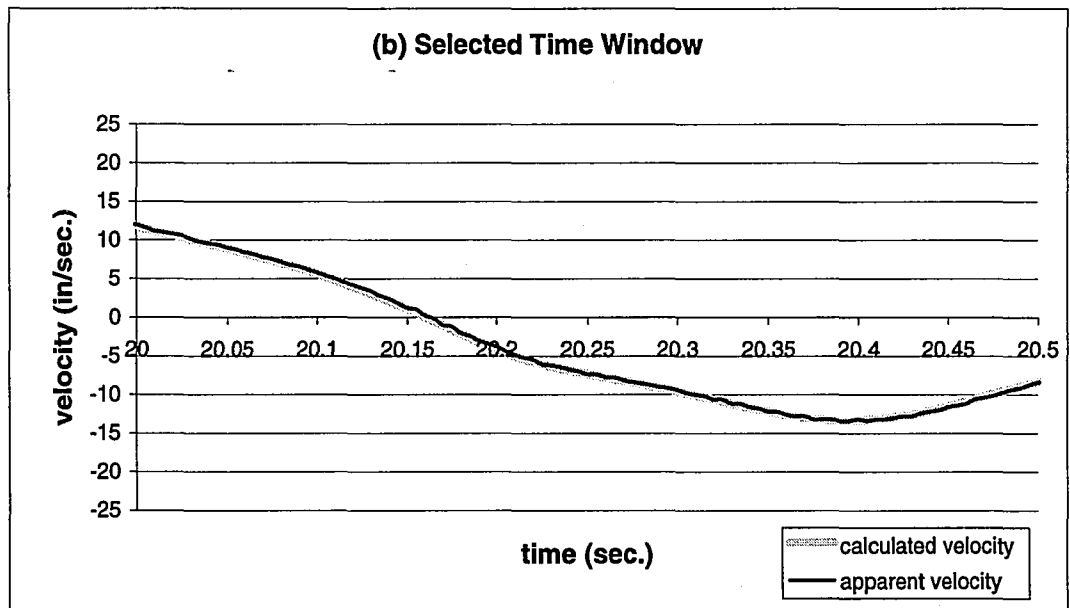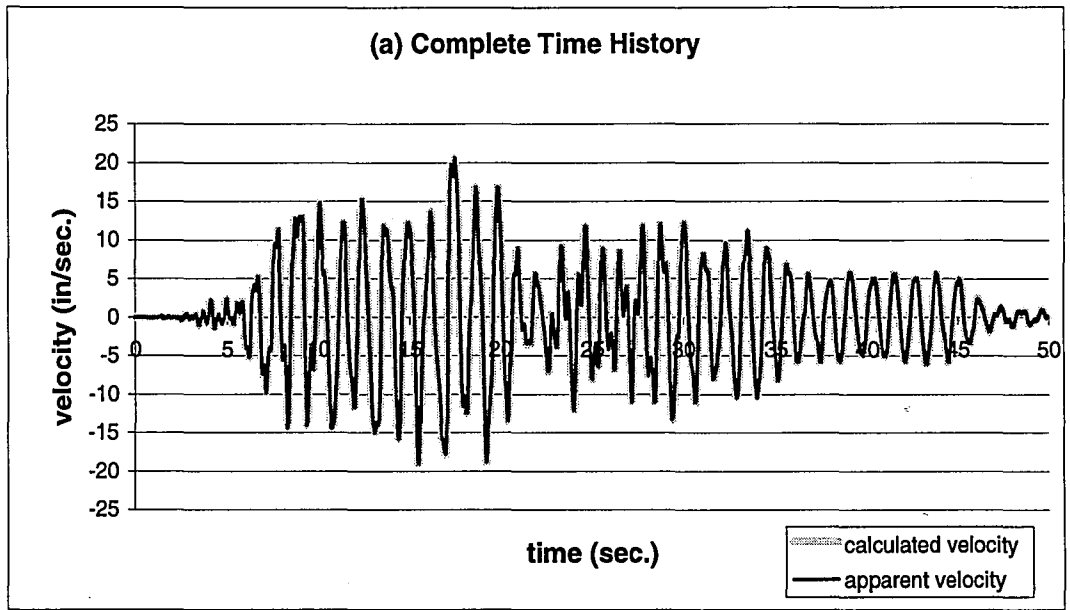
Figure 6.1 Comparison of Apparent and Calculated Velocity

for Newmark Explicit Method, Inelastic MRF without VE Dampers

109

(a) Complete Time History

(b) Selected Time Window
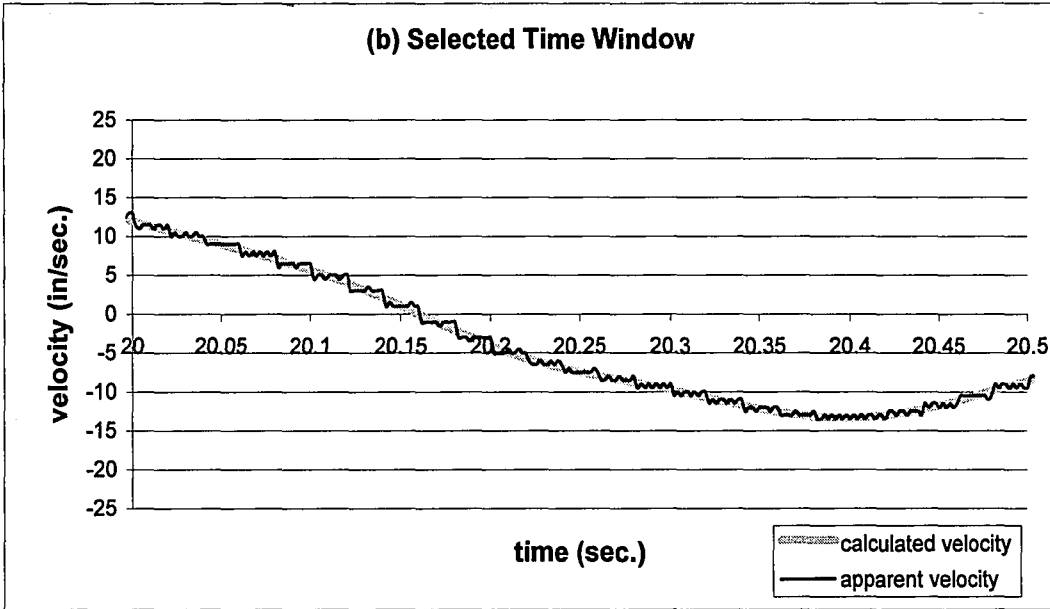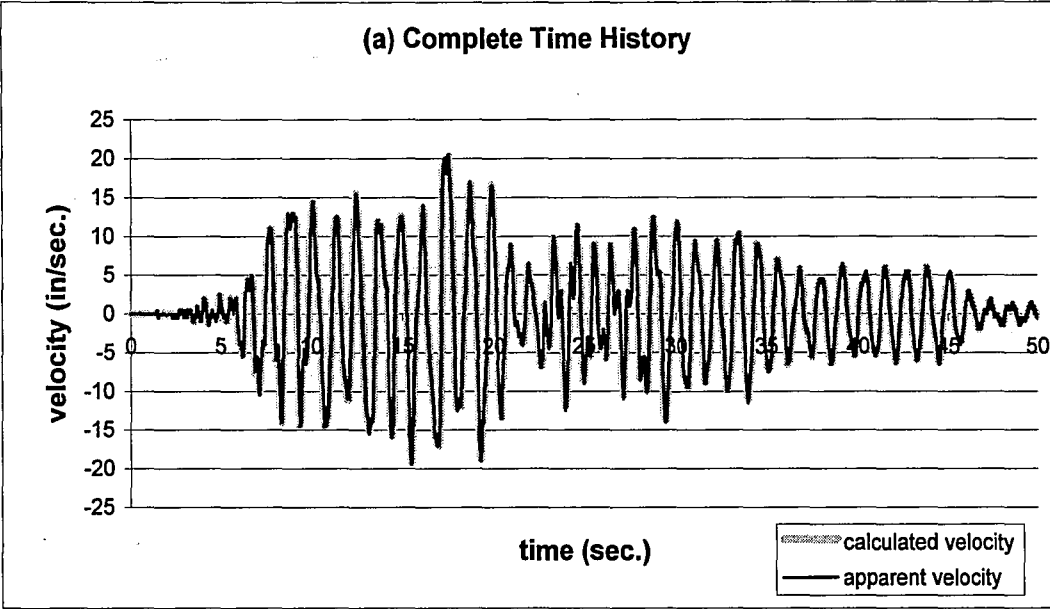
Figure 6.2 Comparison of Apparent and Calculated Velocity

for Alpha Method with a Fixed Number of Iterations, Inelastic MRF without VE Dampers

110
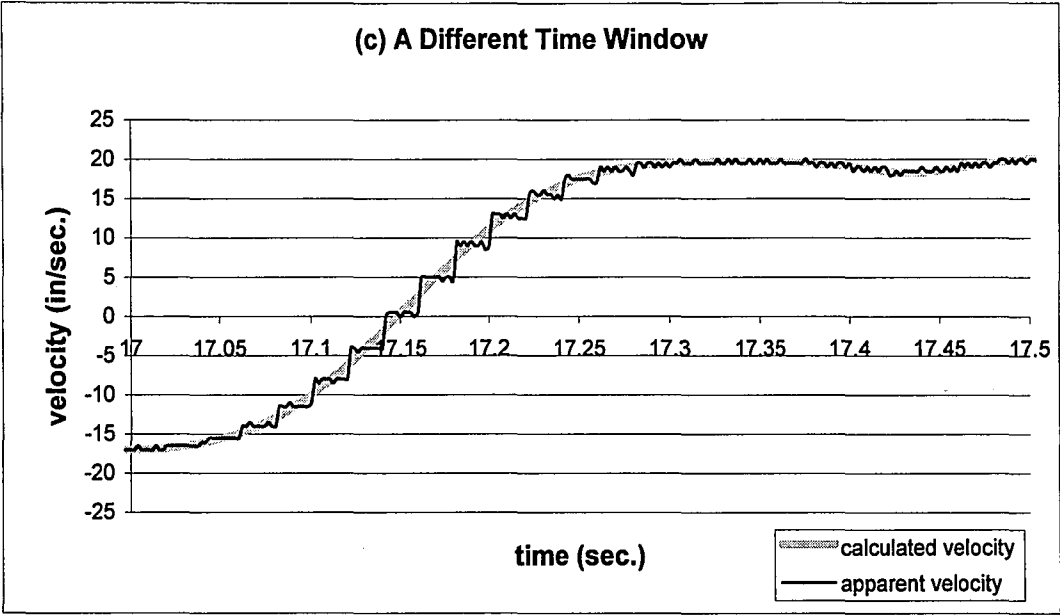
Figure 6.2 (Continued) Comparison of Apparent and Calculated Velocity for Alpha Method with a Fixed Number of Iterations, Inelastic MRF without VE Dampers

(a) Complete Time History

(b) Selected Time Window
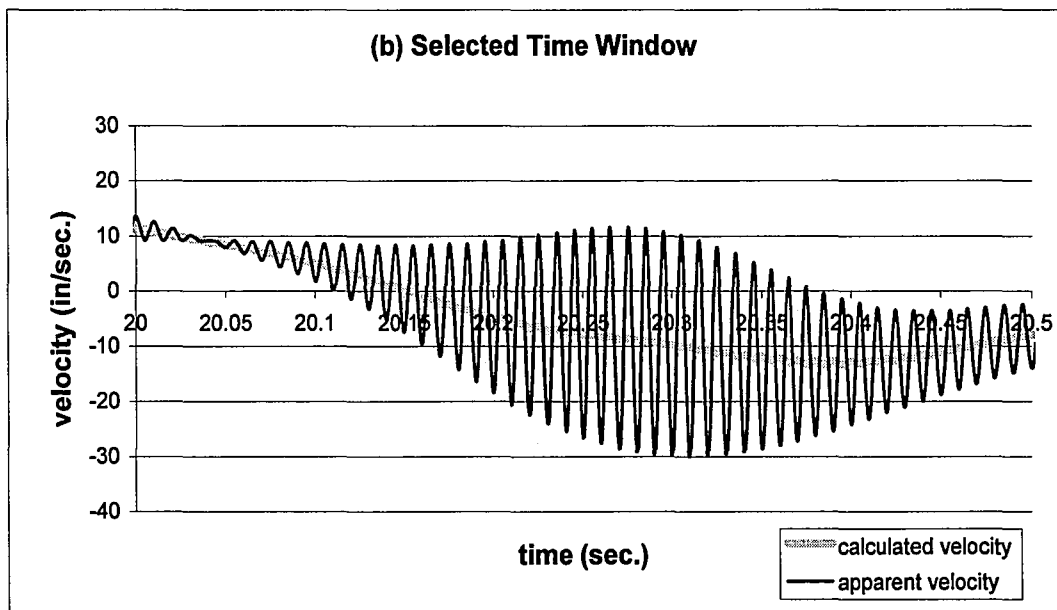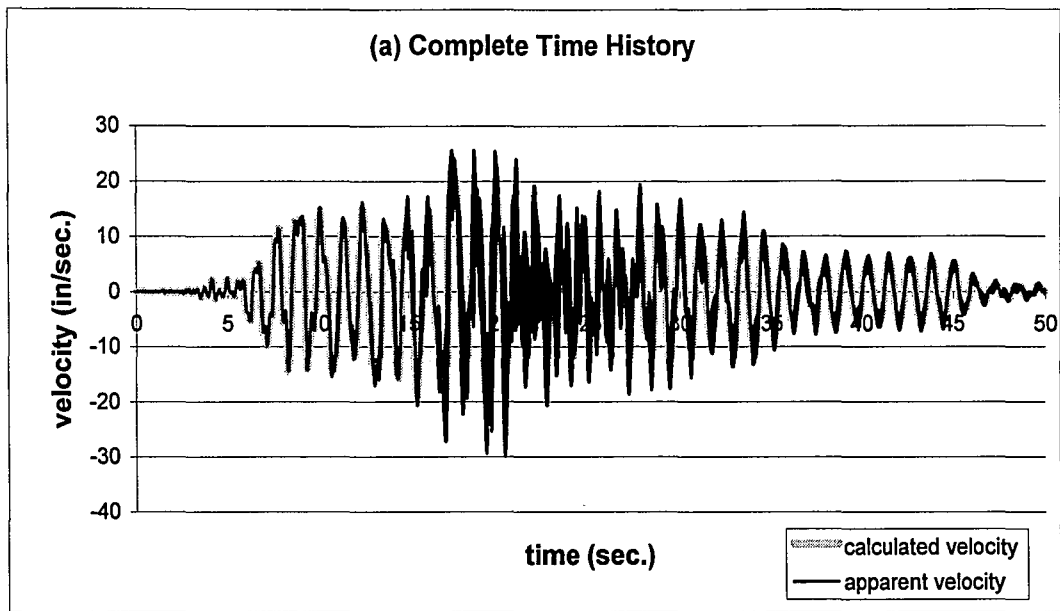
Figure 6.3   Comparison of Apparent and Calculated Velocity
for Newmark Explicit Real-Time Algorithm without Alpha-Beta Tracker Filter,
Inelastic MRF without VE Dampers

112
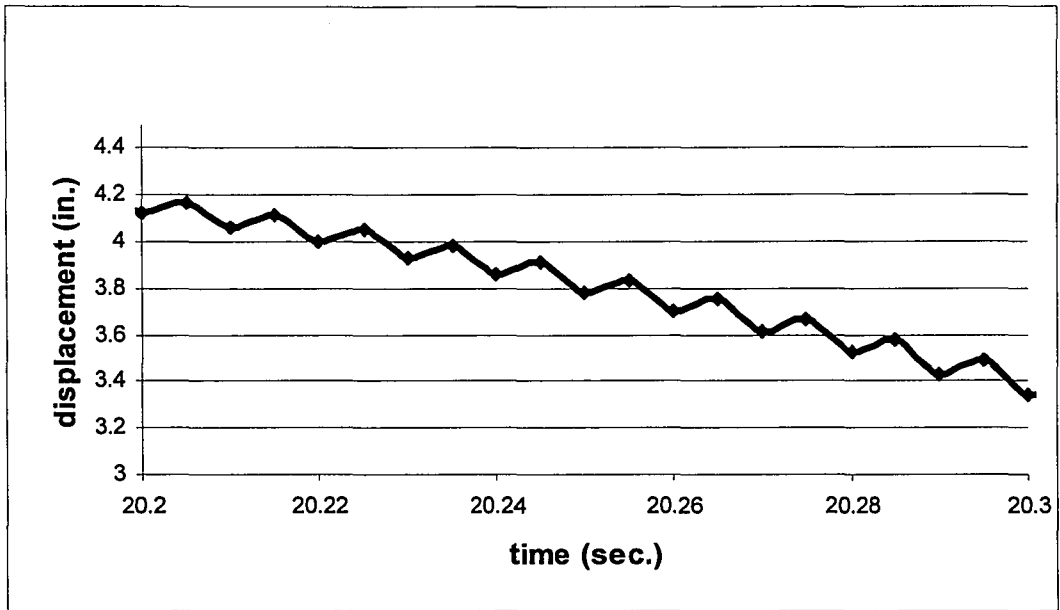
Figure 6.4 Local Maxima and Minima

in Displacement Response History Resulting from the Staggered Integration

113
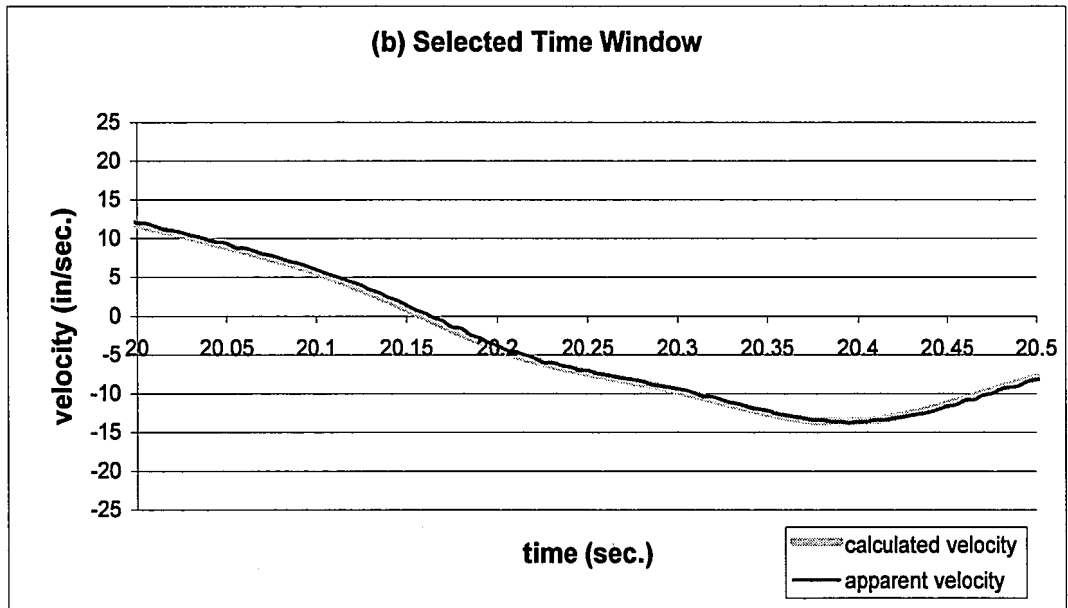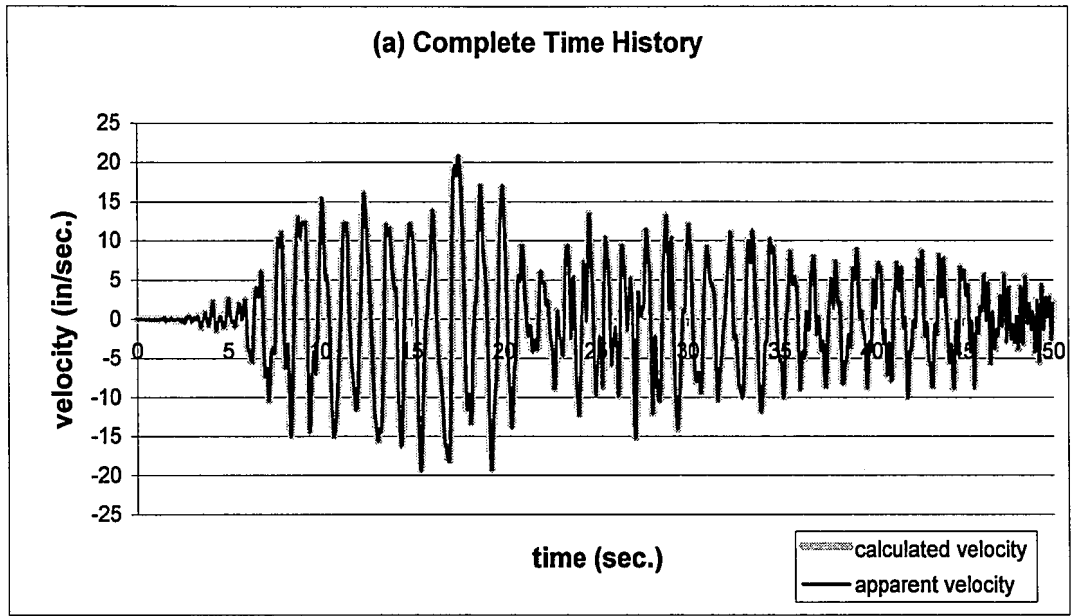
Figure 6.5 Comparison of Apparent and Calculated Velocity

for Newmark Explicit Real-Time Algorithm with Alpha-Beta Tracker Filter,

Inelastic MRF without VE Dampers

114
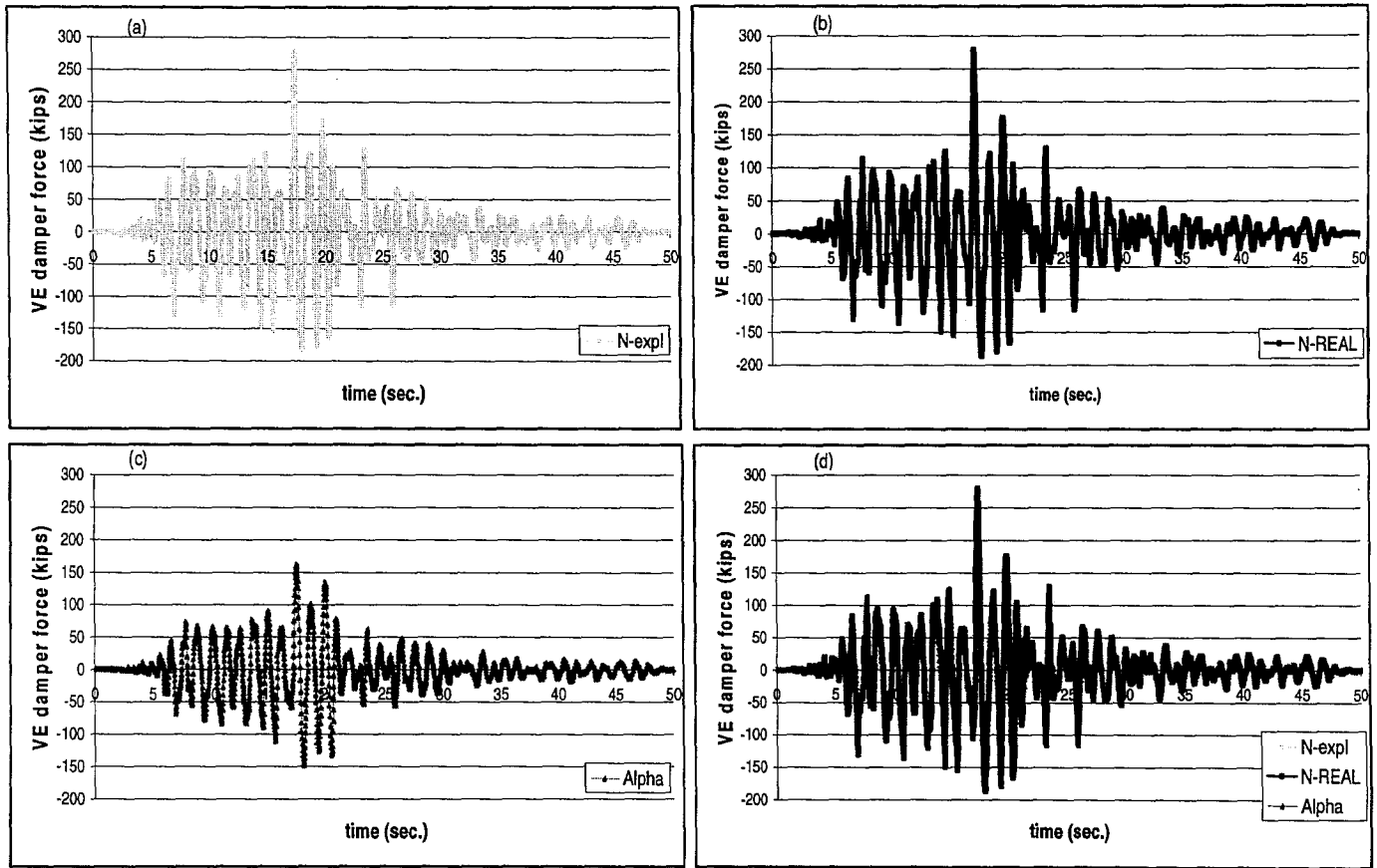
Figure 6.6   Comparison of VE Damper Force, Linear Elastic MRF with VE Dampers

Figure 6.6   Comparison of VE Damper Force, Linear Elastic MRF with VE Dampers
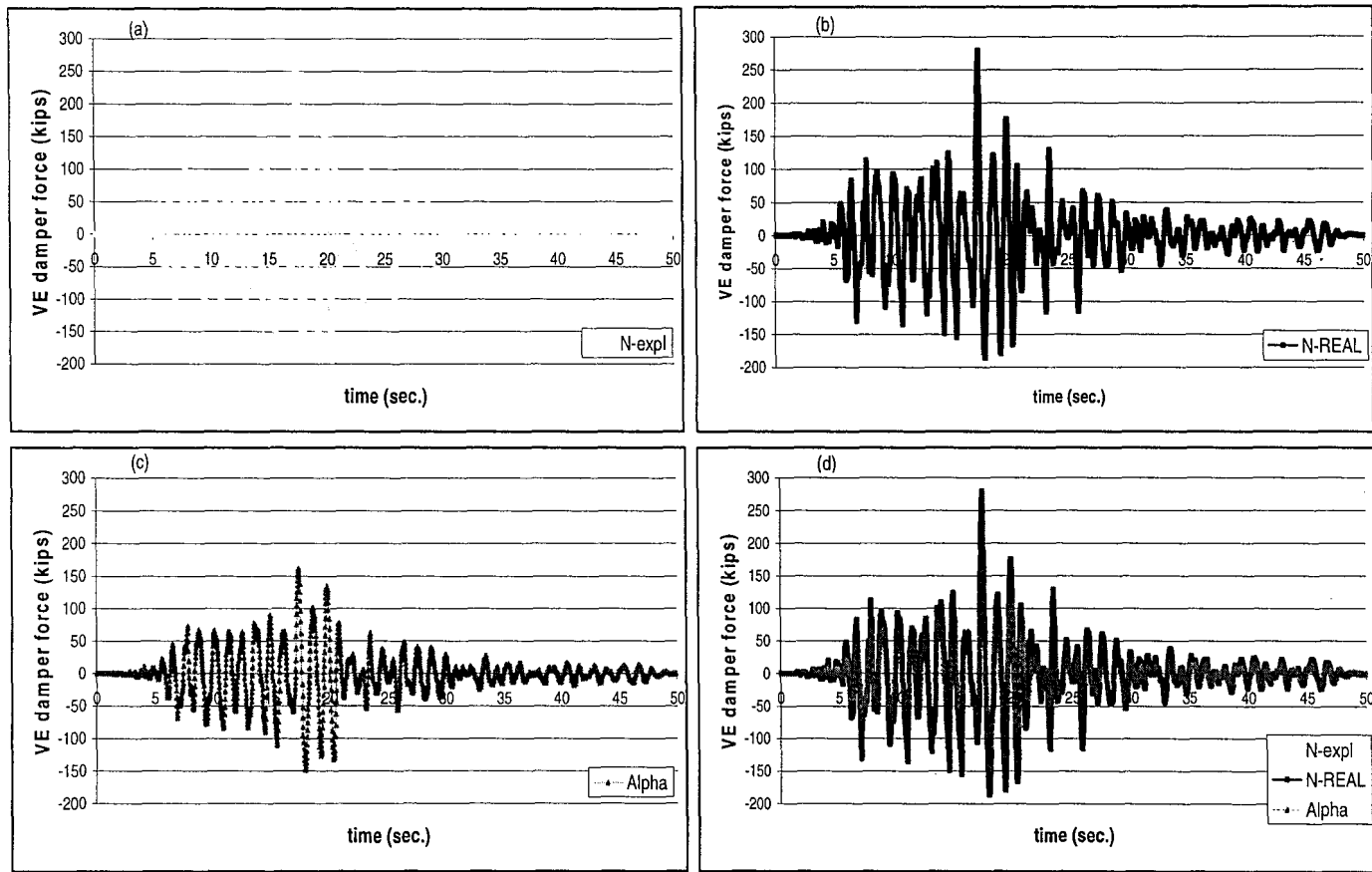
115

Chapter 7 Error Propagation Analysis Background

7.0 General

This chapter gives the background information related to the error propagation analysis that was conducted on the three PSD testing algorithms. After classifying the experimental errors, previous studies on this subject are presented. The error types and the considered combination cases of these errors for which the numerical simulations were performed are also explained.

7.1 Error classifications

Errors are inevitable during a PSD test, due to reasons such as electrical noise, loss of significant figures in analog to digital conversion, as well as the resolution and accuracy limitations of measurement and control instruments. In order for the experimental results to be acceptable, the errors introduced should be reasonably small. Although these errors cannot be completely eliminated, one can reduce their magnitudes considerably with a careful setup and good instrumentation.

In the pseudodynamic test method, the restoring forces of the system are not modeled, rather they are directly measured from the tested structure. This experimental feedback is used in the step-by-step numerical integration. For instance, in a PSD test that uses the Newmark Explicit algorithm for numerical integration, the target displacement for the next step ($i+1$) is calculated using the measured displacement, velocity and acceleration values of the current time step (i). This calculated displacement is imposed to the

116

structure, resisting forces developed in the structure are measured and used to determine the acceleration and velocity of the new step $(i+1)$. Then the target displacement for the next time step (i.e., $(i+2)$) are determined.

Errors introduced in any time step will be carried over to subsequent time steps. Although the magnitudes of the error within each individual step are small, the error can accumulate over the large number of computation steps involved in the test, and consequently the result may diverge significantly from the correct results as the experiment proceeds. The rate of error propagation depends on the numerical scheme used and the nature of these errors.

Shing and Mahin (1983) defined control and measurement errors as the two components of the total feedback error introduced in each time step. The displacement computed in a time step may not be accurately imposed to the structure due to displacement control errors. Moreover, the actually imposed displacement and the restoring force developed by the structure may be incorrectly measured and returned to the computer (measurement errors).

Shing and Mahin (1983) listed the causes of control errors as:

- inaccurate calibration of displacement transducers used in the closed-loop feedback system, which controls the hydraulic actuators.

- resolution limit imposed by the analog to digital (A/D) conversion of control signals transferred by the microprocessors.

- movement or deformation of the test specimen's support.

- response time of the actuators to control signal (i.e., latency between time of command issue and actual actuator movement)

Similarly the measurement errors can be caused by:

- inaccurate measurement transducers.

- the A/D conversion of the data transferred.

- electrical noises.

- frictional forces in actuator system connections.

These control and measurement errors may consist of systematic and random parts. Systematic errors are those for which a regular pattern of occurrence can be identified. They are usually caused by persistent inaccuracy in instrumentation and experimental setup, and can have a significant influence on the experimental results. Fortunately, these errors can often be avoided or reduced to insignificant levels with careful instrumentation and test design.

The causes of systematic errors can be summarized as follows:

- transducer calibration errors.

- actuator displacement errors.

- friction.

- A/D conversion of electrical signals.

- support movement.

• inconsistent actuator motion.

Random errors, on the other hand, don't have a regular pattern of occurrence and are more difficult to predict and control.

They result from many causes including:

• random electrical noise in wires and the electrical system.

• random rounding off or truncation in the A/D conversion of electrical signals.

• inconsistent actuator motion.

• transducer readings contaminated by some external mechanical disturbances.

Random errors can be so irregular that no specific physical effects can be anticipated.

Nakashima and Kato (1987) examined the stages in which the experimental error could be generated during testing. The conclusions are summarized in a flow chart in Figures 7.1 and 7.2.

As can be seen from above, there are several source of error in the closed loop of the control mechanism. All of these errors accumulate during each time step, and are finally combined into one reactional force error quantity.

7.2 Previous Studies on PSD Testing Error Analysis

Propagation of experimental error appears to be the major source of inaccuracies in a PSD test. This drawback led several researchers to focus on error analysis. The cumulative nature of experimental errors in pseudodynamic tests using explicit numerical integration algorithms was studied by Shing and Mahin (1983,1987). Nakashima and

Kato (1987) performed PSD tests on a 2-DOF and a 6-DOF specimen to examine the effects of the experimental error on the response. Thewalt and Roman (1994) investigated several parameters such as position error, cumulative over/undershooting, energy error and input energy for identifying errors and quantifying their magnitude and effect in PSD testing.

These studies concluded that systematic undershooting (i.e., achieved displacements are less than the target displacements) numerically adds energy to the system while overshooting errors dissipate energy in the system. It has been suggested to use Fast Fourier Transforms (FFTs) of the displacement error history to identify the existence of systematic errors, where displacement error is defined as the difference between the measured and calculated displacement values. The presence of peaks at discrete frequencies in the FFT of the error shows that the error is systematic in nature, and for random errors the FFT will contain a large bandwidth of frequencies.

In these studies, the systematic over and undershoot errors introduced in the numerical simulations were either a constant value, or obtained by truncating the calculated displacement. For example, Mahin and Shing (1983,1987) used both truncation error and constant over and under shooting of 0.02 mm or 1.75 mm (Shing and Mahin, 1987; Shing and Vannan 1990, 1992). More recently Chang et al. (Chang et al., 1998; Chang, 2002) introduced a constant undershooting error of 0.1 mm and 0.02 mm in their numerical simulations.

The reason for the problems due to systematic undershoot error was explained by Nakashima (1987). Unless the distribution of the undershoot error in a PSD test coincides

with the first mode, the higher modes will be excited and the response will be overshadowed by the higher modes of vibration that normally would not participate in the response. Several improvement methods to suppress the spurious growth of the high frequency modes in an MDOF system have been suggested, such as numerical damping (Shing and Mahin, 1983), I Modification (Nakashima and Kato, 1987), T Modification (Nakashima and Kato, 1987), or using an integral form of the Newmark explicit algorithm (Chang et al., 1998).

Most pseudodynamic test systems are capable of recording the history of position errors for each actuator. Therefore, after the experimental setup is ready, preliminary pseudodynamic testing within the linear elastic range of the test specimen is always recommended before any destructive test. By computing the FFT results for the monitored error signals, the nature of the errors can be identified. Also, linear elastic pseudodynamic test results should closely match analytical results obtained with available appropriate structural models. The degree of discrepancy between the two will give an idea about the magnitude of the errors introduced.

Special attention should be given towards using appropriate instrumentation with proper calibration, reliable test apparatus, and good experimental techniques in order that the PSD test simulates the real seismic behavior.

7.3   Error Types Considered in Error Propagation Analyses

7.3.1   Displacement errors

Two types of displacement errors were introduced into the algorithms, which were used to perform the PSD test simulations presented in Chapter 5 and 6. These included: systematic displacement error and random displacement error. The objective was to calculate the performance of these algorithms when experimental error was presented.

A systematic error in the simulation was represented by a factor (called "q"), which has a constant value.

During the PSD test, the reaction wall, against which the actuators are placed to apply the command displacement to the test specimen may not be infinitely rigid. Even though the actuators may be either extended or retracted to the exact amount of the command displacement, due to the elastic deformation of the reaction wall only a certain percentage of the calculated displacement might be imposed to the structure. If, for example the structure was displaced 99% of each computed displacement value, it is considered as an 'undershoot' case and incorporated into the simulation by using q=0.99 to adjust the target displacement for a time step.

Because of miscalibration, it may be possible that the structure is consistently displaced more than it was actually supposed to. This scenario was incorporated into the PSD test simulations by considering values of q greater than one, resulting in overshooting the target displacement.

Nakashima and Kato (1987) conducted a series of on-line test using a two story steel braced frame model. From those results they concluded that random displacement errors are either uniformly distributed or Gaussian distributed.

At the beginning of the study, to represent random error, both normal and uniform distributed errors were considered. Preliminary studies were conducted on how to best represent the random error. Random variables with a Gaussian and uniform distribution were separately considered. It was found that a random error having a Gaussian distribution is more conservative. Therefore the error analysis study proceeded using a random variable with a Gaussian distribution.

The random displacement error in the simulations was represented by a factor called "rd", which is an array having as many number of elements as the number of time steps in the analysis. The elements are normally distributed with a mean of zero and a specified standard deviation.

The normal probability function is a two-parameter function; one parameter, μ, is the mean of the outcomes, and the other parameter, σ, is the standard deviation. The mean μ locates the peak of the curve and is the most likely value to occur. The width, or spread of the curve is described by the parameter σ. The probability density function $p(x)$ of a Gaussian random variable is given by the following equation:

$$p(x) = \frac{1}{\sigma\sqrt{2\pi}}\exp(-\frac{1}{2}\left(\frac{x-\mu}{\sigma}\right)^2)$$ (7.1)

The area under the probability density function curve gives the probability that a range of outcomes will occur, where for example:

$$p(\mu - \sigma \leq x \leq \mu + \sigma) = \int_{\mu-\sigma}^{\mu+\sigma} p(x)dx = 0.68268 \qquad (7.2a)$$

$$p(\mu - 2\sigma \leq x \leq \mu + 2\sigma) = \int_{\mu-2\sigma}^{\mu+2\sigma} p(x)dx = 0.954499 \qquad (7.2b)$$

$$p(\mu - 3\sigma \leq x \leq \mu + 3\sigma) = \int_{\mu-3\sigma}^{\mu+3\sigma} p(x)dx = 0.9973 \qquad (7.2c)$$

Thus, if a variable is normally distributed, there is a 68 % chance that a randomly selected sample will lie within one standard deviation of the mean, 95.5% chance that it will lie within two standard deviations, and, a 99.7% chance that it will lie within three standard deviations.

In the PSD test simulations, the magnitude of the random displacement error is specified by its standard deviation. For example, for rd=0.02, from the above explanation a selected random error (rd_i) is expected to be within $-0.02 < (rd_i) < 0.02$ 68 % of the time (where the mean of the error is taken as zero).

For the PSD test simulations with error, the systematic and random error were implemented into the algorithms where the target displacement is multiplied by (q+rd) to find the actually "imposed displacement", which in turn is used in the calculation of the resisting force. Thus,

$$imposed\_displacement = calculated\_displacement * (q + rd) \qquad (7.3)$$

7.3.2 Force error

As pointed out previously, all errors introduced during a given time step in a PSD test are finally combined in the force error quantity as follows:

$$force\_error = f(displacement\_error) + force\_measurement\_error \qquad (7.4)$$

where the first term is associated with the structure's restoring force due to the actual displacement (which may contain error), the second term is associated with the force measurement error.

The force measurement error is accepted as random, represented by a factor called 'rf'. Like 'rd', it is an array having as many of elements as the number of time steps in the analyses and its magnitude is specified by its standard deviation, such as $rf = 0.002$.

Since the error in a load cell is usually around $load/1000$, $rf = 0.002$ was used in all the numerical simulations and implemented in the following way:

$$measured\_restoring\_force = calculated\_restoring\_force * (1 + rf) \qquad (7.5)$$

where the calculated restoring force is based on the actual imposed displacements which contains displacement errors.

7.4 Error Analysis Matrix

In addition to the case of no errors, ten different combinations of 'q', 'rd' and 'rf' were considered in the numerical simulations of PSD testing of rate-dependent and independent structures using the three different integration algorithms. Thus, a total of 11 cases were considered. The cases are summarized in Table 7.1, and included:

Case 1: This is the 'no error' case. The other cases, where different combinations of error were introduced, are compared to Case 1.

For the remaining ten cases 'rf' was set equal to 0.002.

Case 2: This is the upper limit of random displacement error. 99% of the time, the introduced random displacement error was less than 3%.

Case 3: In this case, 99% of the time the random displacement error is less than 1%.

Case 4: This case is to observe the combined effect of a 2% systematic 'overshoot' error combined with random displacement error, that is less than 1%, 99% of the time.

Case 5: This case is to observe the combined effect of 2% systematic 'undershoot' error combined with random displacement error, that is less than 1%, 99% of the time.

Case 6: Case 6 considers a random displacement error that is less than 2%, 99% of the time, and without any systematic error.

Case 7: The combined effect of a 2% systematic 'overshoot' and random displacement that is less than 2%, 99% of the time was evaluated in Case 7.

Case 8: The combined effect of a 2% systematic 'undershoot' and random displacement that is less than 2%, 99% of the time was evaluated.

Case 9: This case is to observe the effect of random force error that is less than 0.6%, 99% of the time.

Case 10: Case 10 is to see the effects of a 2% systematic 'overshoot' without any random displacement error, and a random force error that is less than 0.6%, 99% of the time.

<u>Case 11</u>: In case 11 the effects of a 2% systematic 'undershoot', combined with a random force error that is less than 0.6%, 99% of the time was investigated.

The 'rd' and 'rf' arrays have been generated by the random number generator in Mathcad (Mathcad 2000 Professional, MathSoft Inc.) with a mean of zero and the specified standard deviation. In the simulations, a separate random error array per floor was used, since the error magnitude induced in the actual test will differ from one story to the other.

The structure used in the numerical simulations was a 4 DOF system; hence for a given standard deviation only four arrays were generated (one for each story). These arrays were stored and used to compare the error propagation characteristics of the different algorithms. Since the same random errors were used for the three different integration schemes, the effect of introducing different random errors to each algorithm was eliminated.

In the Alpha Method with a Fixed Number of Iterations, arrays of random numbers had only as many elements as the number of time steps. The same random errors rf_i and rd_i were introduced in each iteration (sub step), of a given time step.

Table 7.1 Error Analysis Matrix

Case	Displacement Error		Force Error
	Systematic (q)	Random (rd)	Random (rf)
1	1.0	0	0
2	1.0	0.01	0.002
3	1.0	0.0033	0.002
4	1.02	0.0033	0.002
5	0.98	0.0033	0.002
6	1.0	0.0067	0.002
7	1.02	0.0067	0.002
8	0.98	0.0067	0.002
9	1.0	0	0.002
10	1.02	0	0.002
11	0.98	0	0.002

```
┌──────────────┐                    ┌──────────────┐                              ┌──────────────┐
│ calculated   │                    │ command      │                              │ achieved     │
│ displacement │         ▷          │ displacement │              ▷               │ displacement │
│              │  resolution limit of│              │ finite accuracy of          │              │
│              │  D/A converter     │              │ displacement                 │              │
│              │                    │              │ sensors, limitations         │              │
│              │                    │              │ of servo-control             │              │
└──────────────┘                    └──────────────┘ mechanism                    └──────────────┘
```
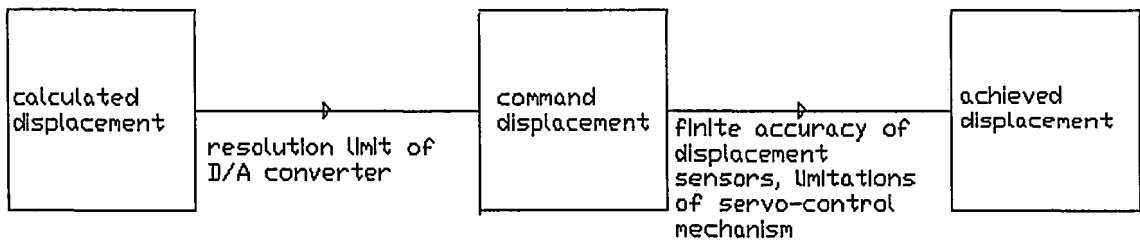
Figure 7.1   Errors associated with a displacement quantity

```
┌──────────────┐                    ┌──────────────┐                              ┌──────────────┐
│ reaction     │                    │ measured     │                              │ feedback     │
│ force due to │         ▷          │ reaction     │              ▷               │ reaction     │
│ achieved     │  finite accuracy of│ force        │ A/D converter               │ force        │
│ displacement │  load measuring    │              │ resolution limit            │              │
│              │  sensors           │              │                              │              │
└──────────────┘                    └──────────────┘                              └──────────────┘
```
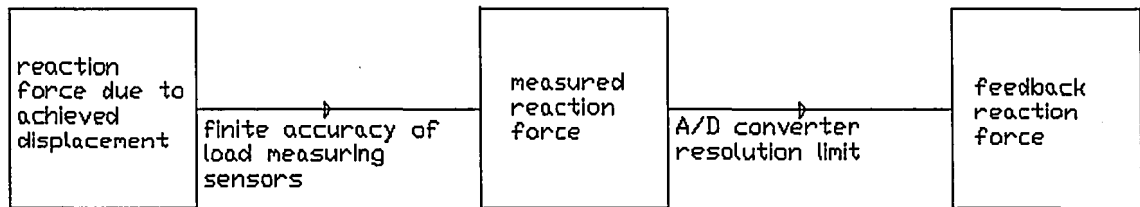
Figure 7.2   Errors associated with a force quantity

Chapter 8 Error Propagation Analysis Results

8.0 General

This chapter presents the error propagation simulations for PSD tests on structures with and without load rate-dependent elements (i.e., VE dampers) using the three different integration algorithms. The results are summarized and the main observations are provided.

8.1 Numerical Simulations of PSD Tests Considering Experimental Error

Numerical simulations of the error combination cases explained in Chapter 7 (Table 7.1) were performed. The maximum and minimum drift ratios were selected as the parameters to compare the response of various simulations with error due to errors of different types and magnitudes introduced into the algorithms. The maximum drift ratio is the ratio of the maximum value of drift for the error case to maximum value of drift for the case without error (i.e., Case 1). Similarly, the minimum drift ratio is the ratio of the minimum value of drift for the error case to the minimum value of drift when there is no error (Case 1).

The reason why drift ratio was selected as the quantity for comparison is because drift is directly related to structural damage.

For each of the 11 error analysis cases, 6 PSD test simulations were performed:

(1) Newmark Explicit Algorithm, Inelastic MRF without VE dampers.

(2) Newmark Explicit Algorithm, Elastic MRF with VE dampers.

(3) Alpha Method with a Fixed Number of Iterations, Inelastic MRF without VE dampers.

(4) Alpha Method with a Fixed Number of Iterations, Elastic MRF with VE dampers.

(5) Newmark Explicit Real-Time Algorithm, Inelastic MRF without VE dampers.

(6) Newmark Explicit Real-Time Algorithm, Elastic MRF with VE dampers.

For the various test algorithms, the effects of having 1%, 2% and 3% random displacement error (i.e., rd=0.0033, 0.0067 and 0.01) alone (i.e., q=1) are compared for cases with a similar random displacement error combined with a 2% over, or undershooting, displacement error (i.e., q=1.02 or q=0.98) in Figures 8.1 through 8.6.

8.1.1 Load Rate-Independent PSD Test Simulation with Newmark Explicit Method

Figure 8.1 summarizes the drift ratios obtained for the ten different error scenarios (Cases 2 through 11), using the Newmark Explicit integration scheme. The simulations were carried out for the idealized MRF presented in Chapter 4.

For no systematic error with random displacement error (q=1,rd=0.01) it is apparent that the drift ratio is around 2.6 in the fourth floor (i.e., the maximum deformation in the fourth floor is 2.6 times larger than that of the solution without error). A random error of rd=0.01 is therefore not acceptable. For rd=0.0033 the drift ratio in the fourth floor is around 1.2, which is more acceptable.

131

8.1.2 Load Rate-Dependent PSD Test Simulations with Newmark Explicit Method

Figure 8.2 summarizes the error analyses results using Newmark Explicit Method for an MRF with VE dampers.

There are only slight changes between cases of q=0.98, q=1, q=1.02. This means that the effect of random displacement errors are more severe compared to systematic errors in the rate dependent simulations with the Newmark Explicit Algorithm.

8.1.3 Load Rate-Independent PSD Test Simulations with Alpha Method with Fixed Number of Iterations

Figure 8.3 summarizes the results of the error analyses performed using the Alpha Method with a Fixed Number of Iterations for the MRF without VE dampers.

From Figure 8.3 it can be observed that Alpha Method is more sensitive to systematic undershoot error (q=0.98). For no systematic error and overshoot cases combined with random displacement error the drift ratios obtained from the Alpha Method are comparable to those from Newmark Explicit Algorithm (see Figures 8.1 and 8.3).

8.1.4 Load Rate-Dependent PSD Test Simulations with Alpha Method with Fixed Number of Iterations

Figure 8.4 summarizes the error propagation characteristics of the Alpha Method for the load-rate dependent PSD test simulations.

For this load rate-dependent case, when Figure 8.4 is compared to Figure 8.2, it can be seen that the Alpha Method has a similar sensitivity to over/undershoot systematic error as the Newmark Explicit scheme.

8.1.5 Load Rate-Independent PSD Test Simulations with Newmark Explicit Real Time Method

Figure 8.5 shows the results of the error propagation simulations using the Newmark Explicit Real-time Method with Alpha-Beta Tracker Filter for load rate-independent PSD tests.

Essentially, the Newmark Explicit Real-Time Method follows a trend very similar to that of Newmark Explicit algorithm results (See Figure 8.1). There are only slight changes in drift ratios for some cases at some floor levels.

8.1.6 Load Rate-Dependent PSD Test Simulations with Newmark Explicit Real Time Method

Figure 8.6 shows the error propagation simulation results for a VE-damped MRF using the Newmark Explicit Real Time Method with Alpha-Beta Tracker Filter.

Similar to the Newmark Explicit algorithm (Section 8.1.2), for the Newmark Explicit Real-Time Method with a filter, the random displacement errors, rather than over/undershooting systematic displacement errors have a greater effect in the result.

Since the ranges of drift ratios are slightly larger than the other two integration schemes for load-rate dependent case it appears that the Newmark Explicit Real-Time Method with a filter is more sensitive to experimental error propagation.

8.1.7 General Observations

In every one of the error cases (both load rate dependent and independent simulatons), for no systematic and random displacement error (i.e., q=1,rd=0), but with random force error (rf=0.002), the maximum and minimum drift ratios are 1 at all floor levels (see Figures 8.1 through 8.6). Therefore it can be concluded that the random force error 'rf=0.002' does not affect the response. As explained in Section 7.3.2 the measurement error in a load cell is around $load/_{1000}$, therefore 0.002 is a conservative value for rf.

The previous error propagation studies (see Section 7.2) concluded that, systematic undershooting errors should especially be avoided, for they numerically add energy to the system. In this study however, this problem with systematic undershoot error was not observed, mainly because of the way the errors were introduced. Since the systematic error was a percentage of the response, and since the response is mainly in the first mode, higher modes were not excited and the energy effect was not detected.

When the error propagation characteristics of the same algorithm for load rate-dependent and independent simulations are compared to each other, it is noticed that the load rate-independent simulations are much more sensitive to experimental error. This can be explained by the fact that the displacement quantities, as well as the error magnitudes introduced, are smaller in the simulations with VE dampers than those in the load rate-independent simulations.

Of the two real-time PSD test algorithms investigated via load rate-dependent PSD test simulations, the Alpha Method with a Fixed Number of Iterations performs slightly

better than the Newmark Explicit Real-Time Method with a filter as far as experimental error propagation is concerned. However it should also be kept in mind that, the use of Alpha Method could lead to incorrect results in a PSD real-time test of a structure with rate dependent elements as explained in Chapter 6.
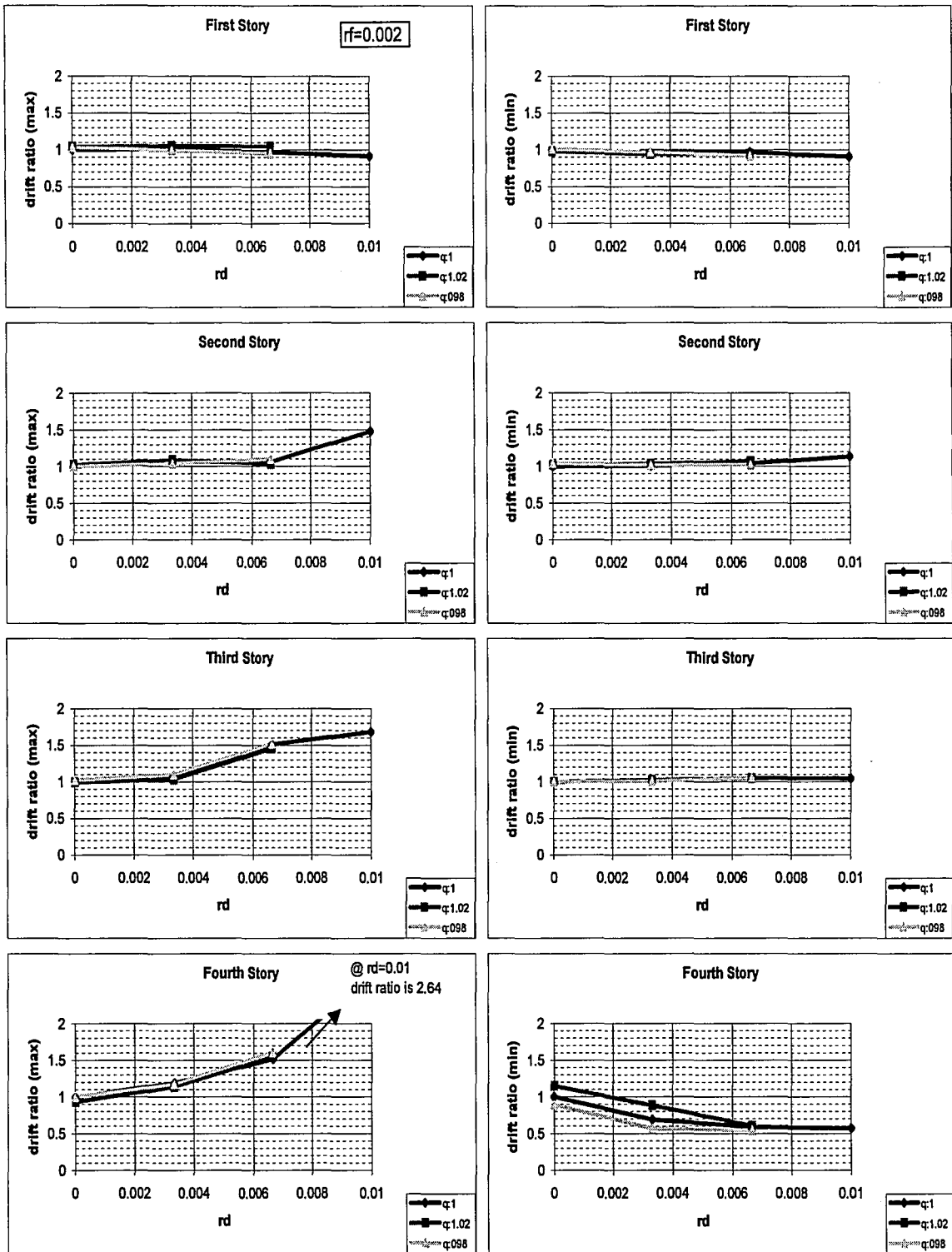
Figure 8.1 Load Rate-Independent PSD Test Simulations,

Newmark Explicit Algorithm (rf=0.002)

136
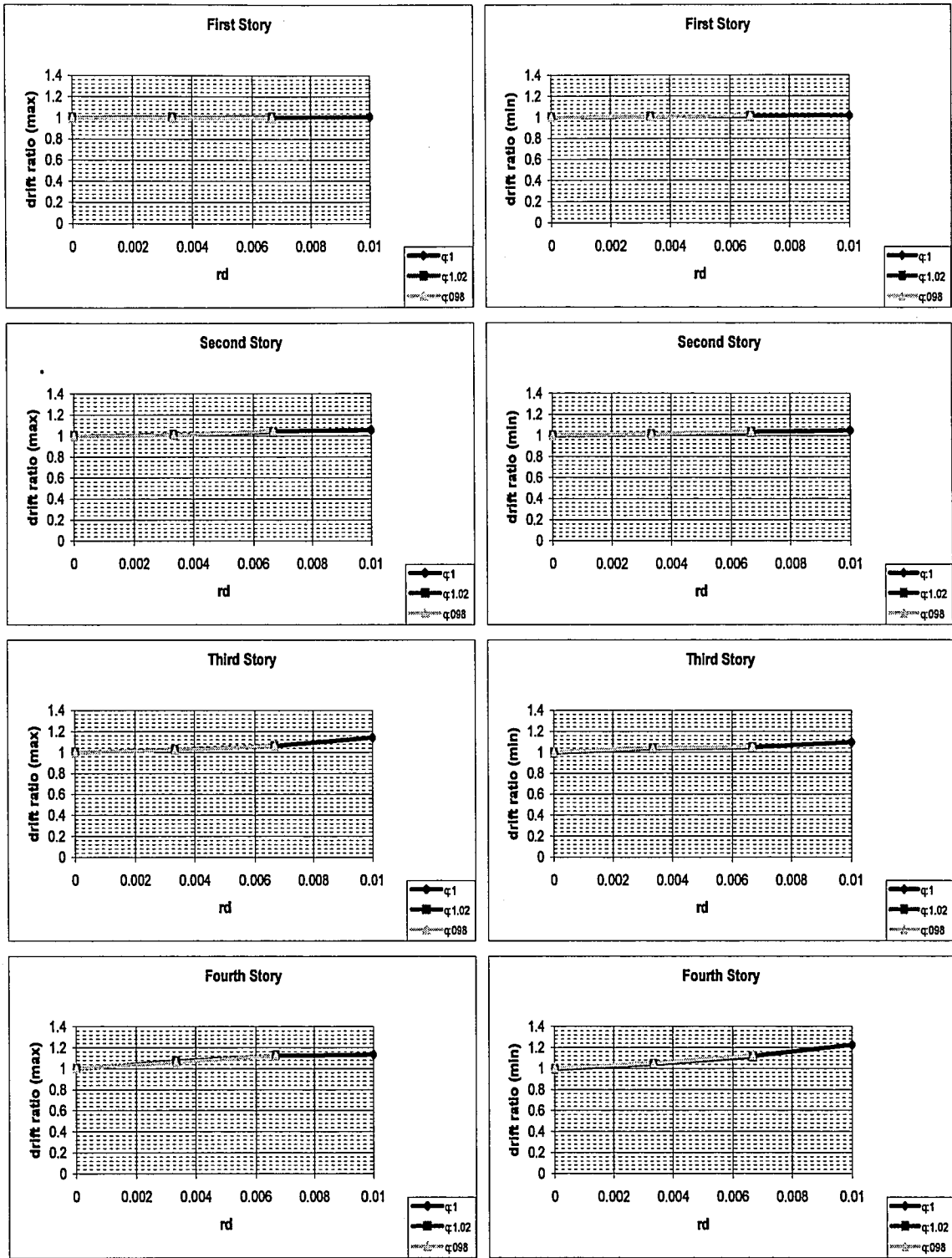
Figure 8.2   Load Rate-Dependent PSD Test Simulations,

Newmark Explicit Algorithm (rf=0.002)

137
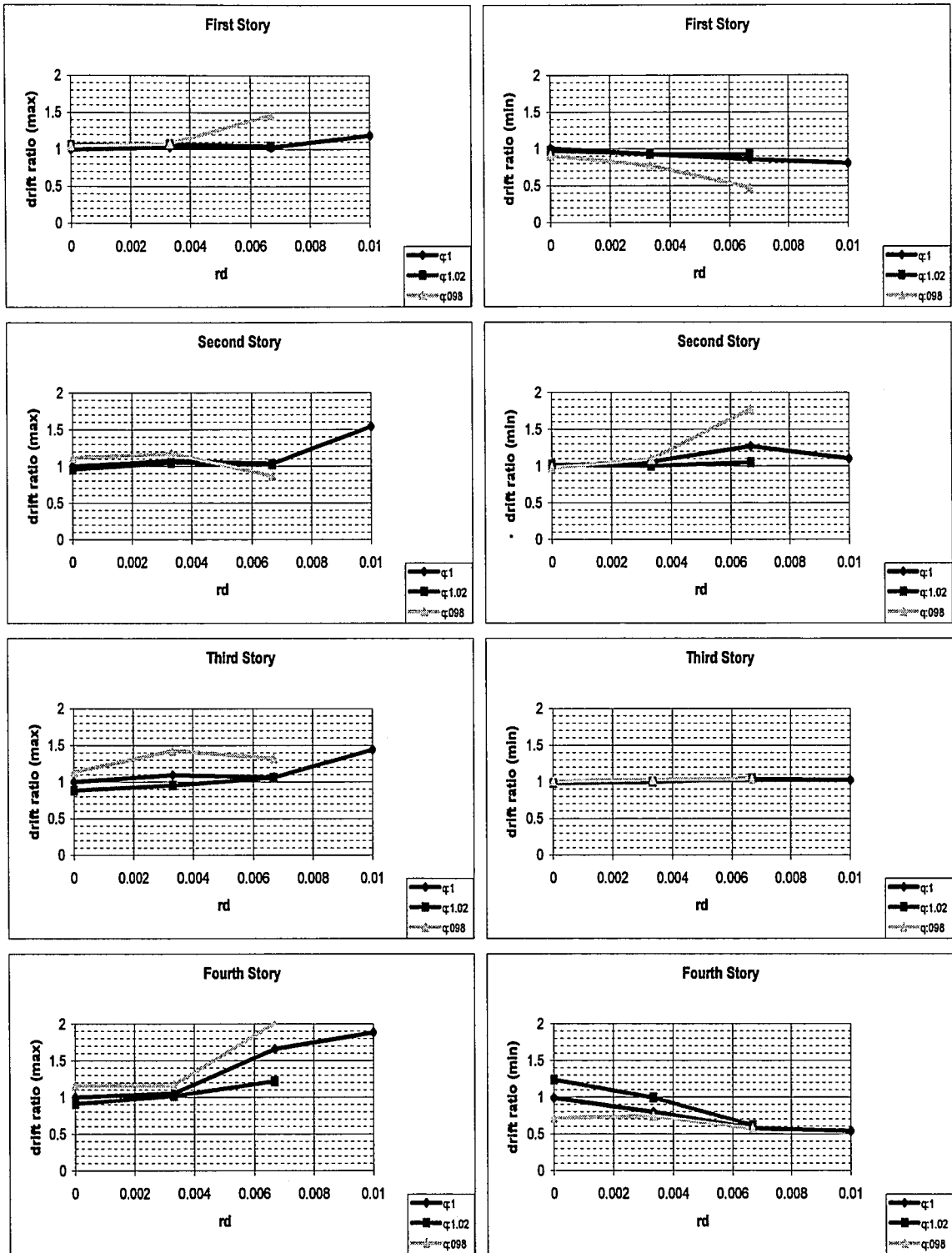
Figure 8.3   Load Rate-Independent PSD Test Simulations,

Alpha Method with Fixed Number of Iterations (rf=0.002)

138
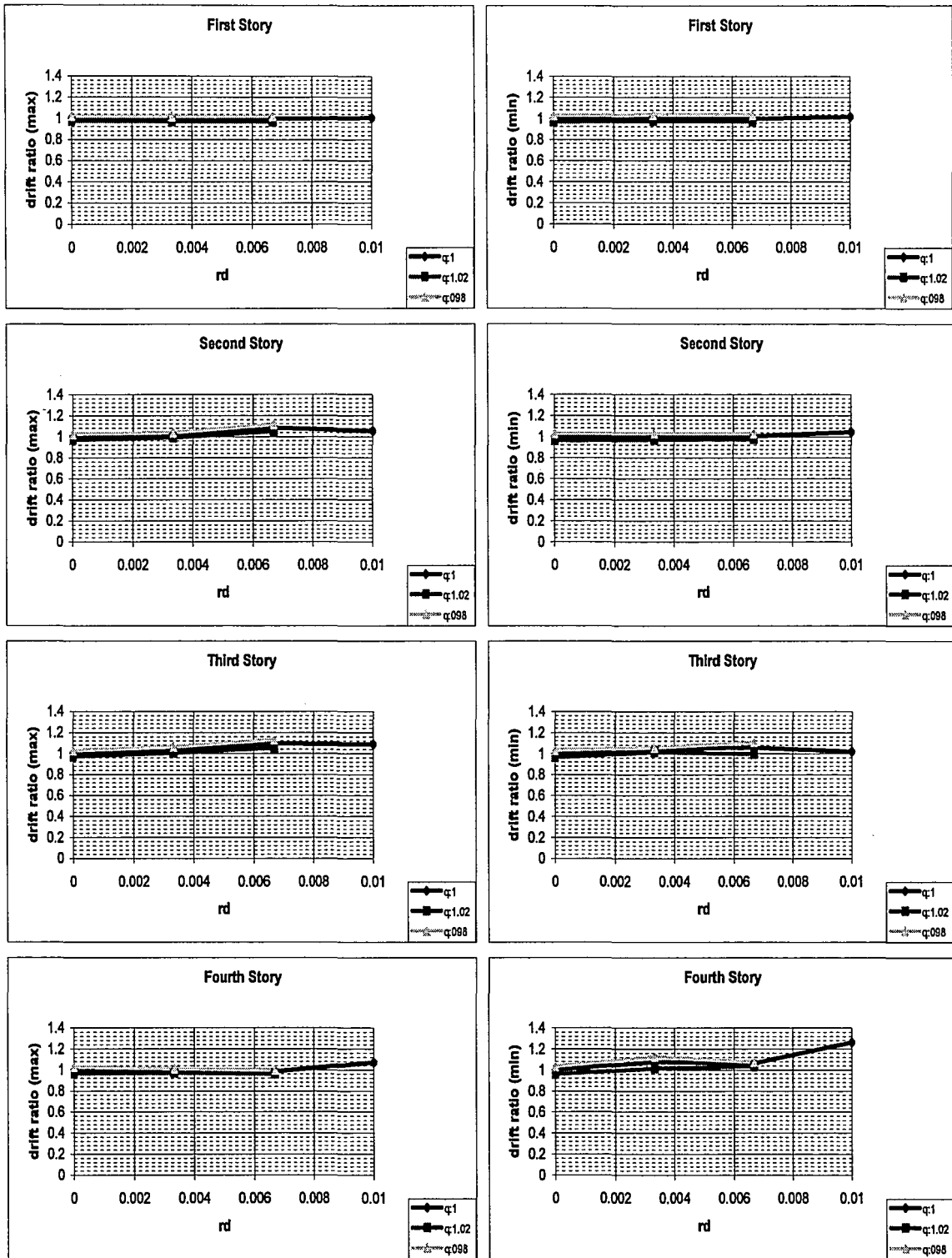
Figure 8.4   Load Rate-Dependent PSD Test Simulations,

Alpha Method with Fixed Number of Iterations (rf=0.002)
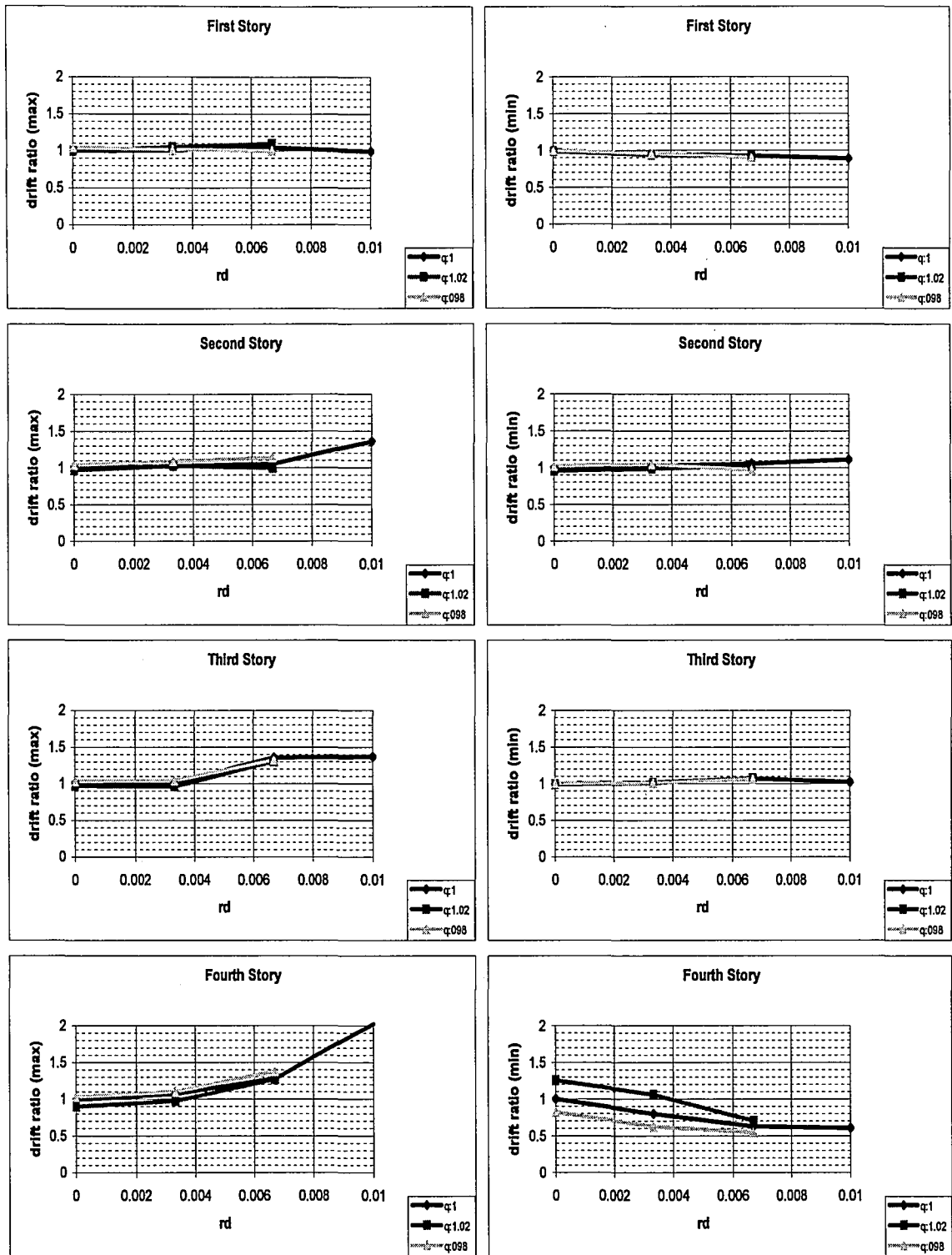
Figure 8.5   Load Rate-Independent PSD Test Simulations,

Newmark Explicit Real Time Algorithm   (rf=0.002)

140
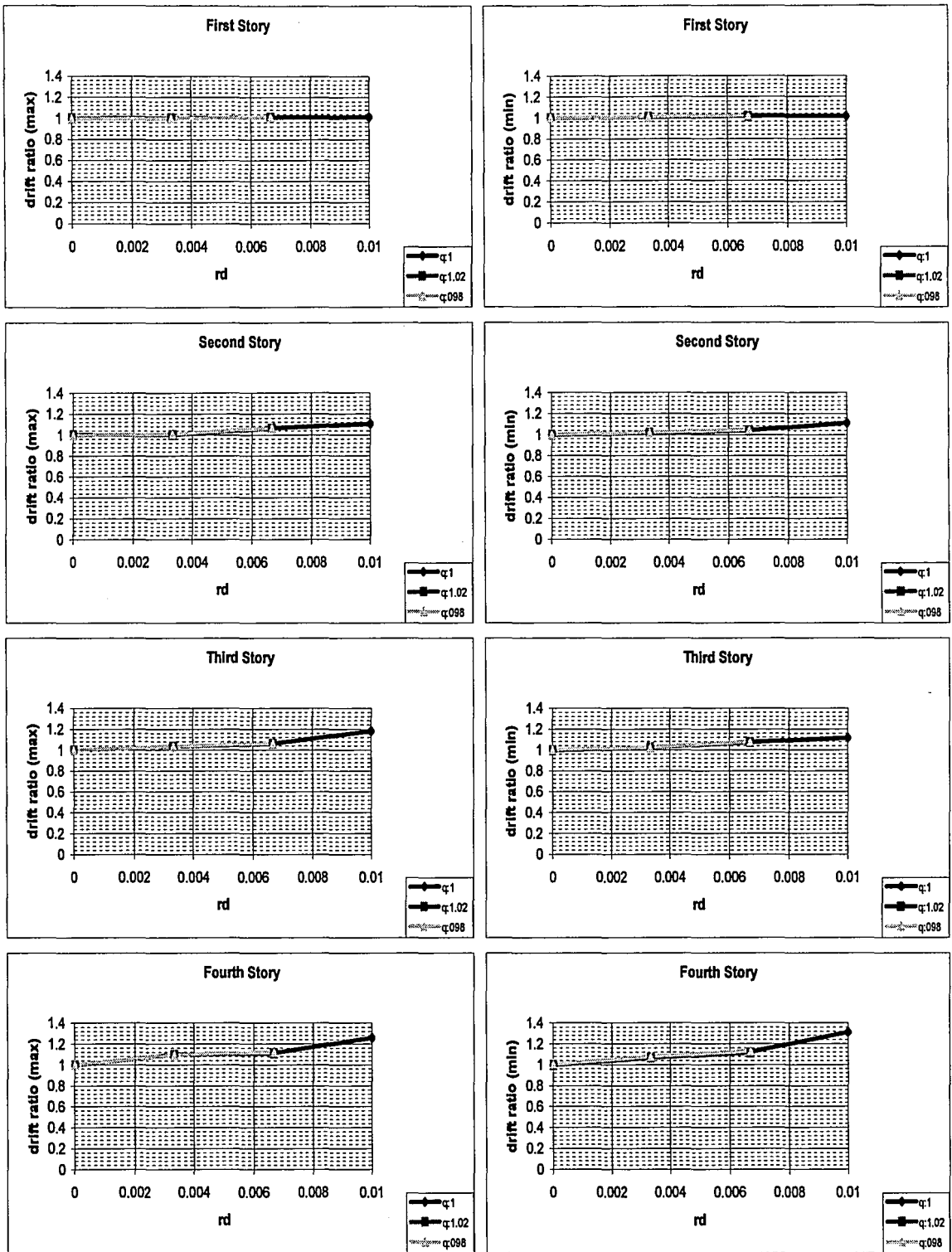
Figure 8.6   Load Rate-Dependent PSD Test Simulations,

Newmark Explicit Real Time Algorithm (rf=0.002)

141

Chapter 9 Summary and Recommended Future Research

9.1   Summary and Conclusions

This study evaluated a total of three numerical integration algorithms for load rate dependent and independent PSD testing.

The necessary background about conventional and real-time PSD testing, together with detailed information about the numerical integration schemes and the structures with and without load rate-dependent devices that were used in the numerical simulations were provided. The error propagation characteristics of the algorithms were systematically examined using ten different error scenarios. Previous research results were included wherever necessary.

A new integration scheme based on the Newmark Explicit method, which is appropriate for real-time PSD testing was presented and evaluated.

For the numerical simulations of load rate-independent linear and nonlinear PSD tests it was observed that all three algorithms gave an accurate response. However, load rate-dependent linear and nonlinear PSD test simulations showed that the Alpha Method with a Fixed Number of Iterations resulted in larger deformations and permanent drift, whereas although conditionally stable, the newly proposed algorithm (Newmark Explicit Real-Time Method with an Alpha-Beta Tracker filter) enabled real-time testing and agreed well with the 'true solution'.

It was found that the 'apparent velocity' characteristics of the algorithms were very important for a real-time PSD test in order to simulate the true seismic response of a

structure with load rate-dependent components. The apparent velocity features of the three algorithms were investigated and the rate-dependent force effect, which was responsible for the discrepancy in the response when different algorithms were used in load rate-dependent PSD test simulations, was also explained.

The error propagation analyses were methodically carried out for both load-rate dependent and independent simulations. The results of all the analyses were summarized by selecting the drift ratio as the quantity of comparison. The observations for the load rate-independent case in the error propagation analyses were compared to those of the previous studies on the same subject.

This report provides the first systematic error analysis for load rate-dependent PSD testing where it was observed that load rate-dependent simulations were not as sensitive to experimental error as the load rate-independent ones.

Of the two real-time PSD test algorithms investigated via load rate-dependent PSD test simulations, the Alpha Method with a Fixed Number of Iterations performed slightly better than Newmark Explicit Real-Time Method with a filter as far as experimental error propagation was concerned. However, as noted earlier, the Alpha Method was found to lead to incorrect results in a real-time PSD test of a structure with load rate-dependent elements.

9.2   Recommended Future Work

Time delay (i.e., latency), which occurs due to several reasons such as the time taken in online data acquisition, filtering and processing and transmission of the control signal,

and time taken between the command issue and actual actuator movement, has not been considered in the numerical simulations in this study.

Because of the time delay, unsynchronized control forces may be applied to the structure, which may cause degradation in the efficiency of control or may even render the structure unstable (Agrawal et al, 1993). Therefore, for a more realistic simulation of real-time PSD testing, actuator dynamics together with time delay effects should be included in the numerical simulations.

In order to examine the error propagation characteristics of the algorithms, the error signals obtained during preliminary pseudodynamic testing from the real experiment setup should be introduced in the numerical simulations. Also, numerical simulations for the error propagation characteristics should be performed using inelastic MRF with VE dampers.

For the verification of the explanation about the rate-dependent force effect, load rate-dependent PSD test numerical simulation responses should be compared to that from a shake table test.

References

Agrawal A., Fujino Y., Bhartia B., (1993) "Instability Due to Time Delay and Its Compensation in Active Control of Structures" Earthquake Engineering and Structural Dynamics, Vol. 22, 211-224.

Bathe K.J. and Wilson E.L., (1976) "Numerical Methods in Finite Element Analysis" Prentence-Hall, Inc., Englewood Cliffs, New Jersey

Bursi O.S., Shing P.B., (1996) " Evaluation of Some Implicit Time-Stepping Algorithms for Pseudodynamic Tests" Earthquake Engineering and Structural Dynamics, Vol. 25,333-355,

Chang S.Y., (2002) "An Improved On-Line Dynamic Testing Method" Engineering Structures Vol. 24, 587-596.

Chang S.Y., Tsai K.C. and Chen K.C., (1998) "Improved Time Integration for Pseudodynamic Tests" Earthquake Engineering and Structural Dynamics, Vol. 27,711-730.

Cunningham E.P., (1992) "Digital Filtering: An Introduction" Houghton Mifflin Company, Boston,

Dimig J., Shield C., French C., Bailey F., Clark A., (1999) "Effective Force Testing: A Method of Seismic Simulation for Structural Testing" Journal of Structural Engineering, Vol. 125,No. 9.

Fan C.P., (1998) "Seismic Analysis, Behavior and Retrofit of Non-Ductile Reinforced Concrete Frame Buildings with Viscoelastic Dampers" Ph.D. Dissertation, Department of Civil and Environmental Engineering, Lehigh University, December.

Grewal M.S. and Andrews A.P., (1993) "Kalman Filtering: Theory and Practice" Prentice Hall, Englewood Cliffs, NJ.

Herrera R, (2004)"Seismic Behavior of Concrete Filled Tube Columns-Wide Flange Beam Frames" Ph.D. Dissertation, Department of Civil and Environmental Engineering, Lehigh University.

Herrera R., Ricles J.M., Sause R., (2003)"Analytical Studies of Steel MRF's with CFT Columns Under Earthquake Loading Conditions" Proceedings, 4th International Conference on Behavior of Steel Structures in Seismic Areas-STESSA,.

Hilber H.M., Hughes T.J.R. and Taylor R.L., (1977) "Improved Numerical Dissipation for Time Integration Algorithms in Structural Dynamics" Earthquake Engineering and Structural Dynamics, Vol. 5,283-292.

Horiuchi T., Nakagawa M., Sugano M. and Konno T., (1996) "Development of a Real-Time Hybrid Experimental System with Actuator Delay Compensation" Proc. 11th World Conf. on Earthquake Engineering, Paper No. 660.

http://www.nsf.gov

http://www-civil.eng.ox.ac.uk/people/msw/rts.html

Hughes T.J.R. and Liu W.K., (1978) "Implicit-Explicit Finite Elements in Transient Analysis: Stability Theory" Trans. ASME J. Appl. Mech., Vol. 45,371-374.

Kasai K., Munshi J.A., Lai M.L., Maison B.F., (1993) " Viscoelastic Damper Hysteretic Model: Theory, Experiment and Application" Proceedings, ATC 17-1: Seminar on Seismic Isolation, Passive Energy Dissipation, and Active Control, Applied Technology Council, San Francisco, CA., pp. 521-532.

Mahin S.A and Shing P.B., (1985) "Pseudodynamic Method for Seismic Testing", Journal of Structural Engineering, Vol. 111, No. 7, © ASCE, ISSN 0733-9445/85/0007-1482/$01.00.Paper No.19867.

Mathcad 2000 Professional, MathSoft Inc.

Nakashima M. and Kato H., (1987) "Experimental Error Growth Behavior and Error Growth Control in On-Line Computer Test Control Method" Building Research Institute, Ministry of Construction, JAPAN.

Nakashima M. and Masaoka N., (1999) "Real-Time On-Line Test for MDOF Systems" Earthquake Engineering and Structural Dynamics, Vol. 28,392-420.

Nakashima M. (1993) ,"Extensions of On-Line Computer Control Method" Disaster Prevention Research Institute, Kyoto University, Gokasho, Uji, Kyoto 611 JAPAN Proceedings of the U.S.-Japan Seminar on Development and Future Dimensions of Structural Testing Techniques, Waikiki, Hawaii.

Nakashima M., Kaminosona T., Ishida M., Ando K., (1990)" Integration Techniques for Substructure Pseudodynamic Test" Proceedings of Fourth U.S. National Conference on Earthquake Engineering May 20-24,1990, Palm Springs, California (Volume 2)

Nakashima M., Kato H., Takaoka E., (1992) "Development of Real-Time Pseudodynamic Testing" Earthquake Engineering and Structural Dynamics, Vol. 21,79-92.

Shing P.B. and Mahin S.A., (1987) "Cumulative Experimental Errors in Pseudodynamic Tests" Earthquake Engineering and Structural Dynamics, Vol. 15,409-424.

Shing P.B. and Mahin S.A., (1987) "Elimination of Spurious Higher-Mode Response In Pseudodynamic Tests" Earthquake Engineering and Structural Dynamics, Vol. 15,425-445.

Shing P.B. and Mahin S.A., (1983) "Experimental Error Propagation in Pseudodynamic Testing" UCB/EERC-83/12, Earthquake Engineering Research Center, University of California, Berkeley.

Shing P.B. and Mahin S.A., (1984) "Pseudodynamic Test Method for Seismic Performance Evaluation: Theory and Implementation", UCB/EERC-84/01, Earthquake Engineering Research Center, University of California, Berkeley.

Shing P.B. and Manivannan T., (1990) "On the Accuracy of an Implicit Algorithm for Pseudodynamic Test" Earthquake Engineering and Structural Dynamics, Vol. 19,631-651.

Shing P.B. and Vannan M.T., (1991) "Implicit Time Integration for Pseudodynamic Tests: Convergence and Energy Dissipation" Earthquake Engineering and Structural Dynamics, Vol. 20,809-819.

Shing P.B. and Vannan M.T., Cater E., (1991) "Implicit Time Integration for Pseudodynamic Tests" Earthquake Engineering and Structural Dynamics, Vol. 20,551-576.

Shing P.B., Spacone E., Stauffer E., (2002) "Conceptual Design of Fast Hybrid Test System at the University of Colorado" Proceedings of the 7th U.S. National Conference on Earthquake Engineering, Boston, Massachusetts.

Takanashi K., Udagawa K., Seki M., Okada T. and Tanaka H., (1975) "Nonlinear Earthquake Response Analysis of Structures by a Computer-Actuator On-Line System" Bull. Earthquake Resistant Struct. Res. Center (Tokyo) Issue 8.

Thewalt C. and Roman M., (1994) "Performance Parameters for Pseudodynamic Tests" Journal of Structural Engineering ASCE 120,9,2678-2781.

Thewalt C.R. and Mahin S.A., (1995)"An Unconditionally Stable Hybrid Pseudodynamic Algorithm" Earthquake Engineering and Structural Dynamics, Vol. 24,723-731.

Thewalt, C.R. and Mahin, S.A., (1987)"Hybrid Solution Techniques for Generalized Pseudodynamic Testing" UCB/EERC-87/09, Earthquake Engineering Research Center, University of California, Berkeley.

Vita

Oya Mercan was born on August 17,1978 in Istanbul, Turkey. She was the second child of Ayse and Yasar Mercan. She received a B.S. degree in Civil Engineering from Bogazici University as the first ranking student of Class 2001.She then went to U.S. to pursue a graduate study majoring in Structural Engineering at Lehigh University, Bethlehem, Pennsylvania. In 2003, she received a M.S. degree in Structural Engineering from Lehigh University and she plans to pursue a Ph.D. degree in Civil Engineering at Lehigh University.

END OF
TITLE